# *Advanced SYNCOM*

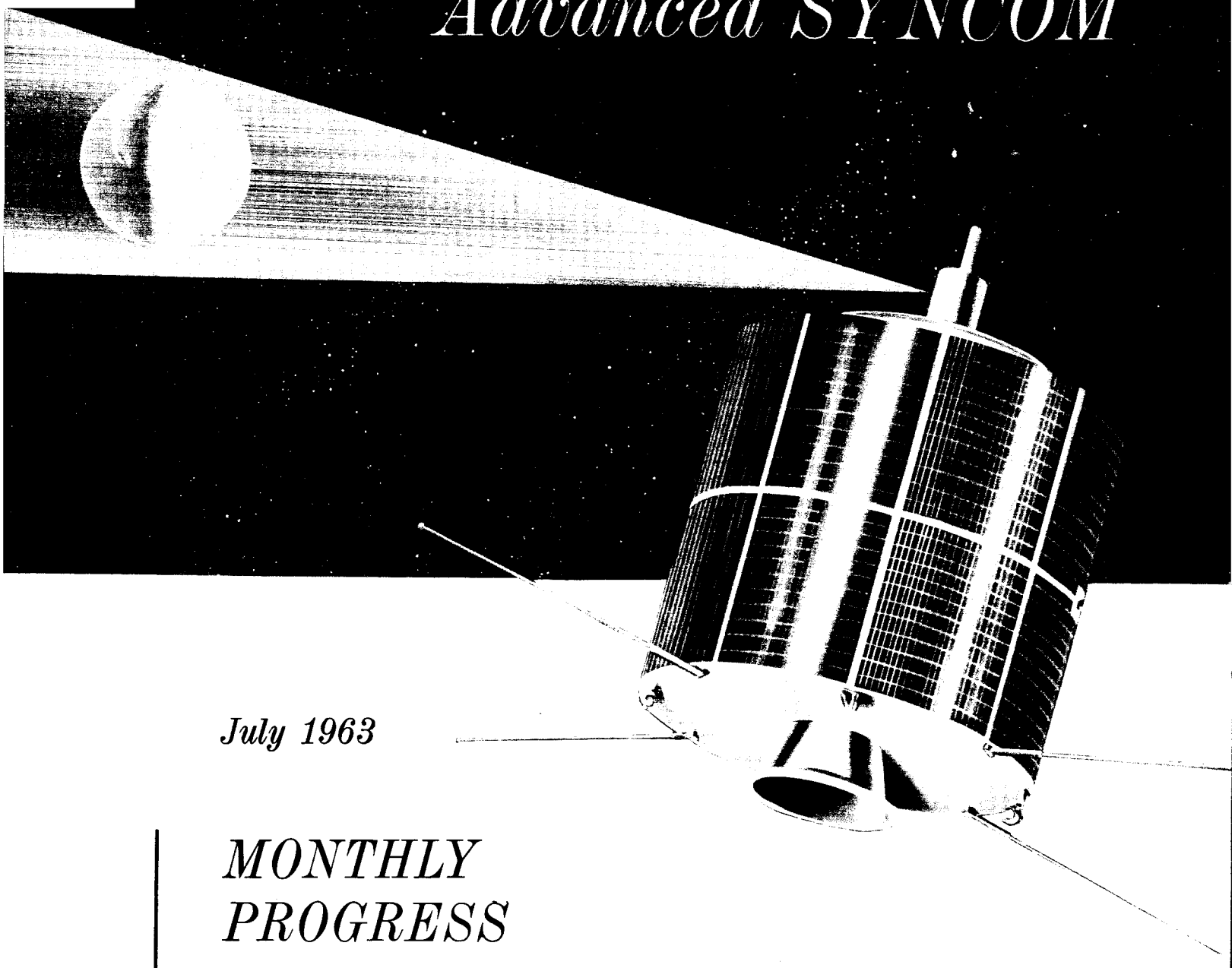

*July 1963*

# *MONTHLY PROGRESS REPORT*



*NASA Contract 5-2797*
*SSD 3464R*

AEROSPACE GROUP
SPACE SYSTEMS DIVISION
HUGHES AIRCRAFT COMPANY
CULVER CITY, CALIFORNIA

HUGHES

**HUGHES AIRCRAFT COMPANY**

AEROSPACE GROUP

SPACE SYSTEMS DIVISION

EL SEGUNDO, CALIFORNIA

19 August 1963

SUBJECT: Advanced Syncom Monthly Progress Report for July 1963

TO: Mr. Robert J. Darcey
Program Manager, Syncom
Goddard Space Flight Center
Code 621
Greenbelt, Maryland

Attached are copies of the Advanced Syncom Monthly Progress Report for July 1963.

The engineering model version of the digital PACE circuitry has been completed, and checkout is well along. All circuits are operating as predicted. The sine wave generators are producing a very true wave with no indications of spikes.

The stripline version of the phased array antenna circuitry is in manufacture with many pieces completed and assembly scheduled for August. The ground planes are being plated, and holes are being punched in the circuit boards. Most of the units of the transponder are in fabrication.

Acceptance tests were run on the reaction control system. A specific impulse of 262 seconds was obtained for a one-sixth duty cycle and 285 seconds for a one-third duty cycle. In a special test of a reworked engine, which ran continuously for 30 minutes, a specific impulse of 262 seconds was obtained.

HUGHES AIRCRAFT COMPANY

Paul E. Norsell

Paul E. Norsell
Manager, Systems Development
Advanced Syncom

cc: H. E. Tetirick
Goddard Space Flight Center
Code 241.4
Greenbelt, Maryland

# *Advanced SYNCOM*

*July 1963*

# *MONTHLY PROGRESS REPORT*

•

*NASA Contract 5-2797*
*SSD 3464R*

AEROSPACE GROUP
SPACE SYSTEMS DIVISION
HUGHES AIRCRAFT COMPANY
CULVER CITY, CALIFORNIA

HUGHES

CONTENTS

# 1. INTRODUCTION

Under NASA Goddard Space Flight Center Contract NAS-5-2797, Hughes is conducting feasibility studies and technological development for an advanced, stationary active repeater communication satellite. A summary report covered the technical progress achieved during the original contract period and detailed the system configuration resulting from the system studies. A subsequent supplementary report covered further studies made under modification two to the above contract and the accompanying technical direction.

These monthly technical letter reports present the technical progress made during the reporting period, critical problems or delays encountered, and plans for the forthcoming reporting period. Separate reports of schedule status are provided through biweekly PERT reports. Monthly financial management reports provide the funding status.

# 2. SPECIAL SYSTEM STUDIES

## PRELIMINARY ANALYSIS OF COMMAND DECODER PERFORMANCE IN PRESENCE OF NOISE

The input to the command decoder consists of a subcarrier which is frequency shifted between 8.0 and 8.6 kc to designate binary states "zero" and "one," respectively. The system is non-return-to-zero (NRZ), and the essential clock pulse frequency is determined from a sinusoidal signal which amplitude modulates the subcarrier 50 percent. The subcarrier, in turn, has been modulated onto the RF carrier with an AM modulation index of about 0.5. The system bit rate is 128 bits per second.

A block diagram indicating elements of the system essential for a basic noise performance analysis is shown in Figure 2-1. The subcarrier is drawn in Figure 2-2 illustrating both amplitude and frequency modulation. The various frequencies have not been drawn to scale; however, the amplitude modulation of 0.5 is shown approximately to scale.

In this system the clock period is determined entirely from the period of the amplitude modulation of the subcarrier. Therefore, any noise disturbing the period of the sinusoidal amplitude modulation is reflected as jitter in the clock pulse period. At some point in the system, a circuit is sampled at a time determined by the clock pulse, and this circuit designates either a zero or a one as the received bit. A significant error in the clock pulse period may result in a bit error.

This analysis attempts to discover what signal-to-noise ratio is required for the bit synchronization tone to ensure satisfactory bit synchronization and what signal-to-noise ratio is required in the frequency shift keying bit detector to ensure a sufficiently small bit error rate. Both questions are examined in the light of preliminary design concepts now available.

### Effect of Noise on Bit Synchronization Tone

The bit synchronization tone is a 128-cps sine wave which amplitude modulates the subcarrier with an AM modulation index of 0.5, as shown in Figure 2-2. One method of processing this tone is indicated schematically in Figure 2-1 A rather wide bandpass filter centered on about 8.3 kc rejects

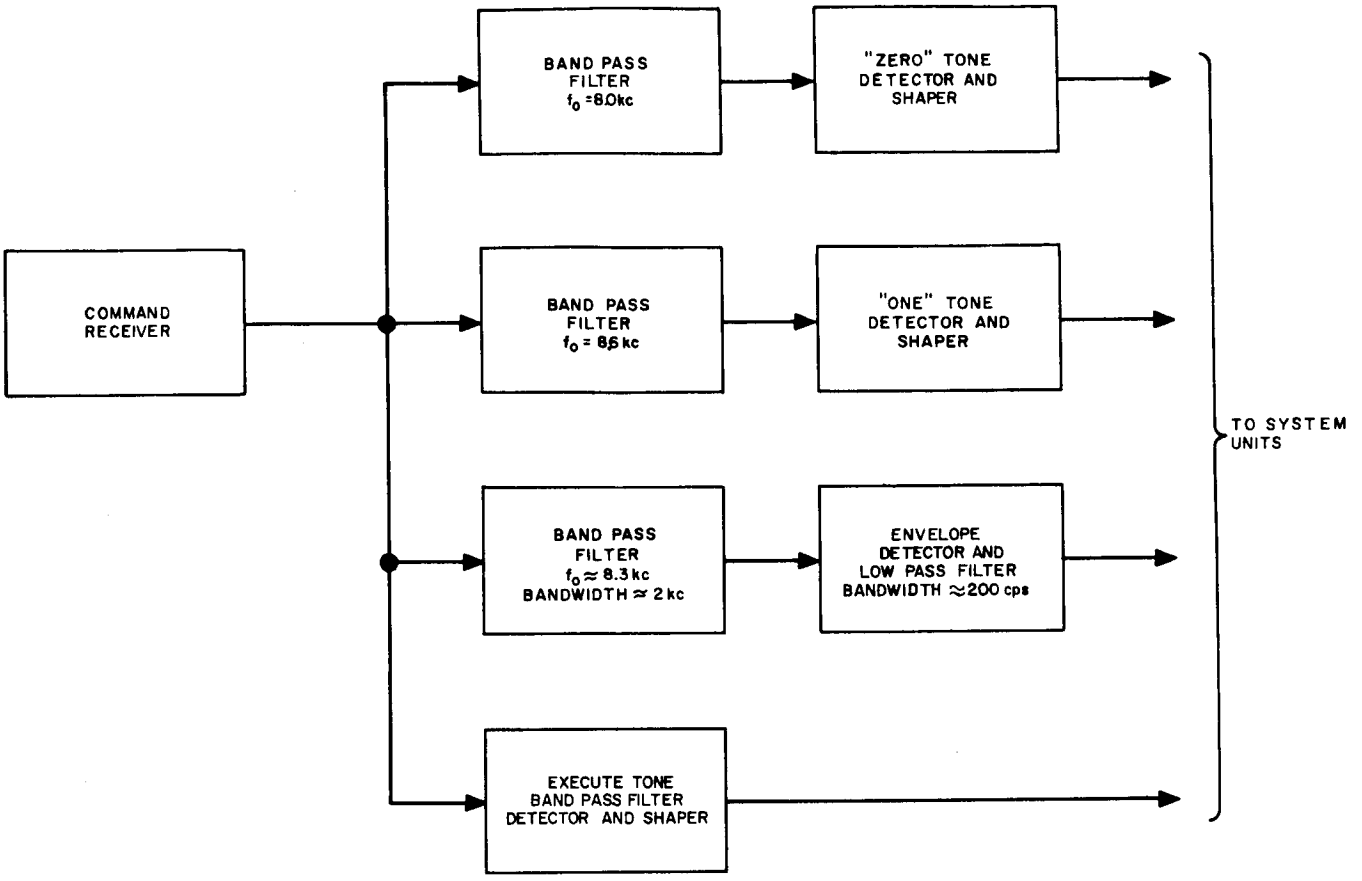


Figure 2-1. Command Decoder Basic Block Diagram

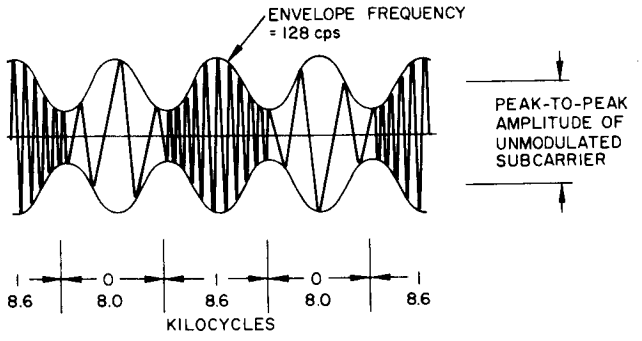


Figure 2-2. Amplitude and Frequency Modulated Subcarrier

much of the noise from the command receiver IF strip and ensures that the envelope detector signal-to-noise ratio (S/N) is above its threshold (S/N > 3 db). The command receiver and many pertinent characteristics of both the ground station and spacecraft are sufficiently similar to those of the Syncom I telemetry and command system that an analogy may be drawn between the Syncom I and Syncom II command systems in many respects. In the analysis of the Syncom I telemetry and command system,* it is shown that the signal-to-noise ratio at the output of the 300 cps bandpass filter is about 30 db when the RF carrier is modulated 50 percent by the 9.745-kc tone. This bandwidth and signal-to-noise ratio will be used as a basis for the following discussions.

Assuming that the noise bandwidth of the bit synchronization tone bandpass filter in Figure 2-2 is 2 kc, the signal-to-noise ratio at the output of this filter is 10 log 2000/300, or 8.2 db less than the 30 db signal-to-noise ratio out of a 300-cps bandpass filter. Therefore,

$$\left(\frac{S}{N}\right)_{\text{input to envelope detector}} = 30 - 8.2 = 21.8 \text{ db}$$

This is well above threshold for an envelope detector.

The signal at the input to the envelope detector is:

$$A_c (1 + M \cos \omega_m t) \cos \omega_c t \qquad (2\text{-}1)$$

where

$A_c$ = peak amplitude of unmodulated subcarrier

$M$ = AM modulation index of tone onto subcarrier

$\omega_m$ = tone frequency = $2\pi(128)$ rad/sec

$\omega_c$ = subcarrier frequency, which shifts between 8.0 and 8.6 kc

The output of the envelope detector enters a low-pass filter, and the final output signal is

$$a A_c M \cos \omega_m t$$

*"Project Syncom: Syncom Mark I Telemetry and Command System Analysis," Hughes Aircraft Company SSD 3017R, January 1963, p. 32.

where a is a constant proportionality of the filter. Therefore the signal power is

$$S_o = \frac{a^2 A_c^2 M^2}{2} \tag{2-2}$$

The original unmodulated subcarrier power is

$$S_c = \frac{A_c^2}{2} \tag{2-3}$$

Therefore, the ratio of the output signal power to subcarrier power is

$$\frac{S_o}{S_c} = a^2 M^2 \tag{2-4}$$

or the signal power varies as the square of the modulation index. For large signal-to-noise ratios, the output signal-to-noise ratio may be expressed as

$$\frac{S}{N} = M^2 \frac{C}{N} \frac{B_1}{2B_o} \tag{2-5}$$

where

$\frac{S}{N}$ = signal-to-noise ratio at the output of the low-pass filter

$M$ = AM modulation index

$\frac{C}{N}$ = subcarrier-to-noise ratio at a reference point in the system

$B_1$ = noise bandwidth at the reference point of $\frac{C}{N}$

$2B_o$ = noise bandwidth of the low-pass filter

For the system under consideration, C/N = 30 db at a reference bandwidth of 300 cps. The output low-pass filter must pass the 128-cps tone so a 3-db point of 150 cps is assumed. The noise bandwidth $2B_o$ of a simple low-pass filter is about $2(\pi/2)$ times its 3-db frequency, or

$$2B_o = 2\left(\frac{\pi}{2}\right)(150) = 470 \text{ cps}$$

Therefore,

$$10 \log \frac{S}{N} = 20 \log M + 10 \log \frac{C}{N} + 10 \log \frac{B_1}{2B_o}$$

$$= -6 + 30 - 2 = 22 \qquad (2\text{-}6)$$

or

$$\frac{S}{N} = +22 \text{ db}$$

The effect of a finite signal-to-noise ratio on the clock pulse jitter may be determined by examining the effect of noise on a sine wave. Consider a single small component of noise separated by $\omega$ from the tone frequency $\omega_m$. The tone plus this single noise component may be written as

$$A_o \cos \omega_m t + A_n \cos(\omega_m + \omega)t$$

where

$A_o$ = amplitude of tone signal

$A_n$ = amplitude of noise signal

$\omega_m$ = tone frequency

$\omega$ = frequency separation between tone and noise component

This may be rewritten as

$$A_o \cos \omega_m t + A_n \cos(\omega_m + \omega)t$$

$$= \sqrt{(A_o + A_n \cos \omega t)^2 + (A_n \sin \omega t)^2} \cos \left( \omega_m t + \tan^{-1} \frac{A_n \sin \omega t}{A_o + A_n \cos \omega t} \right)^*$$

Note that the phase deviates from that of a clean sine wave by the term

$$\tan^{-1} \frac{A_n \sin \omega t}{A_o + A_n \cos \omega t} \qquad (2\text{-}7)$$

*M. Schwartz, "Information Transmission, Modulation, and Noise," McGraw Hill, p. 297.

By invoking the central limit theorem it may be shown that the sum of a large number of sine waves of different frequencies and random phases approaches a normal distribution whose variance is equal to the total mean power, or the sum of the powers, in each incremental sinusoidal component. The standard deviation, $\sigma$, of the resulting power is the square root of this variance. To be consistent with the terminology of Equation 2-6, the total noise signal will first be expressed as a sine wave of equal variance (and therefore equal $\sigma$). Again, the total noise signal, $A_{n_T}$, is assumed small in comparison with the signal tone amplitude $A_o$. For small $A_{n_T}$, Equation 2-6 is

$$\tan^{-1} \frac{A_{n_T} \sin\omega t}{A_o + A_{n_T} \cos\omega t} \approx \tan^{-1} \frac{A_{n_T}}{A_o} \sin\omega t \qquad (2\text{-}8)$$

or

$$\theta \approx \frac{A_{n_T}}{A_o} \sin\omega t \qquad (2\text{-}9)$$

where $\theta$ is the phase deviation in radians. This geometry is illustrated in Figure 2-3. The rms value of $\theta$ is therefore

$$\theta_{rms} \approx \frac{A_{n_T}}{A_o\sqrt{2}} \qquad (2\text{-}10)$$

Assuming that clock pulses are generated at positive going axis crossing of the bit synchronization tone as indicated in Figure 2-4, it is evident that phase jitter $\epsilon$ on the tone results in an equivalent jitter in the clock pulse period. Since the rms value of the composite noise signal $A_{n_T}/A_o \sin\omega t$ from Equation 2-8 is

$$\frac{A_{n_T}}{A_o\sqrt{2}}$$

it is seen that this is equal to the rms value of the phase jitter $\theta$. The term $A_o/A_{n_T}$ is the voltage signal-to-noise ratio at the output of the low-pass filter. Therefore,

$$\frac{S}{N} = \left(\frac{A_o}{A_{n_T}}\right)^2 = \frac{1}{2\theta^2_{rms}} \qquad (2\text{-}11)$$

or

$$\boxed{\theta_{rms} = \frac{1}{\sqrt{2}\sqrt{\frac{S}{N}}}} \qquad (2\text{-}12)$$

This equation indicates that for large signal-to-noise output values, the rms value of the jitter is inversely proportional to the square root of the signal-to-noise output.

Now assume that $\epsilon$ should generally not exceed $1/8\ \tau$ where $\epsilon$ and $\tau$ are as shown in Figure 2-4. Since $\theta$ is $\epsilon$ expressed in radians,

$$\theta \leq \frac{2\pi}{8} = 0.785 \text{ radian}$$

A $3\sigma$ confidence level will be assumed for the $\theta$ extreme. Therefore the rms value of $\theta$ should be

$$\frac{0.785}{3} = 0.262 \text{ radian}$$

Under these conditions $\theta$ will be less than its peak value 99.73 percent of the time. Therefore, from Equation 2-10,

$$\frac{S}{N} = \frac{1}{2\theta^2_{rms}} = \frac{1}{2(0.262)^2} = 7.30 \longrightarrow 8.6 \text{ db} \qquad (2\text{-}13)$$

Thus, in answer to the question posed at the beginning of this analysis, it is seen that a signal-to-noise ratio of 8.6 db at the output of the bit synchronization tone filter will ensure that 99.7 percent of the time the clock pulse jitter does not exceed 1/8 of the clock period.

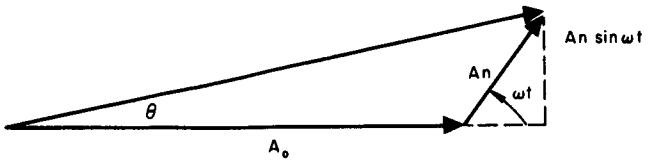


Figure 2-3. Geometry of Noise Modulated Tone

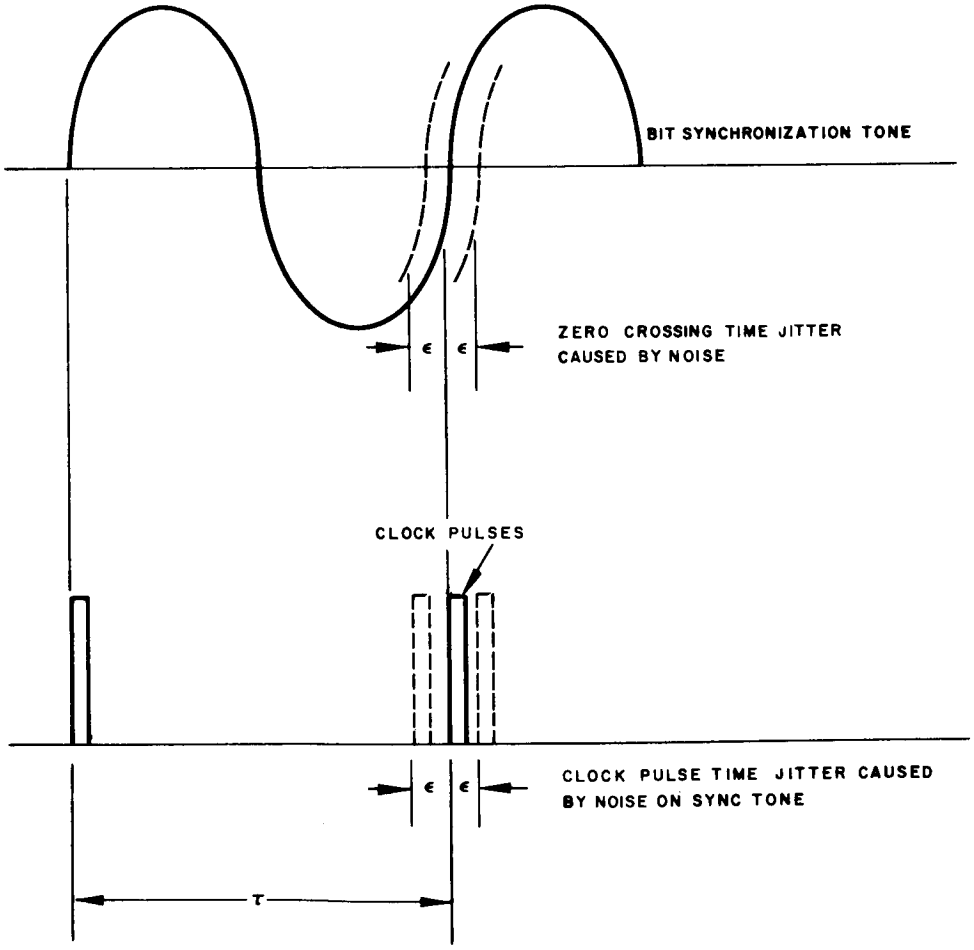


Figure 2-4. Effect of Noise on Clock Pulse Period

Consider now the values in the proposed system,

$$\frac{S}{N} = 22 \text{ db} = \frac{158}{1}$$

$$\sqrt{\frac{S}{N}} = 12.6$$

$$\theta_{rms} = \frac{1}{\sqrt{2}\sqrt{\frac{S}{N}}} = \frac{1}{\sqrt{2}(12.6)} = 0.056 \text{ radian}$$

For a $3\sigma$ confidence factor, it may be stated that 99.7 percent of the time the jitter will be less than 3 x 0.056 or 0.168 radian or less than 0.0268 of a clock pulse period. Based on the results of Equation 2-12 the system contains a safety factor of 22.0 - 8.6 = 13.4 db.

Effect of Noise on Bit Error Rate

The bit error rate is a function of the signal-to-noise ratio at that part of the system where a decision is made as to whether a bit is a zero or a one. The signal-to-noise ratio however is a function of the noise bandwidth of the low-pass filter used in the tone detector of Figure 2-1. For a simple low-pass filter (RC), the 3-db cutoff frequency is given by

$$\omega_{3db} = \frac{1}{T}$$

where

$\omega_{3db}$ = 3-db cutoff frequency in radians per second

T = time constant of filter (RC)

Five time constants will permit the filter output to approach closely its maximum value during each bit period. Since each bit period is 1/128 second,

$$5\,T = \frac{1}{128} \text{ second}$$

$$T = 0.00156 \text{ second}$$

Therefore,

$$\omega_{3db} = \frac{1}{T} = 642 \text{ rad/sec}$$

or

$$f_{3db} = \frac{642}{2\pi} = 102 \text{ cps} \qquad (2\text{-}14)$$

The noise bandwidth of the filter is 2 $(\frac{\pi}{2})$ times this amount, or

$$2\,B_{LP} = 2\,(\tfrac{\pi}{2})\;102 = 320 \text{ cps} \qquad (2\text{-}15)$$

The tone signal-to-noise ratio in the Syncom I system is about 30 db referred to a 300 cps noise bandwidth. Therefore the signal-to-noise ratio at the output of the tone detector filter will be about 29.7 db.

The bit error probability for a frequency shift keying system similar to the one considered here is given by:

$$P_e = \frac{1}{2}\, e^{-E/2N_o} \qquad (2\text{-}16)$$

where

$P_e$ = bit error probability

$E$ = average signal energy per bit

$N_o$ = noise power density

*A. B. Glenn, "Comparison of PSK vs. FSK Binary Coded Transmission Systems," IRE Trans. on Comm. Sys., June 1960, p. 92.

The ratios $E/2N_o$ may be converted to signal-to-noise ratio by the following manipulation:

$$\frac{E}{2N_o} = \frac{E}{2N_o}\frac{B_{LP}}{B_{LP}}\frac{\tau}{\tau} = \frac{\frac{E}{\tau}}{2B_{LP}N_o}(B_{LP}\tau) \qquad (2\text{-}17)$$

or

$$\frac{E}{2N_o} = \frac{S}{N}(B_{LP}\tau) \qquad (2\text{-}18)$$

Therefore,

$$\frac{E}{2N_o} = \frac{S}{N}\left(\frac{160}{128}\right) = \frac{S}{N}(1.25) \qquad (2\text{-}19)$$

For the system under consideration each word consists of about 14 bits. Therefore an error rate of $10^{-3}$ would be expected to result in an error about every 70 words. Assuming that this is a reasonable error rate,

$$P_e = \frac{1}{1000} = \frac{1}{2e^{E/2N_o}}$$

or

$$e^{E/2N_o} = 500$$

Therefore

$$\frac{E}{2N_o} = 6.22$$

or

$$\frac{S}{N} = \left(\frac{1}{1.25}\right)\frac{E}{2N_o} = 4.97 \rightarrow 7 \text{ db} \qquad (2\text{-}20)$$

Since the actual signal-to-noise ratio is 29.7 db, the system safety margin for the assumed bit error rate is about 22.7 db. The second question proposed at the beginning of this analysis is answered by Equation 2-20.

Consider now the bandpass filter characteristics of the filters preceding the zero and one tone detectors. The 3-db bandwidths of these filters should be over twice the 3-db bandwidths of the low-pass filters so that the low-pass filter dominates in determining the rise time. This would require the bandpass filters to exceed 300 cps in bandwidth. This, however, conflicts with the close separation of only 600 cps specified between the center frequencies of the two filters. It therefore appears desirable to increase the separation between the filters to, say, 1200 cps. The frequency separation between the zero and one tones in the frequency shift keying signal must be increased accordingly.

# 3. LAUNCH AND ORBIT ANALYSIS

## PRELIMINARY ORBITAL ANALYSIS

### Detailed Behavior Due to Perturbations of Sun and Moon

A study has been initiated to determine the perturbations of the satellite's behavior caused by gravitational attraction of the sun and the moon. Dependence of this behavior on the satellite longitude will also be investigated.

The method used is to linearize the equations of motion obtained in the presence of a small perturbation:

$$\ddot{r} - rw^2 + \frac{k^2}{r^2} = a_r$$

$$\frac{d}{dt}(r^2 w) = ra_\theta$$

$$\ddot{z} = -\frac{k^2}{r^3} z + a_z$$

where $a_r$, $a_\theta$, and $a_z$ are the radial, tangential, and normal components of the perturbing acceleration. The resultant linearized equations are then solved by the method of variation of constants to obtain explicit formulas for $\delta r(t)$, $\delta\lambda(t)$, and $z(t)$, the radial, tangential, and normal deviations from the synchronous equatorial orbit (in terms of the acceleration components).

From the equation of motion of the satellite relative to the earth, in the presence of the gravitational attraction of the sun and the moon, the perturbing acceleration is determined. The necessary acceleration components are then expressed in terms of series involving Legendre polynomials and associated Legendre functions. These expressions show explicitly the dependence of the initial longitude on the acceleration components. The expressions are then analyzed to determine significant terms and substituted into the formula for $\delta r(t)$, $\delta\lambda(t)$ and $z(t)$.

A computer program will then be obtained and used in conjunction with a Jet Propulsion Laboratory ephemeris tape to indicate the detailed perturbed behavior of the satellite. The perturbed position of the satellite at 6-hour intervals over a 5-year period at various initial longitudes will be obtained and analyzed. The program can also be used to determine the effect of gravitation attractions other than the sun and the moon on the satellite.

# 4. SPACECRAFT SYSTEMS DESIGN

## GENERAL STATUS REPORT

The engineering model transponder effort is proceeding, and most units are now in some phase of the fabrication cycle. Communications test equipment required to evaluate the transponders is being designed and will be available when transponder fabrication is complete. The stripline version of the phased array feed system is almost entirely fabricated, and assembly will start shortly. The breadboard version of the PACE circuitry is now undergoing electrical checkout, and only minor problems have been encountered.

Telemetry and command formats have been defined, and circuit design is continuing. Details of structural design are being established. Location and content of electronic quadrants and other electronic packages is being decided, and the required interconnections are being generated.

Definition of spacecraft subsystems requirements is continuing. Detailed reports on progress of all subsystems are given in the following sections.

## SPACECRAFT BLOCK DIAGRAM

The revised Advanced Syncom system block diagram is shown in Figure 4-1. Major revisions include the command decoder, telemetry encoder, and telemetry format. Tentative flight plug connections and test access points are also shown.

## COMMUNICATION TRANSPONDERS

### Components of the Multiple Access Transponder

Preamplifier (130). One unit has been fabricated and adjusted. Bandwidth, gain, and noise figures were satisfactory.

Filter Amplifier (141). Two laboratory models were built for use in the ground test equipment. One engineering model is being fabricated.

Phase Modulator (131).

Doubler Amplifier (132).

Master Oscillator Amplifier (123). The circuits for these units have been released, and fabrication has been initiated.

Master Oscillator (122). Circuit design has been released and fabrication initiated. Temperature tests on the steel block, which will contain the oscillator, are being conducted in a vacuum to determine the thermal inertia of the block.

Frequency Components Common to Frequency Translation Transponder

Preamplifier (110).

Intermediate Amplifier (104).

Post Amplifier (111). All amplifier units are being fabricated. Preliminary temperature tests on the breadboard units indicated no major problem areas.

Master Oscillator (113). Circuit design has been released, and fabrication is under way.

Limiter Amplifier (109). Laboratory model is operating satisfactorily except for the output circuit which will be finalized after checkout with the high-level mixer.

High-Level Mixer (112). Performance of the unit using RF and IF signal generators appeared satisfactory. Measurements of IF impedance are being made to aid tie-in with the limiter amplifier.

Components Common to the Multiple Access and Frequency Transponders

X32 Multipliers (114). These units are being fabricated.

Input Mixer (100). Initial performance was satisfactory, meeting all of the tentative RF specifications. The noise figure, measured with a 3.6 db noise figure RF amplifier, was 9 db. These units are shown in Figures 4-2 and 4-3. Two OSM connectors are used for the RF connections and an OSSM connector is used for IF. An improved choke on the IF lead resulted in less RF to IF leakage than was present in previous units.

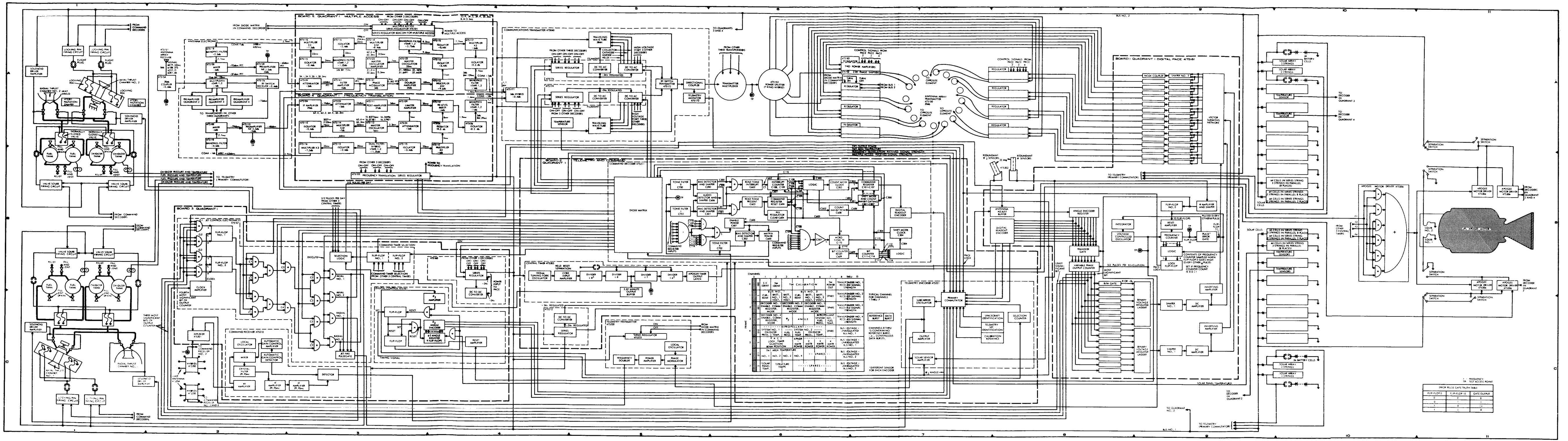

Figure 4-1. Spacecraft Block Diagram

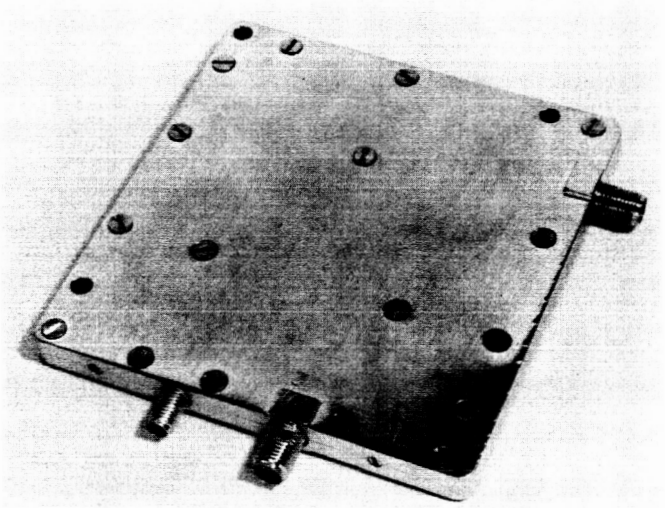

Figure 4-2. Assembled Input Mixer

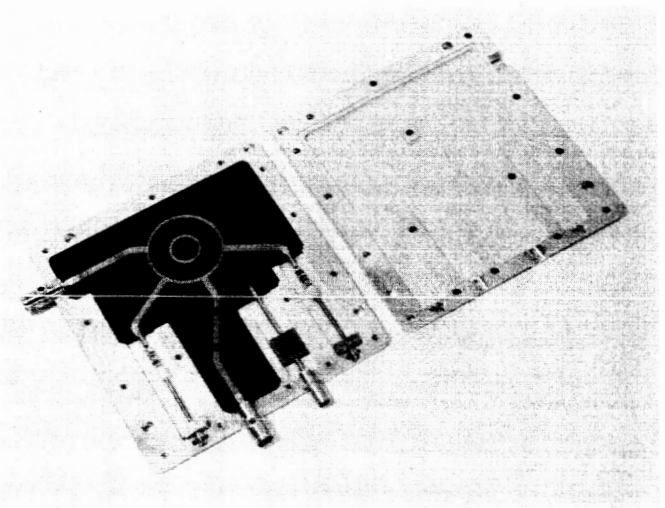

Figure 4-3. Input Mixer Disassembled to Show Stripline Circuits

Receiver 20 db Coupler (103)

Transmitter 20 db Coupler (172). Photographs of these units are shown in Figures 4-4 and 4-5. The detector mount is on order, while all OSM loads are on hand. RF performance of both units is satisfactory.

Local Oscillator Bandpass Filter (118). This component is pictured in Figure 4-6. The sides have been squared off to reduce weight, and OSM connectors are used. A total of 14 units have been fabricated and assembled, including four transponder units and spares and six test equipment units.

Bandpass Filters. Delivery of all of these filters is expected 15 August 1963.

Multiplexer. Cavity design is proceeding. The waveguide configuration will be determined after the mechanical structure layout in the spacecraft is finalized.

Regulators (101, 102, 174). Breadboard layouts of these units are being assembled. Testing should begin early in the next report period.

Breadboard System. A bench setup using all of the breadboard units for the new block diagram is being assembled.

Special Equipment

Divide-by-32 Unit. The X32 multiplier has been adjusted to operate satisfactorily as a divide-by-32 unit. The test setup is shown in Figures 4-7 and 4-8. The first figure shows an input being provided to the divider. An oscillator and phase modulator drive a normal X32 multiplier. The spectrum at 1800 mc, shown on the analyzer, indicates a high index of modulation. This signal was fed to the divider (Figure 4-8). The resulting compressed spectrum at 60 mc is shown on the analyzer. Further quantitative measurements will be made by comparing the output of the divider with the input to the X32 multiplier to determine linearity and frequency response.

## TRAVELING-WAVE TUBE POWER AMPLIFIER

### Traveling-Wave Tube Status

Final design tubes have been tested, and the design appears to be optimum for the electrical performance requirements; consequently, the production run of the tubes has been initiated.

In the previous report, the importance of helix structure tolerances was discussed in relation to tube reproducibility. Three tubes furnish an

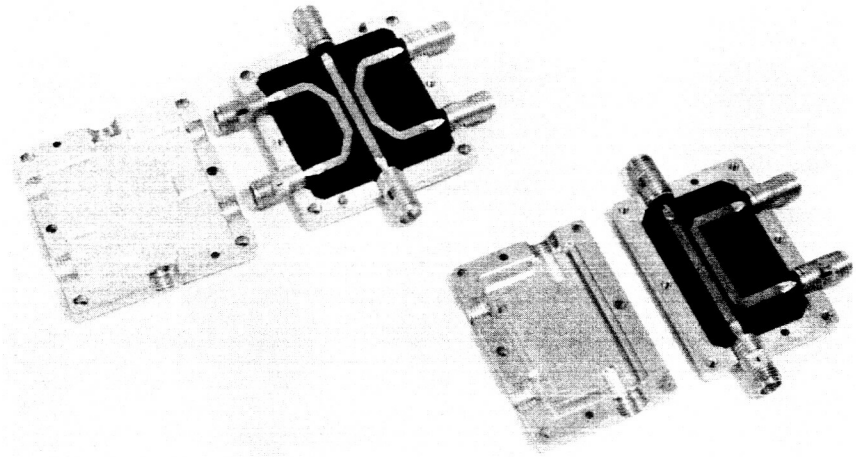

Figure 4-4. Receiver and Transmitter 20 AB Couples Showing Stripline Circuits

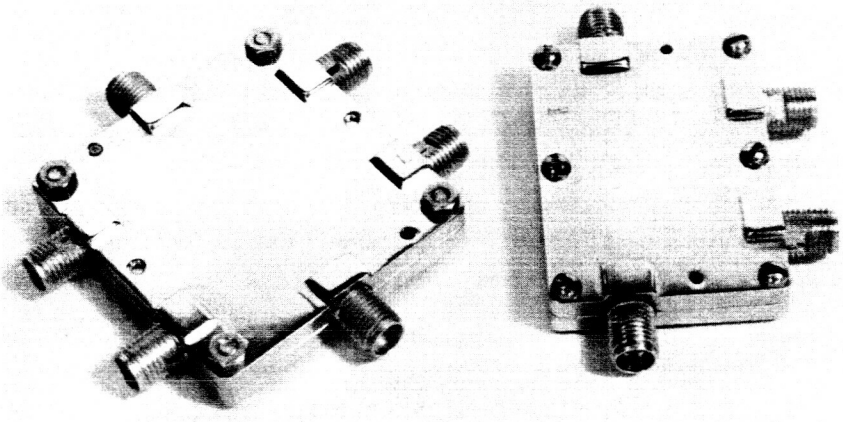

Figure 4-5. Receiver and Transmitter 20 DB Couples Complete units

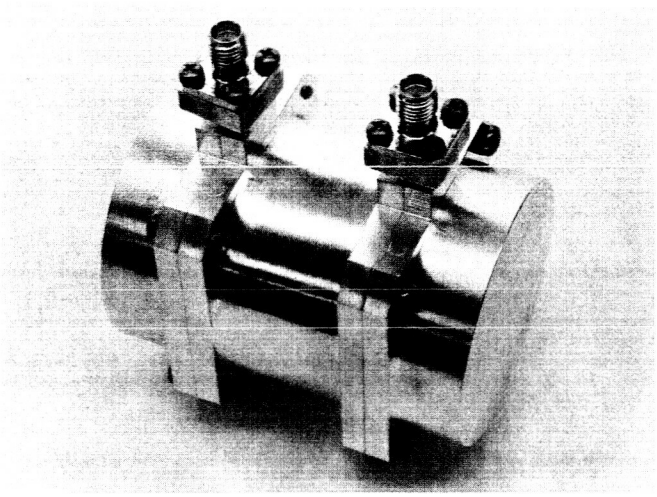

Figure 4-6. Local Oscillator Bandpass Filter

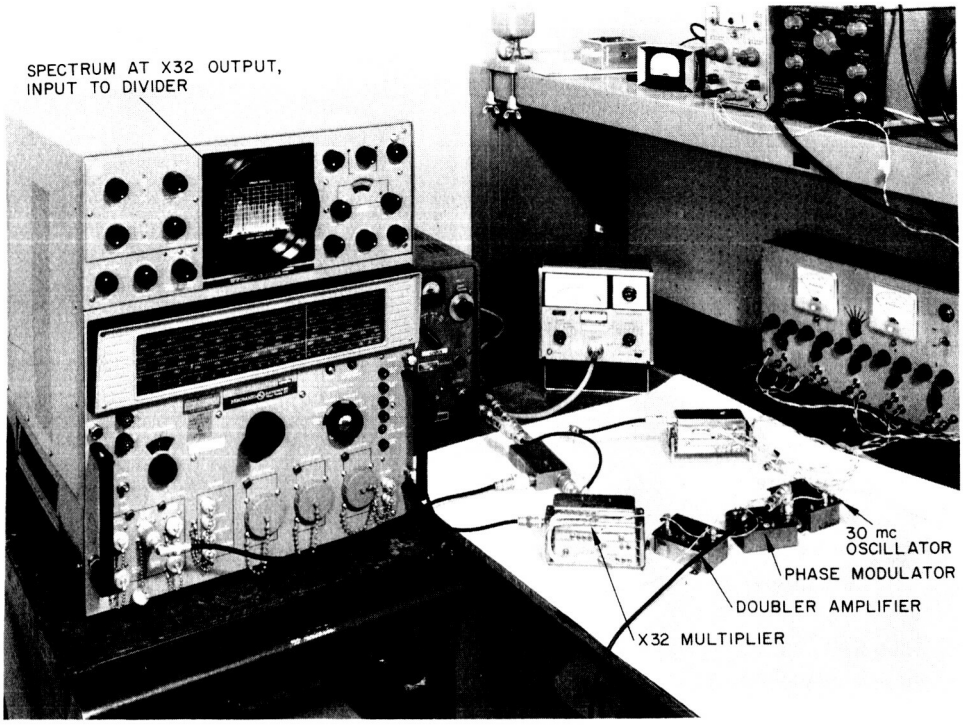


Figure 4-7. Setup for Testing Divide-by-32 Unit 6

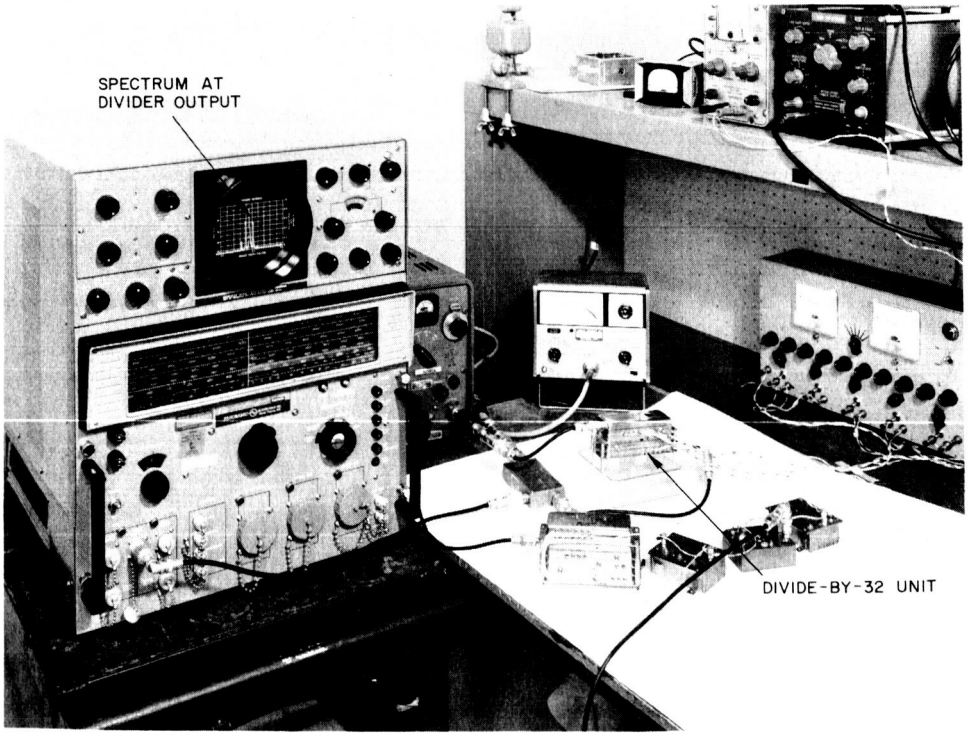


Figure 4-8. Divide-by-32 Unit Under Test

example of the success of these controls. These tubes have met all electrical specifications and are awaiting packaging. Their operation parameters are:

| Tube | $V_a$ | $V_H$ | $V_c$ | $I_a$ | $I_H$ | $I_c$ | $I_T$ |
|---|---|---|---|---|---|---|---|
| 35 | 190 | 1280 | -700 | 0.14 | 1.6 | 18.2 | 19.9 |
| 39 | 180 | 1280 | -700 | 0.04 | 1.15 | 19.0 | 19.2 |
| 40 | 240 | 1275 | -725 | 0.11 | 1.35 | 18.1 | 19.5 |

The variance of the anode voltage can be attributed to electron gun tolerances. Methods of controlling these tolerances are presently being studied.

The production status of tubes at the end of this report period is as follows:

| Stage | Description | Tubes |
|---|---|---|
| I | Clean room assembly | 2 |
| II | Bake-out process | 2 |
| III | Magnet assembly | 1 |
| IV | Focusing and RF testing | 1 |
| V | Packaging | 3 |
| VI | RF testing after packaging | 0 |

A severe problem in production has occurred in the packaging stage. The approved RF connectors that had been on order for 6 weeks were received on 30 July; however, the contact pin in the connectors was not the type specified. Consequently, these contact pins were returned to the vendor. The vendor has promised an immediate partial shipment of the proper contact pins by 15 August. Tubes can not be packaged before the RF connectors are installed.

## Life Improvement Program

Thirty standard 384H cathodes are being subjected to a complete composition analysis. These cathodes were selected at three stages of processing: after cleaning and washing, after wet hydrogen firing, and after

oxidation and reduction in dry hydrogen. The specific elements of interest are sulphur, carbon, zirconium, copper, silicon, tungsten, iron, and manganese. They will also be investigated for gas content.

A similar test will be conducted for cathodes of one-hald and one-quarter thickness to ensure that the machining and assembly process of test vehicle (diode) cathodes does not differ from that for standard cathodes. Assembly of the test diodes was delayed by a vendor problem. The vendor shipped 20 mil diameter thermocouple wire instead of the 2 mil diameter wire.

The diode aging rack should be complete by 1 September.

## PHASED ARRAY TRANSMITTING ANTENNAS

### Advanced Engineering Model Status

During the report period fabrication of the parts for the stripline phase shifter has continued. All needed holes have been drilled in the ground planes, and the planes are being plated. Holes are being punched in the circuit boards. The two ground planes for the power divider are shown, before plating, in Figure 4-9. Figure 4-10 shows the partially punched top circuit board. The waveguide probes are in place in the bottom hole, and the matching "horseshoe" pieces fit at a vertical transition. Most of the miscellaneous hardware associated with the stripline is completed, and assembly should begin during the next period.

New field coils for the phase shifters have been ordered to match the new power amplifier circuits. They will have half the number of turns with twice the wire diameter, thus operating at twice the current and half the voltage. This makes possible a more efficient circuit design.

### Preliminary Environmental Tests

A series of temperature tests was made on the phase shift properties of some of the breadboard phase shifters. The test setup is diagramed in Figure 4-11. A 12-position switch was used to generate the two-phase voltages of the form sin $\theta$ and cos $\theta$, where $\theta$ varied from 0 to 360 degrees in 30-degree steps. A slotted line was used to measure phase, while isolators were employed to maintain a constant load on the phase shifter. The field winding was adjusted so that outputs 1 and 2 were in phase when $\theta = 0$ degrees. The input angle was then varied and the output phase, $\theta_o$, was measured. The difference between $\theta_o$ and a linear output was calculated and the results plotted in Figure 4-12. Five phase shifters were tested at 0°C, 25°C, and 50°C at 4170 mc. The phase difference (with arbitrary zero position) was plotted vertically against input angle. A number of factors were apparent from these curves. All of the phase shifters varied about the same with temperature, increasing in length about 80 degrees when the

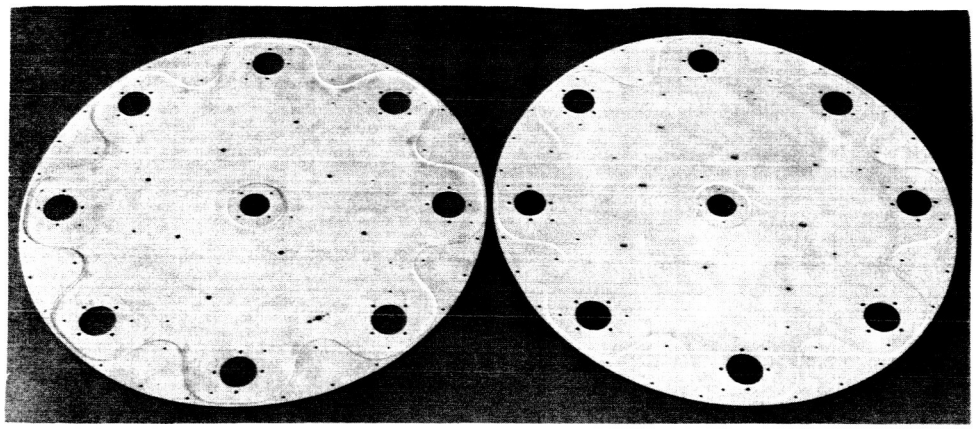

Figure 4-9. Phased Array System Ground Planer for Power Splitter

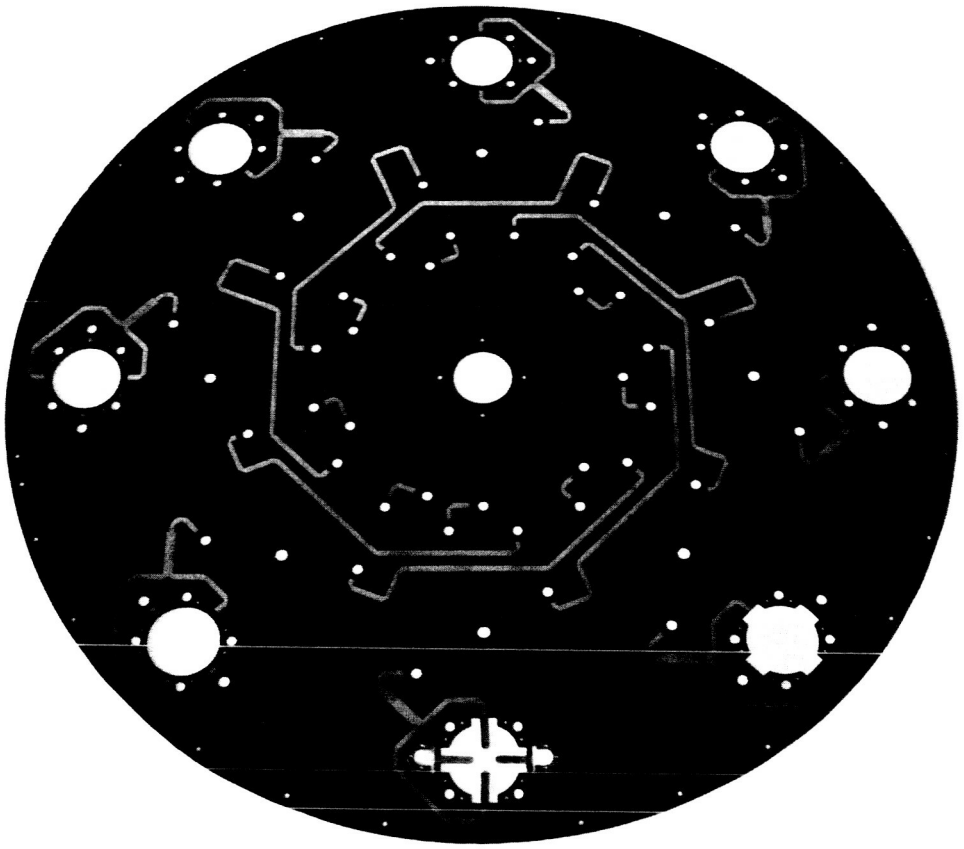

Figure 4-10. Phased Array System Top Stripline Circuit Board

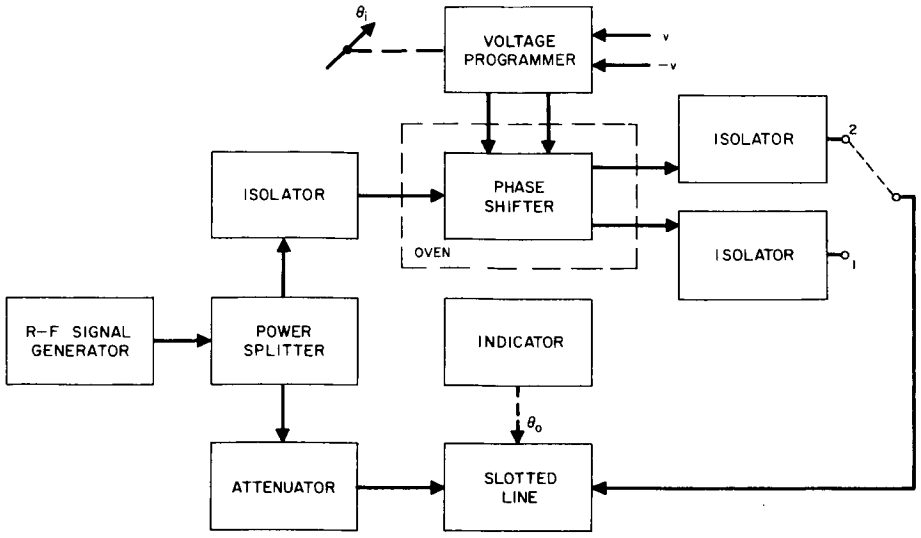


Figure 4-11. Test Setup for Measuring Phase Shift Versus Temperature

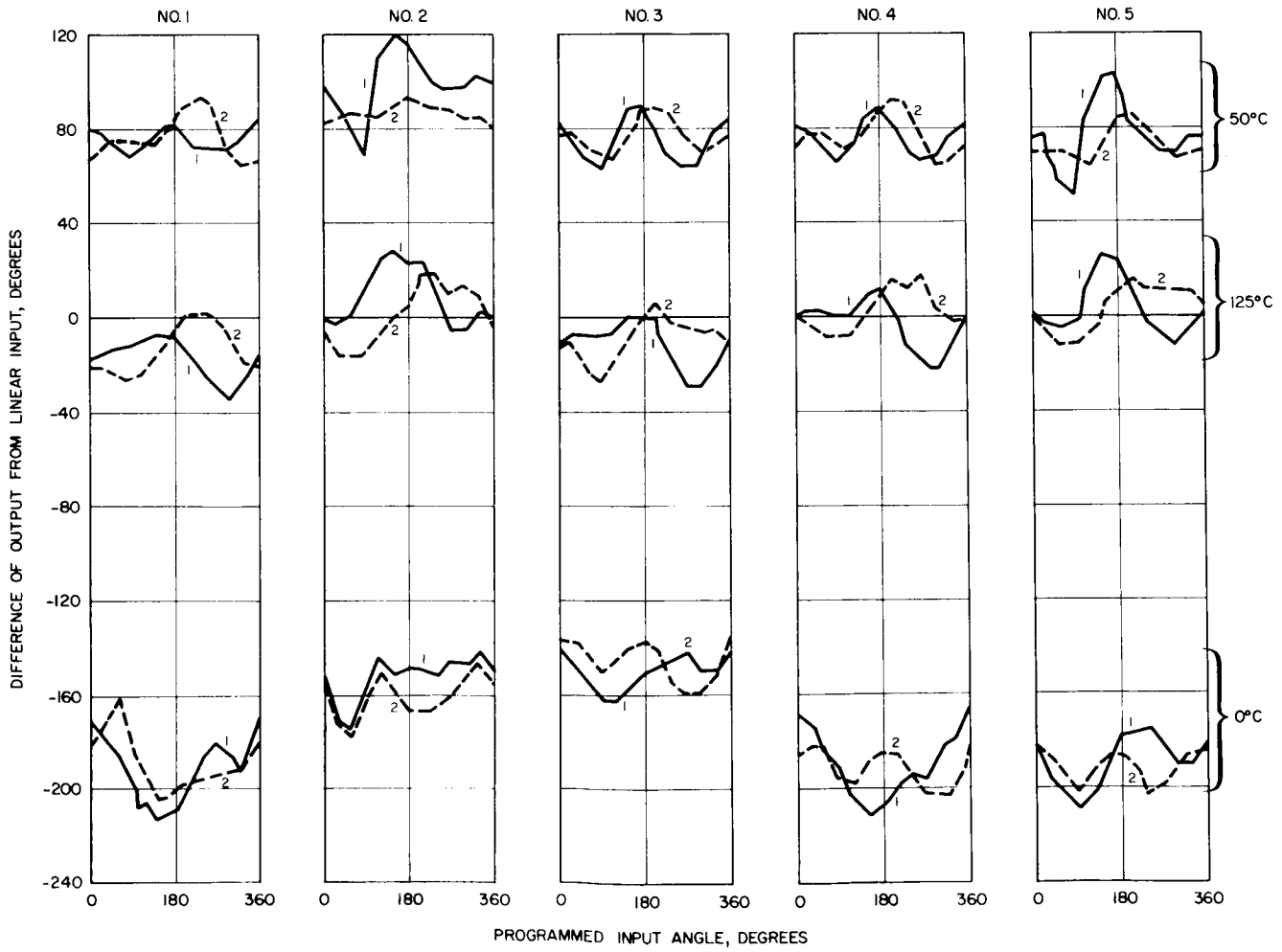


Figure 4-12. Phase Shifter Performance Versus Temperature

temperature was raised from 25°C (room temperature) to 50°C and decreasing about 180 degrees when the temperature was lowered to 0°C. There was a variation in the deviation of output from the desired linear relationship amounting to about 10 degrees rms. The reason for this is not known but could be caused by nonsymmetry of field windings, errors in control voltage, error in the measuring procedure, residual magnetization in the ferrites, or misadjustment of the output couplers. It was also observed, but not recorded, that the amplitude of the phase shifters also fluctuated as the input voltages were varied. It is expected that some of the problems will be alleviated when the stripline circuit is assembled. The general method of measurement appears to be satisfactory.

## PHASED ARRAY CONTROL ELECTRONICS (PACE)

### Status of PACE Circuits

The power amplifiers have been redesigned for the new phase shifters and power supply configuration. Final releases have been completed for all circuits.

The frequency lock-loop block diagram is given in Figure 4-13. The primary function of the loop is to generate pulses at a frequency $2^9 f_s$, where $f_s$ is the spin frequency of the spacecraft. The input reference is one pulse per revolution, normally derived from a sun sensor, but also derived from the command decoder during eclipses. Another output of the loop is $2^{12} f_s$, which is used for on-board measurement of the solar aspect angle.

The input reference pulse triggers F100, causing it to change state with each pulse. When F100 goes from one to zero, the reset amplifier is triggered, which resets the voltage-controlled oscillator and flip-flops F101 through F113 to zero. Flip-flops F101-F112 constitute a binary counter. At the end of the $2^{12}$ voltage-controlled oscillator cycle after reset, F113 is set to one. If the voltage-controlled oscillator frequency is exactly $2^{12} f_s$, F100 will also be set to one at the same time, and there will be zero error. In general there will be some timing error between F100 going to one and F113 going to one, generating an output from the error pulse gate. The logic of the error pulse gate is illustrated in Table 4-1.

TABLE 4-1. ERROR PULSE GATE TRUTH TABLE

| F100 | F113 | V Out |
|---|---|---|
| 0 | 0 | Decoupled |
| 0 | 1 | -V |
| 1 | 0 | +V |
| 1 | 1 | Decoupled |

When F100 and F113 are in the same state, the output of the error pulse gate is decoupled, through very low leakage diodes, from the filter. When F100 and F113 are different, the output of the error pulse gate is either -V or +V, depending on which of the two possible combinations occurs. Figure 4-14 shows the error pulse gate waveforms for both positive and negative errors.

The filter F701A has the configuration shown in Figure 4-15. The filter integrates the error pulses and provides loop compensation.

The amplifier F701B serves to unload the filter and drive the voltage-controlled oscillator. The schematic of amplifier F701B is shown in Figure 4-16. The large input impedance of the field effect transistor is utilized to unload the filter. The amplifier F701B is essentially a source follower circuit. Transistors Q1 and Q2 and zener diode CR1 maintain a constant source-to-drain voltage which minimizes the gate current. Zener diode CR2 shifts the output level as required by the voltage-controlled oscillator circuit. The lock logic detects when the loop is in lock; the "lock" output is telemetered and used to enable the on-board mode of the jet control electronics.

The transient response is illustrated in Figure 4-17, which shows a plot of the width of the error pulse versus time for spin speeds of 50, 100, and 150 rpm. This response was obtained from a digital computer simulation of the frequency lock loop. The steady-state error is a function of the current load on the filter. For zero load, the width of the error pulse continues to decrease exponentially; for a finite, non-zero load, the error pulse width levels off to a constant value. At the present state of development, for nominal spin speed of 100 rpm, the steady-state error pulse width is less than 100 microseconds.

## Status of Jet Control Electronics (JCE) and Solenoid Driver Circuitry

### Jet Control Electronics

Design changes are being made to reduce the number of commands from sixteen to seven. Other minor design changes are being made because of a change in the command decoder output voltage levels.

### Solenoid Driver

The command decoder voltage level change makes possible a change to the input to the solenoid driver. This change saves approximately twelve components (20 percent) per driver and relaxes the tolerance on the input voltage levels. Four models of this driver will be fabricated and delivered to Controls Department for further testing with the Marquardt valves.

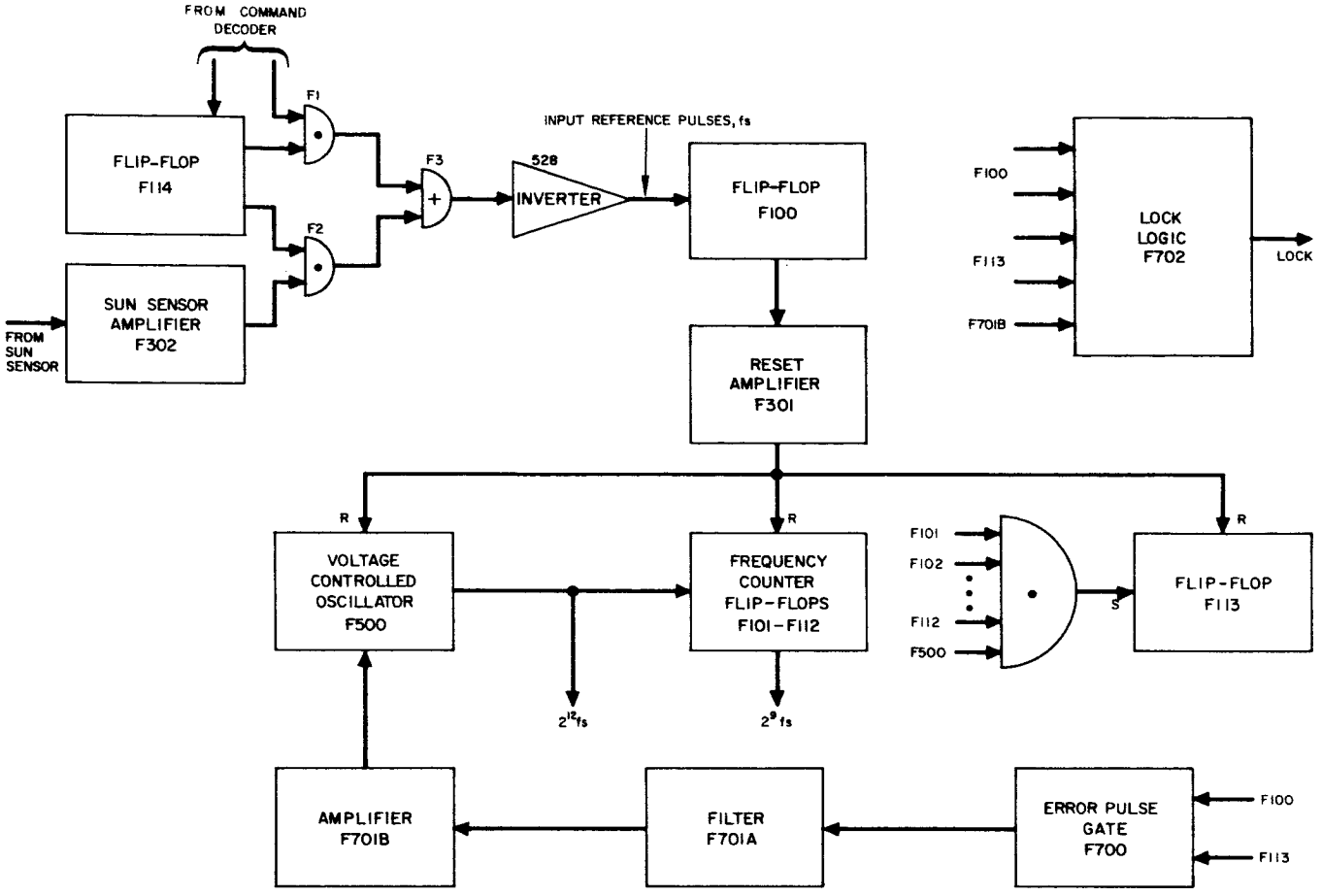


Figure 4-13. Frequency Lock-Loop Diagram

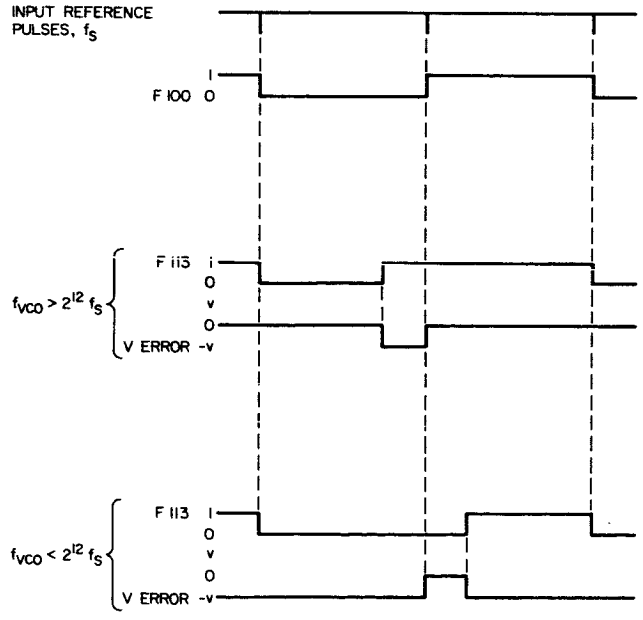


Figure 4-14. Error Pulse Gate Waveforms

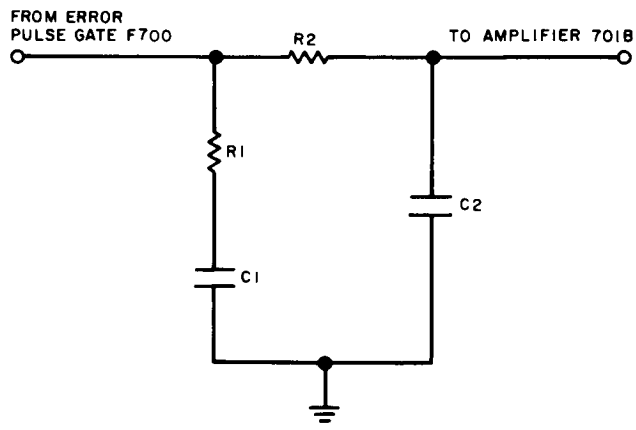


Figure 4-15. Filter F701 A Block Diagram

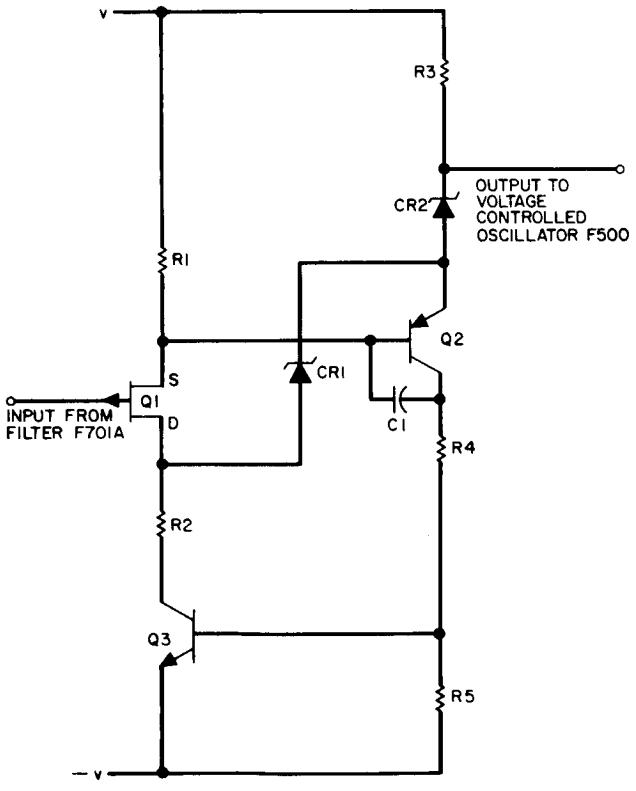


Figure 4-16. Amplifier F701 B Block Diagram

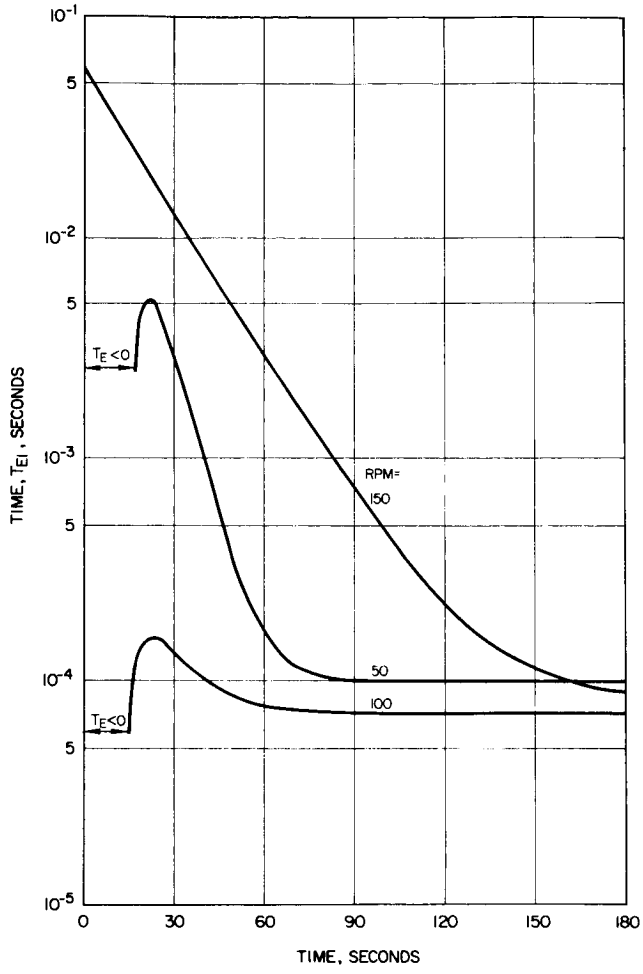


Figure 4-17. Frequency Lock-Loop Transient Response

## Advanced Engineering Model of PACE and JCE

The flat circuit card and chassis fabrication was completed during July. The flat cards for the PACE and JCE subsystems have all been tested, and corrections have been made when necessary with the exception of the solenoid amplifiers. Modifications of the latter will be made to reflect JCE circuit changes.

The chassis has been wire checked. Conversion of the demonstration panel into a unit tester has been completed and this is now being used in the checkout of the engineering model. The frequency lock loop and the output counter portions of the PACE are now functioning correctly.

Figure 4-18 shows the PACE/JCE advanced engineering model. Figure 4-19 shows the advanced engineering model undergoing checkout. Figures 4-20 and 4-21 show power amplifier output waveforms generated by the advanced engineering model.

## Design of the Advanced Development Model of PACE

The welded module version of the basic PACE is now being referred to as the advanced development model of the PACE. Thirty percent of the module assembly drawings were prereleased to fabrication during the reporting period. Layouts of the beam positioner and waveform generator etched circuit boards were completed. The printed wiring on the waveform generator is 100 percent redundant and that on the beam positioner is 100 percent redundant with four jumper wires.

A preliminary unit design was completed and sent to stress analysis along with the results of the environmental testing of a sample function block. The stress analysis confirmed that with minor modifications the design was adequate. Final unit sheet metal design is proceeding.

## Fabrication of the Advanced Development PACE

All component purchase requisitions were written and placed with purchasing and all available 5 percent resistors were obtained.

Fabrication of component holders for seven module types started late in July. Module header plates are being made for evaluation.

# CENTRAL TIMING ELECTRONICS

A preliminary design review of the central timer was held during the report period. The configurations of most of the circuits are firm, and final designs are in progress. Tests to determine the long-term stability of intermediate counts within a core are continuing. To date, no failures have been observed.

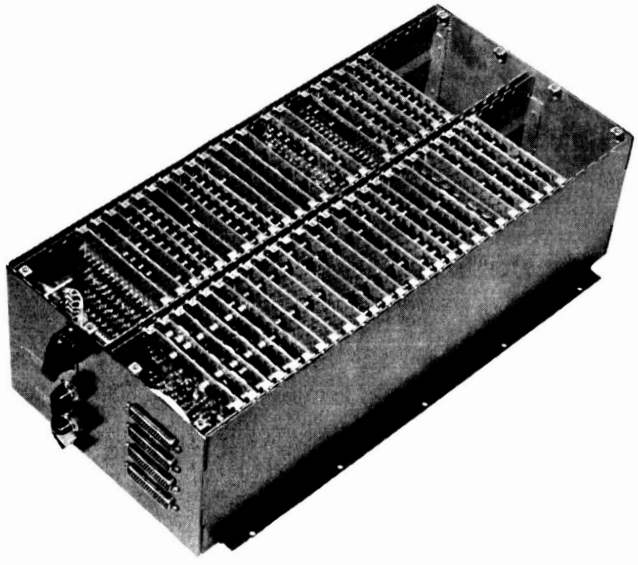

Figure 4-18. PACE/JCE Advanced Engineering Model

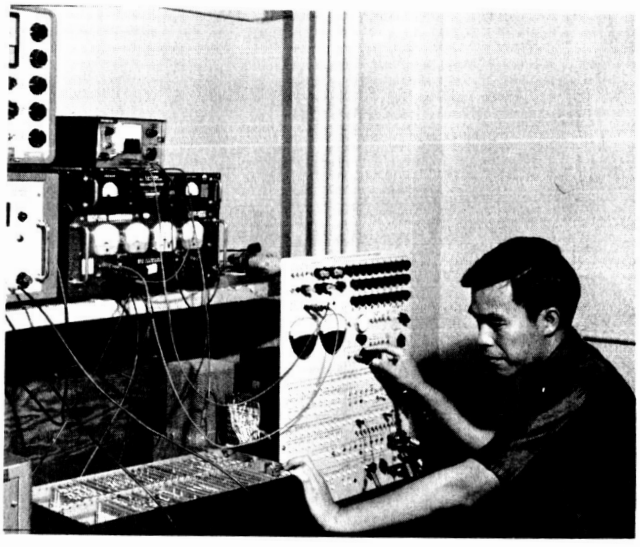

Figure 4-19. PACE/JCE Advanced Engineering Model Undergoing Checkout

Figure 4-20. Sine Wave Output of Power Output Generated by the PACE/JCE Advanced Engineering Model

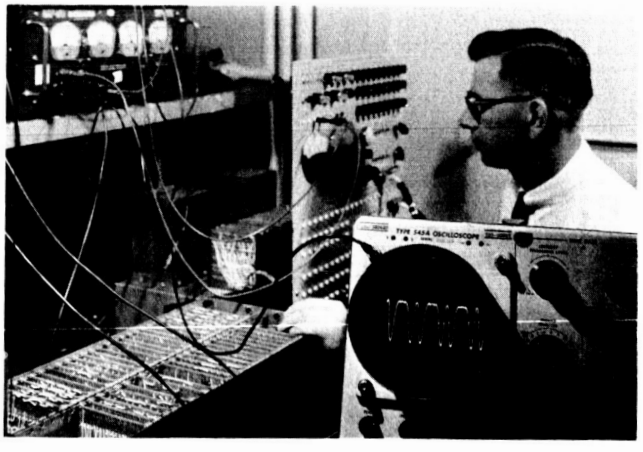

Figure 4-21. Cosine Wave Output Power Output Generated by the PACE/JCE Advanced Engineering Model

## Central Timer

### Advanced Engineering Model Status

Fabrication of the central timer engineering model is complete, and checkout of the unit has begun. Figure 4-22 shows a circuit card containing three "count-of-8" stages. Figure 4-23 shows this card undergoing checkout. Figure 4-24 shows the chassis for the timer advanced engineering model.

### Specifications

The central timer will provide a fire signal to the apogee motor driver 315 minutes $^{+0}_{-21}$ seconds after separation. This then requires that all cores beyond the fifth "count-of-8" stage be held reset until separation. To allow checkout of the timer on the gantry, a flight plug will be connected in series with the reset windings. This plug, when pulled, will remove reset current and allow normal operation of the timer.

In addition to the 2.81-minute output and the apogee motor output, the central timer will provide the commutating clock frequency for the telemetry encoder. The output waveform will be a chain of 10-second pulses at a 194 cps repetition rate. Figure 4-25 is a block diagram of the central timer.

## Apogee Motor Firing

Design of an all-electronic apogee motor driver is in progress. Such a driver will not require the use of either pyrotechnic switches or silicon-controlled rectifiers. Instead, a transistorized one-shot (monostable multivibrator) will provide the required duration of pulse current to fire the apogee motor squib.

## COLLINEAR ARRAY (CLOVERLEAF) RECEIVING ANTENNA (Figure 4-26)

Additional tests have been made on the 6165 mc cloverleaf array. These tests were made while the array was enclosed in a fiberglass sleeve having a wall thickness of .015 inches. The purpose of the sleeve is to add rigidity to the antenna and to support the antenna in its proper operating position. The test results of the cloverleaf array without the sleeve were presented last month. The addition of the sleeve caused appreciable change in beam width and sidelobe level. However, there was an appreciable change in other characteristics of the antenna, i.e., omnidirectionality, beam tilt, voltage standing wave ratio, and gain. These characteristics are shown in Figure 4-27. Maximum gain does not occur at the center frequency; therefore, a matching device will be designed to achieve this result. The beam tilts toward the connector a few degrees. Additional tests will be performed to determine the cause of this, and the necessary steps will be taken to minimize this unwanted characteristic.

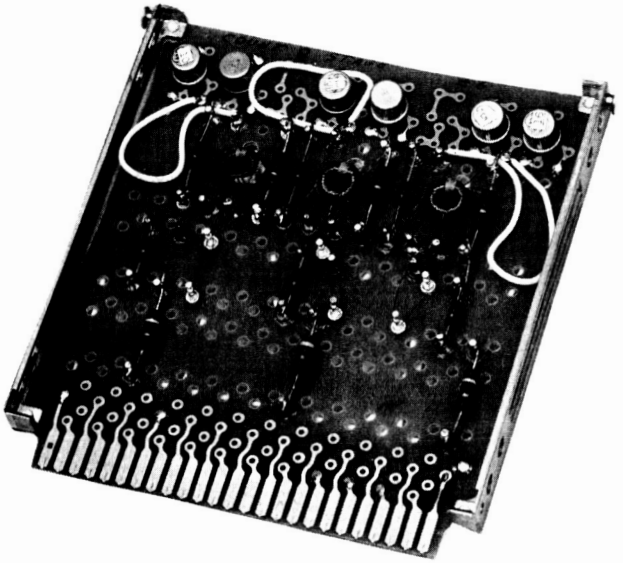

Figure 4-22. Circuit Card Containing Three "Count-of-8" Stages

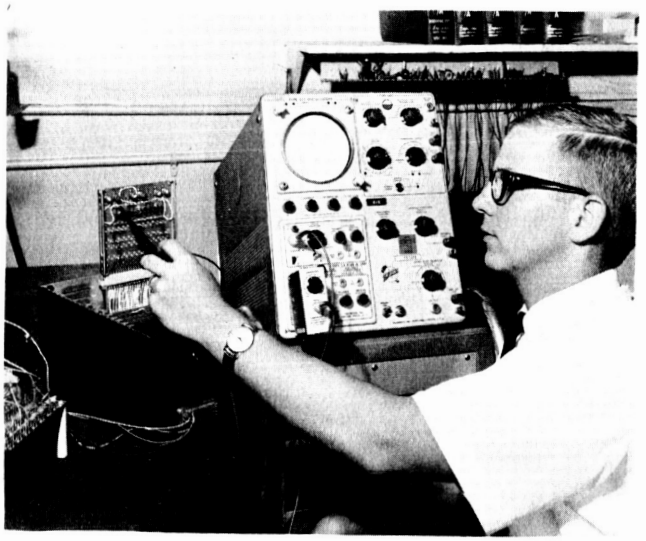

Figure 4-23. Circuit Card Containing Three "Count-of-8" Stages Undergoing Checkout

Figure 4-24. Central Timer Advanced Engineering Model Chassis

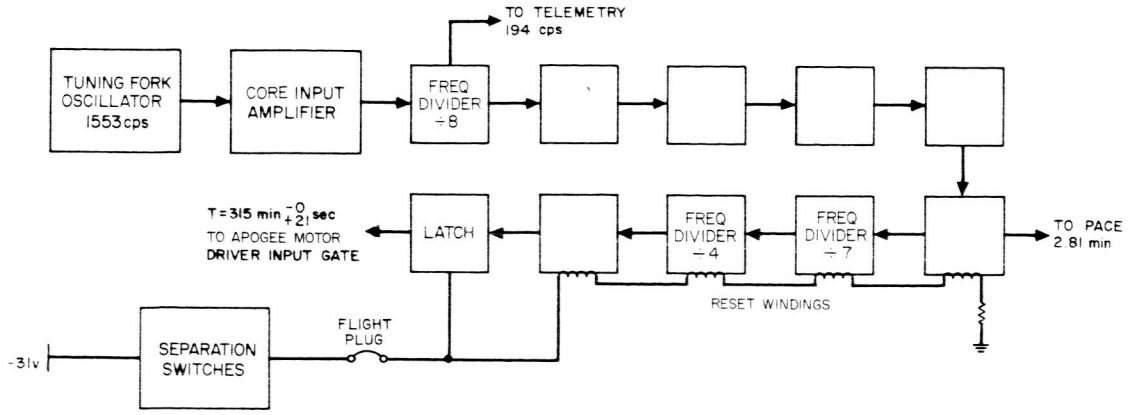


Figure 4-25. Central Timer Block Diagram

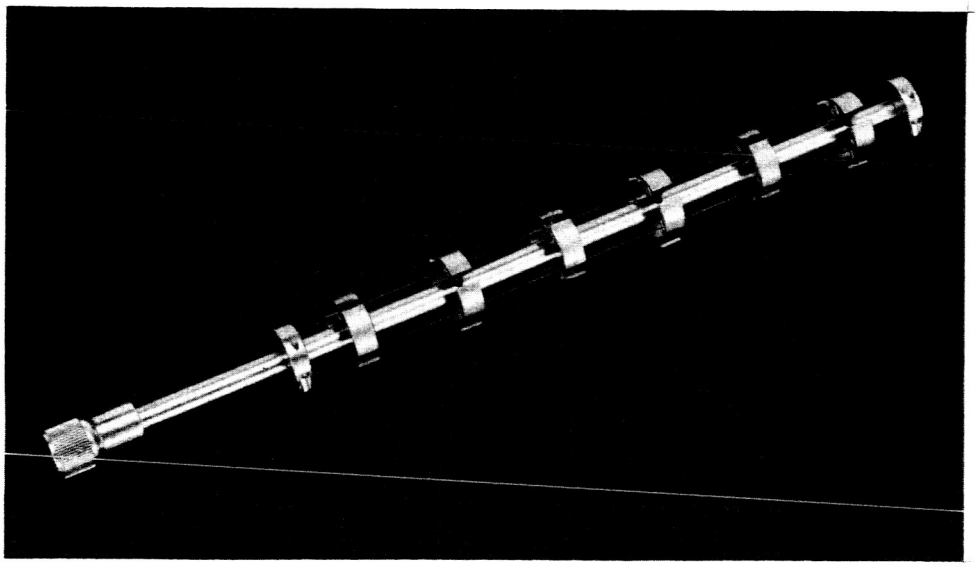

Figure 4-26. Collinear Array (Cloverleaf) Receiving Antenna

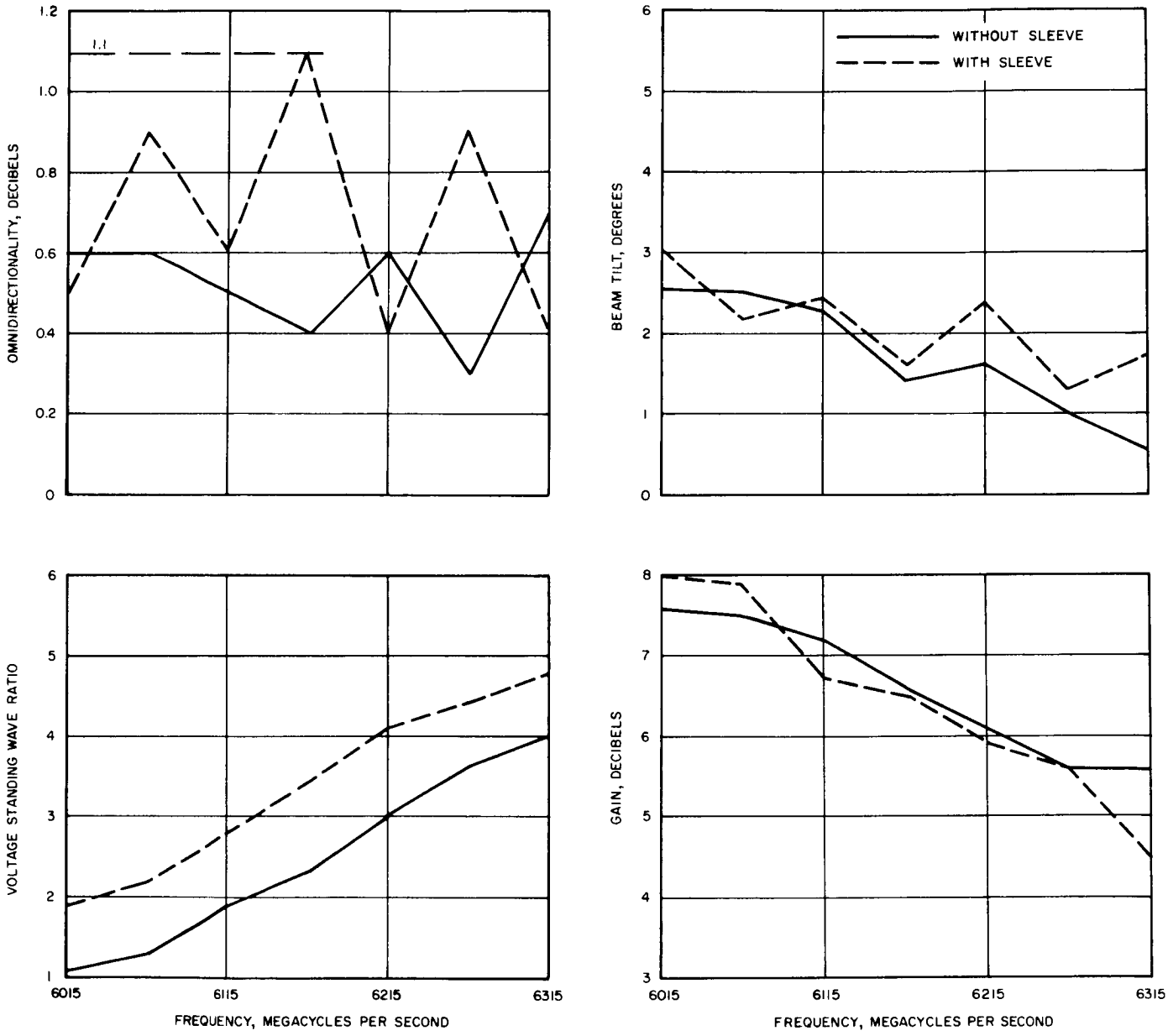


Figure 4-27. Antenna Characteristics

## VELOCITY AND ORIENTATION CONTROL

### Bipropellant Rocket Reaction Control System Development Status

The Marquardt Corporation completed Phase 1 of the Advanced Syncom Reaction Control System Development Program on 15 July 1963. Five significant test events were performed during the final two weeks of this phase.

1) Radial and axial engine acceptance tests

2) Leakage checks and calibration of the engineering model Reaction Control System exclusive of engines

3) Hot-firing spin demonstration of the engineering model at altitude conditions

4) Vibration and burst tests of an engineering model-design propellant tank

5) Steady-state engine durability demonstration.

Acceptance tests of the radial and axial engineering model engines were conducted in both the one-sixth and one-third pulse mode duty cycles. The engines demonstrated a specific impulse of 262 seconds (5-pound thrust level) for the one-sixth duty cycle and 285 seconds (5-pound thrust level) for the one-third duty cycle. Measurements of pulse centroid indicated variations from pulse to pulse of less than the maximum ±5 milliseconds allowed by Hughes Aircraft Company Specification X254044. The acceptance tests were conducted with an oxidizer-fuel ratio of 1.8 (designed value is 1.62). The difference is attributed to calibrating with water. Reworking of the calibrating orifices was deleted by Marquardt because of program time limitations. Hughes has required that the acceptance test be conducted at the proper mixture ratio.

Leakage of the propellant tanks noted in the previous monthly progress report was resolved by gold plating in the vicinity of the leaks. Subsequent leakage checks and calibration of the installed reaction control system were satisfactory.

A hot-firing spin demonstration of the engineering model witnessed by NASA and Hughes was conducted in the Marquardt test facility (Cell 9). Both engines accumulated a total burn time of 2.5 minutes during the demonstration. The program included actuation of the pyrotechnic propellant prevalves and swivel mechanism pin-pullers. With the exception of two discrepancies, the system satisfactorily demonstrated design performance. The axial engine chamber pressure transducer (not a flight component) failed to function as calibrated, and one pin-puller, after firing, interfered

with the gimballing action of the swivel mechanism. Improper installation of the pin-puller was later found to be the cause of interference.

An engineering model design propellant tank was vibrated along three orthogonal axes and subsequently burst. During the vibration test, the tank was half-filled with a test fluid and pressurized to 325 psia, simulating prelaunch conditions. No significant vibratory stress levels were noted, and the hydrostatic burst test resulted in tank rupture at 1190 psia (design value is 940 psia). The rupture did not coincide with any welded seams.

During the reporting period, Marquardt successfully demonstrated continuous, steady-state firing capability of a reworked Syncom II engine assembly. By increasing the fuel injector diameter from 0.016 inch to 0.031 inch, continuous steady-state firing runs, two for 30 minutes and one for 13 minutes, were logged on the engine. A total of 73 minutes of hot-firing time, at a specific impulse of 262 seconds and a thrust chamber wall temperature of 2325°F, were accumulated on the molybdenum disilicide coated chamber with no deleterious effects.

Marquardt Report (Hughes-Edited)*

Engineering

Design. Design support activity included engineering drawing release and maintenance, development test support and manufacturing support.

Drawing changes and maintenance were accomplished on the following:

1) Engineering model assembly: Additional refinements were made as a result of assembly buildup. These changes plus those reported in the previous period are being incorporated on the engineering model assembly drawing.

2) Rocket engine assembly: A design change to the high pressure drop restrictor gaskets was made to eliminate engine performance changes caused by restricted propellant flow. The material was changed from teflon-TFE sheet to glass-filled teflon-TFE bar. In addition a geometry change was made to control void volume displacement. The change was successful as demonstrated in engine acceptance tests.

*The information in this subsection was abstracted from Marquardt Monthly Progress Report MR-1-5, dated 15 July 1963.

3) Fixed restrictors: Additional sizes of high pressure drop restrictors were required to permit proper injector pressure control.

In development test support, additional design support was required for a development test of an engine with a modified injector which permitted operation of the engine at steady state. The flight-type tank development structural test plan was completed. Effort was also expended in preparation of the test hardware and vibration fixture setup. The long-term storage test plan was completed (rough draft) and submitted for approval.

Engineering effort was expended in support of manufacturing activities on the following: tanks (flight type), engine and spin control mount assembly (buildup), and engineering model assembly (buildup). Leakage from tanks on the engineering model was discovered during system pressure test operations. Investigations revealed that improper grain orientation and inclusions in the tank fittings were the cause of pin hole leaks which developed on successive pressure test cycles. Repair entailed placing localized gold plating on each fitting and burnishing.

Development. The component and subassembly acceptance tests have been completed, and the engineering model is presently in the Cell 9 facility for leakage tests and instrumentation checkout prior to the formal firing demonstration.

During engine tests a design modification was incorporated into the engines for the engineering model. High pressure drop orifices, previously located in the engineering model plumbing, were moved to a location in the engine downstream of the injector solenoid valves. The engine acceptance tests with this modification showed that the engine thrust characteristics were improved by elimination of thrust overshoot during the start transient.

A problem was encountered during the acceptance testing with the teflon seal for the relocated restrictors. A redesign of the seal was necessary to control the cold flow of the teflon. Changes in the seal were causing a change in engine pressure drop with subsequent influence on the propellant flow. The preburn and postburn flow calibration of the engines, acceptance tested for the engineering model, showed that engine pressure drop characteristics with the redesigned seal were consistent before and after engine firing.

The engine acceptance test data indicated that at the engineering model initial tank pressure of 300 psia the engines would produce 5.1 pounds of thrust at an O/F ratio of 1.8. The high O/F ratio (1.8 rather than 1.64) can be attributed to higher oxidizer flow during engine operation than was predicted from the preburn pressure drop calibrations using water as the calibrating fluid.

A test was conducted during the report period to demonstrate engine life capability with a modified injector configuration. Previous test data indicated that combustion chamber wall temperatures could be lowered sufficiently to permit continuous engine operation with the modified injector. The engine test was made at an O/F ratio of 1.64 and thrust level of 4.9 pound. Specific impulse was approximately 260 seconds. Steady state engine temperature was 2325°F. Two continuous runs of 30 minute duration and one of 13 minutes were made. The last run was terminated because of facility fuel supply exhaustion. Examination of the combustion chamber at the conclusion of the test showed no evidence of deterioration.

The objectives and results of the engine tests are described in detail below and summarized in Table 4-2.

1) Engine Test 24: To conduct the acceptance test of Serial No. 001 engine for the engineering model; to evaluate change in pressure drop restrictor location and improve engine dynamic characteristics.

   A design modification was incorporated in the engines for the engineering model that consisted of installing the pressure drop restrictors downstream of the engine solenoid valves.

   The engine testing was conducted in accordance with Marquardt Test Specification (MTS) 0608 which consists of preburn tests, engine firing tests, and postburn tests. During preburn tests the pressure drop restrictors are installed in the engine to obtain a pressure drop across the engine for a specified flow condition such that the desired propellant flow rates will be obtained for specified propellant inlet pressure conditions during the engine firing tests. The engine firing tests are conducted at propellant pressures corresponding to the tank pressures during operation of the engineering model, and performance requirements are specified for the particular inlet pressures. The postburn tests consist of pressure drop and leakage tests to verify that the initial preburn calibration is unchanged.

   The engine firing tests indicated that engine start transients had been improved by eliminating thrust overshoot that was experienced prior to the change in restrictor location. Figures 4-28 and 4-29 show the impulse/pulse and thrust/pulse as a function of time during continuous pulse runs at one third and one sixth duty cycles and the 5-pound thrust level. Figure 4-30 shows the same parameters for one sixth duty cycle operation at the 3-pound thrust level.

   During the postburn tests, a change in the engine pressure drop was observed in comparison to the preburn calibration.

## TABLE 4-2. ENGINE TEST SUMMARY

| Test Number | Test Date (1963) | Injector Head | Combustion Chamber | Test Conditions | Number of Runs | Total Burn Time, Seconds | Maximum Single Run Time | Remarks |
|---|---|---|---|---|---|---|---|---|
| 24 | 6/15 | X19151 Serial No. 001 | X19158 Serial No. 008 | Altitude acceptance | 16 | 227 | 3 minutes* 6 minutes** | Postburn tests showed change in engine pressure drop |
| 25 | 6/17 | X19151 Serial No. 003 | X19158 Serial No. 009 | Altitude acceptance | 34 | 216 | 3 minutes* 6 minutes** | Postburn tests showed change in engine pressure drop |
| 26 | 6/28 | X19151 Serial No. 001 | X19158 Serial No. 008 | Altitude acceptance | 9 | 18 | 1 second | Test terminated because of low O/F ratio |
| 27 | 7/1 | X19151 Serial No. 003 | X19158 Serial No. 009 | Altitude acceptance | 26 | 206 | 3 minutes* 6 minutes** | Postburn tests showed change in engine pressure drop |
| 28 | 7/2 | X19151 Serial No. 001 | X19158 Serial No. 008 | Altitude acceptance | 35 | 214 | 3 minutes* 6 minutes** | Postburn tests showed change in engine pressure drop |
| 29 | 7/3 | X19151 Serial No. 006 | X19158 Serial No. 001 | Altitude life capability | 14 | 4420 | 1800 seconds | Test terminated because of fuel exhaustion |
| 30 | 7/6 | X19151 Serial No. 001 | X19158 Serial No. 010 | Altitude acceptance | 25 | 264 | 3 minutes* 6 minutes** | Test objective completed |
| 31 | 7/7 | X19151 Serial No. 003 | X19158 Serial No. 009 | Altitude acceptance | 20 | 200 | 3 minutes* 6 minutes** | Test objective completed |

*Continuous run and duty cycle 1 second on/2 seconds off.
**Continuous run at duty cycle 0.1 second on/0.5 second off.

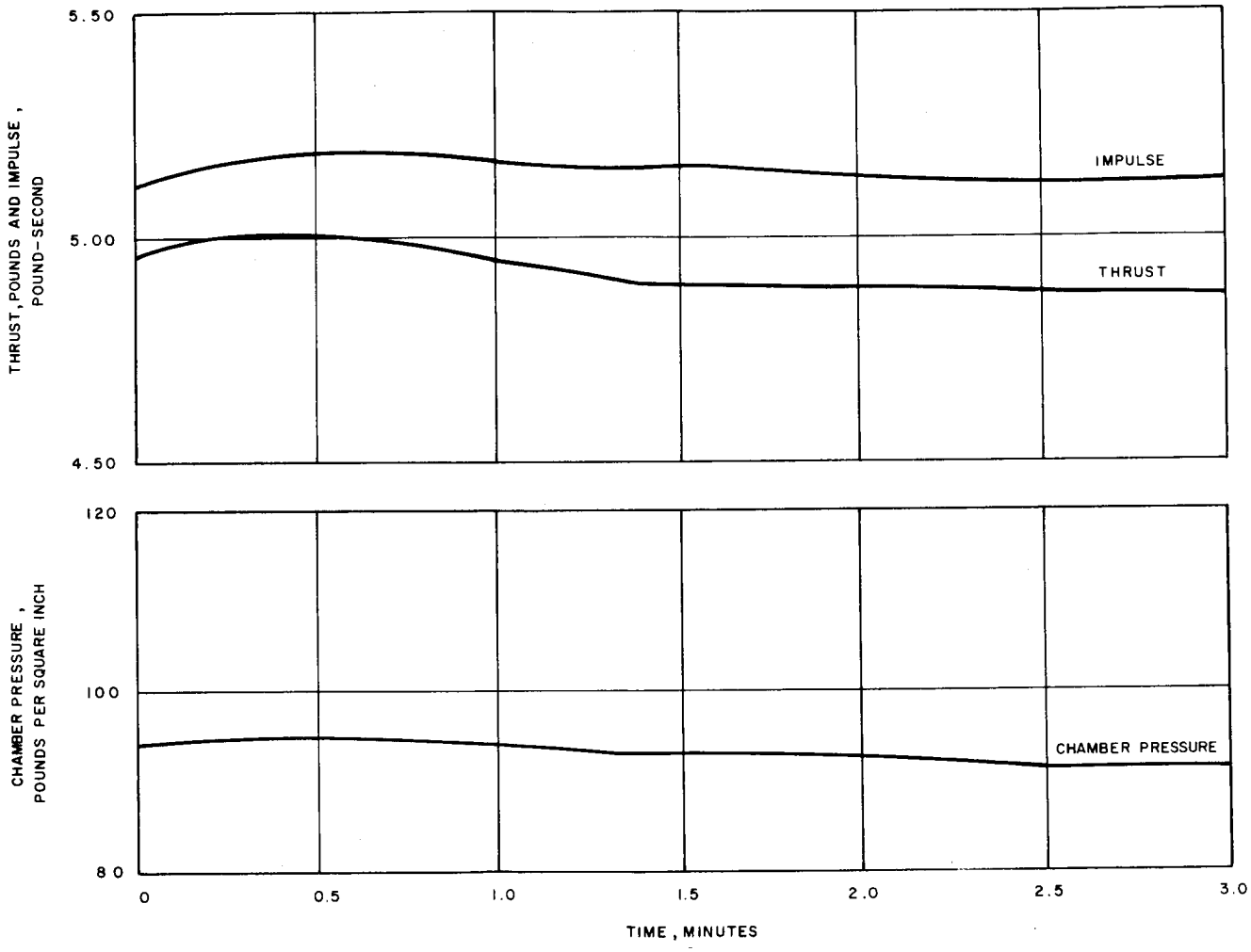


Figure 4-28. Syncom 5-Pound Engine Test
Test 24, 16 June 1963, Run 5

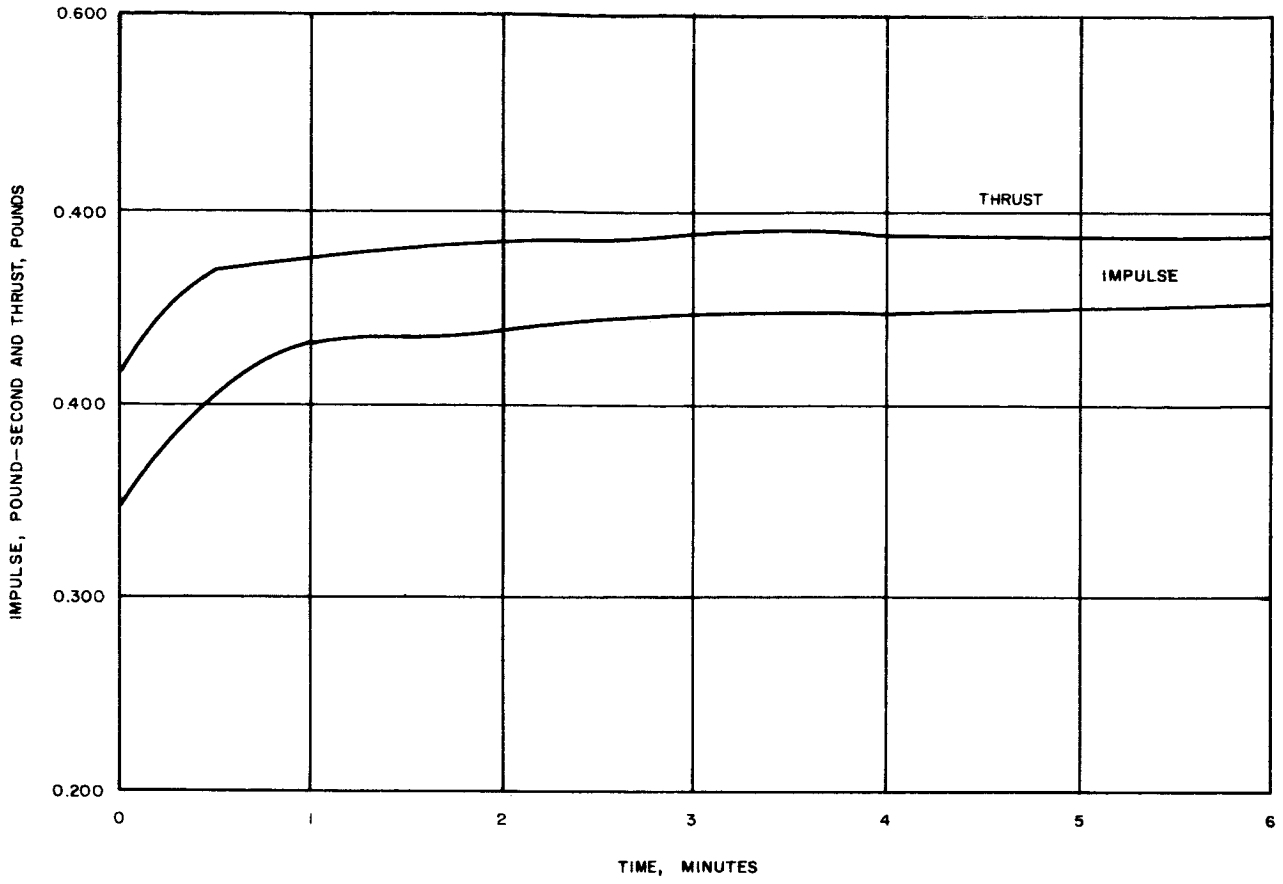


Figure 4-29. Syncom 5-Pound Engine Test
Test 24, 16 June 1963, Run 8

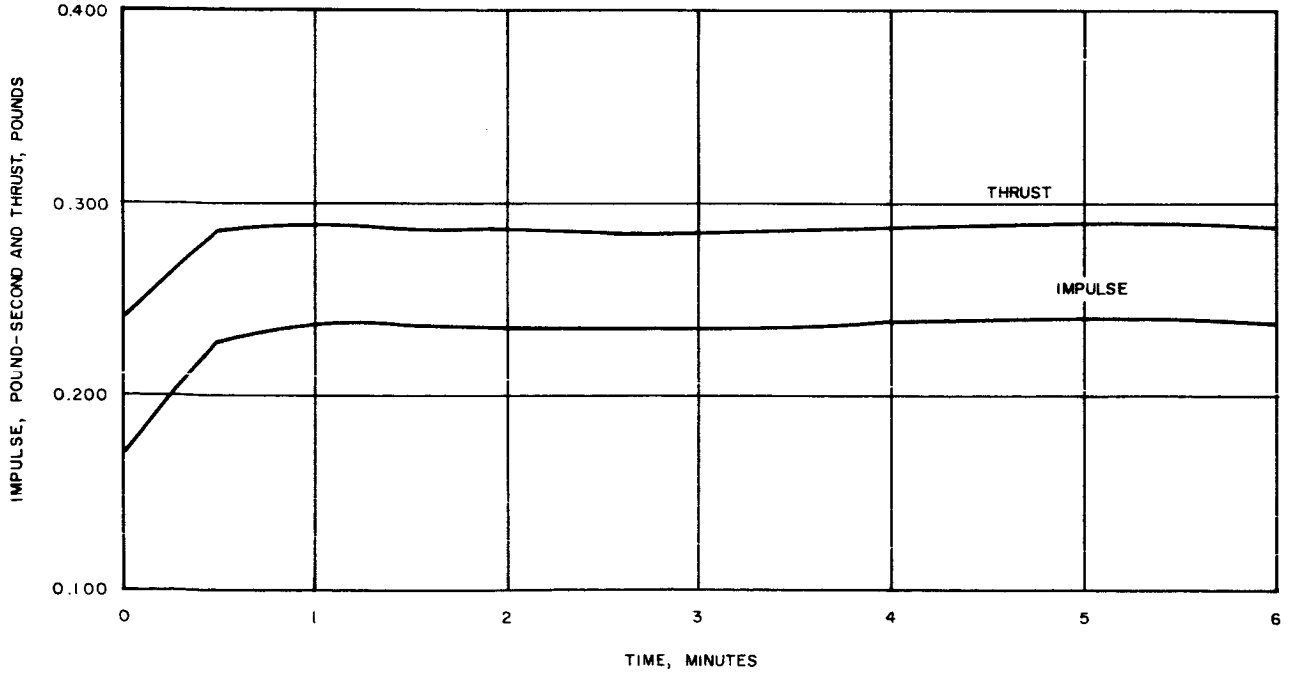


Figure 4-30. Syncom 5-Pound Engine Test
Test 24, 16 June 1963, Run 11

Subsequent investigation showed that the teflon seal for the restrictor was not sufficiently contained and could permit leakage past the restrictor when the teflon cold flowed. Action on the seal was delayed pending results of the postburn tests on the second engine.

2) Engine Test 25: To conduct the acceptance test of Serial No. 002 engine for the engineering model.

Engine test procedures were identical to those employed in Test 24.

During engine firing tests at the one sixth duty cycle at the 5-pound thrust level, there was evidence of a fuel solenoid valve malfunction. The data indicated that this valve did not open, or opened only partially, for a portion of the cycling. Subsequent to the malfunction, valve operation was normal and there was no further evidence of malfunction.

During the postburn testing, a change in engine pressure drop was recorded in relation to the preburn calibration, and action was taken to change the restrictor seal configuration to provide additional squeeze on the teflon seal.

The fuel solenoid valve (X19172 Serial No. 001) was removed from the engine and replaced with a new valve (Serial No. 005). A retest of the solenoid valve (Serial No. 001) in accordance with valve acceptance test procedures showed an increase in the pressure drop of 4.5 psi and a slight decrease in the opening and closing response times in comparison to the initial acceptance test data. Disassembly of the valve showed that armature travel had decreased because of swelling of the teflon seal, accounting for the change in pressure drop and in response time. There was no direct evidence to account for the malfunction observed during the test. One very small metal particle was found on the inlet side of the armature, but there were no gall or scratch marks to indicate that this had contributed to the malfunction.

3) Engine Test 26: To conduct the acceptance test of Serial No. 001 engine for the engineering model using revised restrictor configuration.

The revised restrictor configuration was installed during the engine preburn testing in accordance with the acceptance test procedures (MTS 0608).

The initial engine firing tests indicated excessive restriction in the oxidizer section of the engine, and the test was terminated.

A recheck of the pressure drops in postburn testing showed that the oxidizer pressure drop was excessive, and subsequent examination showed that the teflon restrictor seal had cold flowed through the space between the restrictor and the solenoid valve, partially blocking the restrictor. A dimensional inspection of the parts indicated that squeeze on the teflon was excessive. The engine was repaired by decreasing the thickness of the teflon seal.

The pressure drop through the fuel side of the engine repeated the preburn calibration data.

4) Engine Test 27: To conduct the acceptance test of Serial No. 002 engine for the engineering model.

The postburn tests on this engine showed that engine pressure drop was out of tolerance and was high compared to calibration. Examination of the teflon was excessive, permitting the teflon to cold flow and interfering with flow through the restrictor.

5) Engine Test 28: To conduct the acceptance test of Serial No. 001 engine.

The restrictor seal in the oxidizer side of the engine had been modified following Engine Test 26 to reduce the squeeze and prevent cold flow.

During the engine burning tests, an increase in O/F ratio was observed following the 3-minute duration run at the 1 second on/2 seconds off duty cycle. The subsequent postburn test and investigation showed that the oxidizer pressure drop was satisfactory, but that the fuel restrictor seal had cold flowed to partially block the restrictor.

Action was taken to redesign the seal to make a one-piece seal of glass-filled teflon, tighten the tolerance on the teflon squeeze, and provide a void area to accomodate teflon cold flow such that there would be no interference with the orifice. It was necessary to tailor the dimensions of each individual seal to account for the tolerance stackup at the valve-seal-injector head interfaces.

6) Engine Test 29: To demonstrate engine life capability with modified injector configuration.

The injector head for this engine was modified to produce lower combustion chamber temperatures by a change in the diameter ratio of the fuel and oxidizer injector orifices.

Previous test data had indicated lower combustion chamber temperatures could be obtained by this technique with some decrease in engine efficiency.

The initial 1-second duration runs at a thrust level of 4.5 pounds and an O/F ratio of 1.63 showed a specific impulse of approximately 250 seconds and a 30-second duration run at these conditions showed the maximum nozzle temperature, as measured by thermocouples attached to the combustion chamber wall, was 2235°F. The propellant flow to the engine was increased to obtain 4.9 pounds of thrust at the 1.64 O/F ratio, and a specific impulse of 260 seconds was measured for 1-second duration runs. A continuous run of 30 minutes, limited by propellant run tank capacity, was made at the 4.9 pound thrust level with maximum nozzle steady state temperatures of 2325°F. There was no evidence of thrust degradation during the 30 minutes of run time. The run tanks were reloaded and a second run of 30 minutes was made followed by partial supply tank reloading and a run of 13 minutes. The 13 minute run was concluded by fuel exhaustion of the facility supply tanks.

Inspection of engine following the 73 minutes of burning indicated no evidence of combustion chamber deterioration.

7) Engine Test 30: To conduct the acceptance test of Serial No. 001 engine.

The redesigned restrictor seals were installed in the engine and tests to MTS 0608 were completed. The postburn flow test data agreed with the preburn calibration data indicating no change had occurred in the restrictor seal during the engine firing tests.

Reduction of the engine firing test data indicates that for engine inlet pressures corresponding to the engineering model tank pressures the O/F ratio is approximately 1.8 because of an oxidizer flow rate higher than predicted by the preburn flow calibration. The higher oxidizer flow also increases the engine thrust to approximately 5.1 pounds for the initial engineering model tank pressure of 300 psia.

The cause for the higher oxidizer flow during the burn runs is not well defined, but appears to be viscosity effects and/or orifice coefficient difference between the preburn calibration using water as the calibrating media and the engine tests with the oxidizer. No action was taken to compensate for the higher oxidizer flow during the previous acceptance tests because of the problem with the restrictor seals which also influenced the O/F ratio.

Tabulations showing engine parameters as a function of time for the acceptance tests are shown in Table 4-3.

8) Engine Test 31: To conduct the acceptance test of Serial No. 002 engine.

The acceptance test on the Serial No. 002 engine was similar to the tests with Serial No. 001 engine. Postburn calibration data showed that the restrictor seal redesign was satisfactory.

The performance data is shown in Table 4-4.

Analysis. Test results with the acceptance test engines for the engineering model and with a development engine with an injector $D_F/D_O$ (fuel to oxidizer diameter) of .031 inch/.019 inch indicate that a specific impulse of approximately 280 seconds can be achieved at the 5-pound thrust level at an O/F = 1.62 with a maximum steady state wall temperature of approximately 2800°F. This can be accomplished with the existing thrust chamber design by increasing injector $D_F/D_O$ from 0.84 to approximately 1.2.

The maximum external surface temperature of the breadboard design of the radiation shield reached 380°F. The external surface temperature of the radiation shield is higher than the 200°F allowed by specification X254044 primarily because of the large conduction heat leak from the inner radiation shield to the outer aluminum shell at the downstream end of the shield. An envelope diameter increase at the downstream end from 3 inches to 5 inches is required to reduce the external surface temperature.

Analysis of the 5 to 20 percent increase in impulse (in the first 30 seconds), which is caused by a probable oxidizer flow increase during operation at a one-sixth duty cycle with the current engine configuration, has not resulted in positive determination of the underlying mechanism. The effect is not caused by a density or viscosity change due to increasing temperature of the injector head during the initial pulses, and it is not caused by an increasing temperature in the combustion chamber. This increasing temperature could improve efficiency by reducing heat loss through the chamber walls or by improving combustion: thrust does not significantly increase during a steady state run from the first second to steady state temperatures. The effect does not result from a direct geometry change caused by increasing engine temperature. The increasing impulse is believed to be related to a temperature effect (propellant or metal) on the orifice discharge coefficients or nitrogen entrapped in the propellant lines or a vapor pressure effect in the orifices. A different impulse/pulse number characteristic may result from an increased injector $D_F/D_O$.

Reliability. A reliability apportionment study of components, subsystems, and system was reviewed and is being modified. A failure mode

# TABLE 4-3. REACTION CONTROL ENGINE DATA SUMMARY

## Serial No. 001

| Paragraph 3.2.4.2 | Units | Run 4 | Run 7 | Run 8 | Required |
|---|---|---|---|---|---|
| Run duration | Second | 0.994 | 0.994 | 0.997 | 1.0 ±0.1 |
| Fuel flow, $W_f$ | Pounds | 0.00656 | 0.00656 | 0.00656 | – |
| Oxidizer flow, $W_{ox}$ | Pounds | 0.01136 | 0.01142 | 0.01142 | – |
| O/F ratio, O/F | – | 1.731 | 1.74 | 1.74 | 1.64 ±0.05 |
| Impulse, $I_M$ | Pounds per second | 5.05 | 5.07 | 5.09 | $5.0\ ^{+0}_{-0.5}$ |
| Average thrust, $I_M/t_e$ | Pounds | 5.08 | 5.10 | 5.10 | $5.0\ ^{+0}_{-0.5}$ |
| Specific impulse, $I_{SP}$ | Second | 283.8 | 284.6 | 286.0 | 285 ±15 |
| Char. velocity, C | Feet per second | 5154.5 | 5163.7 | 5190.0 | 4840-5480 |

| Paragraph 3.2.4.3 | Units | Pulse 1 | Pulse 15 | Pulse 30 | Pulse 45 | Last Pulse | Required |
|---|---|---|---|---|---|---|---|
| Run duration | | | | | | | >3 minutes |
| Pulse on time | Second | 0.93 | 0.99 | 0.99 | 0.99 | 0.99 | 1.0 ±0.1 |
| Pulse off time | Second | 2.1 | 2.03 | 2.05 | 2.03 | 2.04 | 2.0 ±0.2 |
| Impulse | Pounds per second | 4.74 | 5.24 | 5.17 | 5.14 | 5.13 | $5.0\ ^{+0}_{-0.5}$ |

| Paragraph 3.2.4.4 | Units | Pulse 1 | Pulse 5 | Pulse 10 | Pulse 15 | Pulse 20 | Last Pulse | Required |
|---|---|---|---|---|---|---|---|---|
| Pulse on time, $t_e$ | Second | 0.09 | 0.09 | 0.09 | 0.09 | 0.09 | 0.09 | 0.10 ±0.01 |
| Pulse off time | Second | 0.51 | 0.51 | 0.51 | 0.51 | 0.51 | 0.51 | 0.50 ±0.05 |
| Fuel flow | Pounds | 0.0006168 per pulse | | | | | | – |
| O/F ratio | – | 1.80 → | | | | | | 1.64 ±0.10 |
| Oxidizer flow | Pounds | 0.001114 per pulse | | | | | | – |
| Impulse | Pounds per second | 0.405 | 0.443 | 0.445 | 0.455 | 0.46 | 0.46 | – |
| Average thrust | Pounds | 4.5 | 4.92 | 4.94 | 5.05 | 5.11 | 5.11 | – |
| Specific impulse | Second | 236.6 | 258.5 | 259.7 | 265.5 | 268.3 | 268.3 | 265 ±15 |
| Pulse centroid, $t_c$ | Second | 0.059 | 0.059 | 0.06 | 0.059 | 0.059 | 0.06 | – |

| Paragraph 3.2.4.5 | Units | Pulse 1 | Pulse 100 | Pulse 200 | Pulse 300 | Pulse 400 | Pulse 500 | Last Pulse | Required |
|---|---|---|---|---|---|---|---|---|---|
| Run duration | | | | | | | | | 6 minutes |
| Pulse on time | Second | 0.09 | 0.09 | 0.09 | 0.09 | 0.09 | 0.09 | 0.09 | 0.1 ±0.01 |
| Pulse off time | Second | 0.51 | 0.51 | 0.51 | 0.51 | 0.51 | 0.51 | 0.50 | 0.5 ±0.05 |
| Impulse | Pounds per Second | 0.415 | 0.445 | 0.435 | 0.435 | 0.335 | 0.325 | 0.315 | |
| Pulse centroid | Second | 0.059 | 0.059 | 0.059 | 0.059 | 0.059 | 0.06 | 0.06 | |

| Paragraph 3.2.4.7 | Units | Pulse 1 | Pulse 5 | Pulse 10 | Pulse 15 | Pulse 20 | Last Pulse | Required |
|---|---|---|---|---|---|---|---|---|
| Pulse on time | Second | 0.09 | 0.09 | 0.09 | 0.09 | 0.09 | 0.91 | 0.1 ±0.01 |
| Pulse off time | Second | 0.51 | 0.51 | 0.51 | 0.51 | 0.51 | 0.51 | 0.5 ±0.05 |
| Fuel flow | Pounds | 0.0004020 per pulse | | | | | | |
| Oxidizer flow | Pounds | 0.0007300 per pulse | | | | | | |
| O/F ratio | – | 1.815 | | | | | | 1.64 ±0.10 |
| Impulse | Pounds per second | 0.22 | 0.246 | 0.25 | 0.25 | 0.25 | 0.253 | |
| Average thrust | Pounds | 2.44 | 2.73 | 2.77 | 2.77 | 2.77 | 2.78 | |
| Specific impulse | Second | 198.5 | 221.5 | 225 | 225 | 225 | 227.7 | 240 ±15 |
| Pulse centroid | | 0.06 | 0.061 | 0.061 | 0.06 | 0.06 | 0.059 | |

| Paragraph 3.2.4.8 | Units | Pulse 1 | Pulse 100 | Pulse 200 | Pulse 300 | Pulse 400 | Pulse 500 | Last Pulse | Required |
|---|---|---|---|---|---|---|---|---|---|
| Run duration | | | | | | | | | 6 minutes |
| Pulse on time | Second | 0.09 | 0.09 | 0.09 | 0.09 | 0.09 | 0.09 | 0.09 | 0.1 ±0.01 |
| Pulse off time | Second | 0.51 | 0.51 | 0.51 | 0.51 | 0.51 | 0.51 | 0.51 | 0.5 ±0.05 |
| Impulse | Pounds per second | 0.216 | 0.240 | 0.225 | 0.220 | 0.218 | 0.218 | 0.218 | |
| Pulse centroid | Second | 0.062 | 0.06 | 0.06 | 0.06 | 0.061 | 0.062 | 0.06 | |

# TABLE 4-4. REACTION CONTROL ENGINE DATA SUMMARY

## Serial No. 002

| Paragraph 3.2.4.2 | Units | Run 1 | Run 2 | Run 3 | Required |
|---|---|---|---|---|---|
| Run duration | Second | 1.03 | 1.02 | 1.03 | 1.0 ±0.1 |
| Fuel flow | Pounds | 0.00630 | 0.00639 | 0.00629 | – |
| Oxidizer flow | Pounds | 0.01186 | 0.01195 | 0.01171 | – |
| O/F ratio | – | 1.88 | 1.87 | 1.86 | 1.64 ±0.05 |
| Impulse | Pounds per second | 5.13 | 5.11 | 5.10 | $5.0\ ^{+0}_{-0.5}$ |
| Average thrust | Pounds | 5.04 | 5.07 | 4.99 | $5.0\ ^{+0}_{-0.5}$ |
| Specific impulse | Second | 278 | 277 | 277 | 295 ±15 |
| Char. velocity | Feet per second | 5169 | 5145 | 5214 | 4840-5480 |

| Paragraph 3.2.4.3 | Units | Pulse 1 | Pulse 15 | Pulse 30 | Pulse 45 | Last Pulse | Required |
|---|---|---|---|---|---|---|---|
| Run duration | | | | | | 182 seconds | 3 minutes |
| Pulse on time | Second | 1.03 | 1.02 | 1.03 | 1.01 | 1.02 | 1.0 ±0.1 |
| Pulse off time | Second | 2.05 | 2.05 | 2.05 | 2.05 | 2.05 | 2.0 ±0.2 |
| Impulse | Pounds per second | 6.00 | 5.85 | 5.85 | 5.85 | 5.85 | $5.0\ ^{+0}_{-0.5}$ |

| Paragraph 3.2.4.4 | Units | Pulse 1 | Pulse 5 | Pulse 10 | Pulse 15 | Pulse 20 | Last Pulse | Required |
|---|---|---|---|---|---|---|---|---|
| Pulse on time | Second | 0.093 | 0.093 | 0.094 | 0.093 | 0.093 | 0.094 | 0.10 ±0.01 |
| Pulse off time | Second | 0.514 | 0.505 | 0.505 | 0.504 | 0.506 | – | 0.50 ±0.05 |
| Fuel flow | Pounds | 0.0006216 per pulse | | | | | | |
| O/F ratio | – | 1.83 | | | | | | 1.64 ±0.10 |
| Oxidizer flow | Pounds | 0.001138 per pulse | | | | | | |
| Impulse | Pounds per second | 0.40 | 0.425 | 0.435 | 0.437 | 0.440 | 0.450 | |
| Average thrust | Pounds | 4.37 | 4.64 | 4.69 | 4.78 | 4.78 | 4.85 | |
| Specific impulse | Second | 248 | 264 | 267 | 272 | 272 | 276 | 265 ±15 |
| Pulse centroid | Second | 0.063 | 0.060 | 0.061 | 0.061 | 0.060 | 0.063 | |

| Paragraph 3.2.4.5 | Units | Pulse 1 | Pulse 100 | Pulse 200 | Pulse 300 | Pulse 400 | Pulse 500 | Last Pulse | Required |
|---|---|---|---|---|---|---|---|---|---|
| Run duration | | | | | | | | 364 seconds | 6 minutes |
| Pulse on time | Second | 0.095 | 0.094 | 0.094 | 0.094 | 0.093 | 0.095 | 0.094 | 0.1 ±0.01 |
| Pulse off time | Second | 0.504 | 0.505 | 0.505 | 0.508 | 0.504 | – | 0.503 | 0.5 ±0.05 |
| Impulse | Pounds per Second | 0.415 | 0.467 | 0.467 | 0.474 | 0.474 | 0.476 | 0.483 | |
| Pulse centroid | Second | 0.063 | 0.064 | 0.063 | 0.063 | 0.063 | 0.064 | 0.064 | |

| Paragraph 3.2.4.7 | Units | Pulse 1 | Pulse 5 | Pulse 10 | Pulse 15 | Pulse 20 | Last Pulse | Required |
|---|---|---|---|---|---|---|---|---|
| Pulse on time | Second | – | 0.093 | 0.092 | 0.090 | 0.090 | 0.090 | 0.1 ±0.01 |
| Pulse off time | Second | – | 0.509 | 0.510 | 0.512 | 0.512 | – | 0.5 ±0.05 |
| Fuel flow | Pounds | 0.0003978 per pulse | | | | | | |
| Oxidizer flow | Pounds | 0.0007480 per pulse | | | | | | |
| O/F ratio | – | 1.88 | | | | | | 1.64 ±0.10 |
| Impulse | Pounds per second | – | 0.227 | 0.233 | 0.240 | 0.240 | 0.241 | |
| Average thrust | Pounds | – | 2.49 | 2.58 | 2.72 | 2.72 | 2.73 | |
| Specific impulse | Second | – | 218 | 226 | 237 | 237 | 238 | 240 ±15 |
| Pulse centroid | – | – | 0.062 | 0.062 | 0.061 | 0.061 | 0.061 | |

| Paragraph 3.2.4.8 | Units | Pulse 1 | Pulse 100 | Pulse 200 | Pulse 300 | Pulse 400 | Pulse 500 | Last Pulse | Required |
|---|---|---|---|---|---|---|---|---|---|
| Run duration | | | | | | | | 374 seconds | 6 minutes |
| Pulse on time | Second | 0.096 | 0.096 | 0.093 | 0.093 | 0.093 | 0.094 | 0.095 | 0.1 ±0.01 |
| Pulse off time | Second | 0.506 | 0.501 | 0.505 | 0.504 | 0.505 | 0.504 | – | 0.5 ±0.05 |
| Impulse | Pounds per Second | 0.225 | 0.246 | 0.248 | 0.250 | 0.250 | 0.246 | 0.247 | |
| Pulse centroid | Second | 0.069 | 0.065 | 0.065 | 0.065 | 0.066 | 0.066 | 0.066 | |

and effects analysis has been completed and is being reviewed. A performance analysis and estimate of achieved reliability is in process.

A tentative outline of a Quality Control Plan has been completed and is being expanded before release. A one-day conference was held with Hughes Aircraft Company on Quality Control specification and audit. A survey of and report on the certification of soldering personnel is in process and is programmed for completion in September 1963. A general Quality Control auditing procedure has been written and a standard audit form designed. These are being reviewed for final approval.

A dry run of the Radiographic Inspection Section was conducted with the general auditing procedures and an X-ray activity audit form. The results were excellent, but indicated minor modifications of the procedural coverage of some process details would be an even greater improvement. These modifications have been incorporated in the general auditing procedures.

Purchase Request and Purchase Order reviews are continuing with Quality Assurance requirements being added as required.

Materials and Process. Design support included the following activities:

1) A laboratory evaluation has been started on the test fired altitude chamber made from 90Ta-10W with tin-aluminide coating. This effort is sponsored by TMC.

2) Emittance evaluations have been started on 90Ta-10W with and without tin-aluminide coating. This effort is sponsored by TMC. Project will arrange for machining of test tubing 6.25 inches long, 0.5 inch in diameter, and with a wall 0.030 inch thick.

3) Metallurgical evaluation was conducted on chembers Serial Nos. 006 and 007 after breadboard test firing on 24 May 1963. On Serial No. 006, the low heat indications at the fracture surfaces near the chamber skirt area indicated rupture occurred after test firing or at the tail off of the run. On Serial No. 007, a crack 0.25 inch long was positioned axially approximately 0.5 inch upstream of the throat. The presence of oxide diffusion indicated the crack was present during test firing. This crack was not present on X-ray films made after coating and after smoke testing.

Manufacturing support included monitoring the following activities:

1) Repair of leaky fittings for engineering model propellant tanks Serial No.'s 001, 002, 007 and 008. Leaks apparently due to axially oriented loose inclusions. A repair was effected by localized brush (Dalic process) plating with gold to 0.010 inch thickness.

2) Vendor brazing of injector head assembly P/N T8557 (modified X-19151).

## Manufacturing

Breadboard Assembly. Complete.

Engineering Model Structure Assembly. The Hughes structure was completed minus the two motor assemblies and delivered to the test facility. One motor assembly was assembled to the swivel mount and one to the heat shield. Manufacturing mounted the two assemblies on the Hughes structure in the test facility. Some minor modifications were made in the Hughes structure.

## Test

This evaluation of the instrumentation systems used at MJL for Syncom rocket engine testing is limited to steady state conditions: evaluations are not yet available for dynamic conditions. The approach was to consider the accuracy and precision of the systems used for measuring pressures, flow, temperature and thrust.*

*Tests were conducted in accordance with procedures outlined in R. J. Horak, "Evaluation of Instrumentation Procedures at the Air Force-Marquardt Jet Laboratory," HAC Report No. 5661, 24 July 1957, Appendix J, p. 112, and with Frank Ernest, "Electrical Measurement Analysis," McGraw Hill, 1959, pp. 109-114.

Since the standard practice for accuracy is to comply 100 percent with NASA Quality Publication 200-2, and MIL-C-45662A, "Calibrator System Requirements," this evaluation is centered around determining precision of the measurement systems according to information supplied in the major component manufacturer's literature. The information supplied by the manufacturer is used as the statistical evaluation data (SED). This data is used to arrive at an overall standard deviation for the various instrumentation systems used.

The standard deviation described is based on a Gaussian distribution due to the random variation of an infinite number of samples (N). The standard deviation indicates the degree of dispersion of the values about the mean ($\bar{x}$) in Figure 4-31. In other words, if repetitive calibrations are made with one measurement system, say pressure, the mean value is found by taking the sum of all measurements (x) at one particular pressure and dividing by the number of samples (N) to obtain $\bar{x}$. Then the deviation from $\bar{x}$ is found by the following formula:

$$\sigma = \frac{\sqrt{(\bar{x}-x)^2}}{N-1}$$

This formula will reproduce the Gaussian distribution curve shown in Figure 4-31 provided enough points are taken. Generally, 20 calibrations are sufficient to define the limits for a first approximation. From this curve, it can be seen that 68.26 percent of all errors lie between $\pm 1\sigma$, 95.46 percent of all errors lie between $\pm 2\sigma$, and 99.73 percent of all errors lie between $\pm 3\sigma$.

Standard deviations are also expressed as confidence levels of 68.26 percent, 95.46 percent, and 99.73 percent. An error expressed as being at the 68.26 percent confidence level contains 68.26 percentage of the random deviation from the mean within the standard deviation ($\sigma$); one time in three such a measurement will be in error. If a statement is made that a specified precision is guaranteed at the $3\sigma$ or 99.73 percent confidence level, repetitive tests must have been performed to establish this fact. If this happens to be a piece of equipment with an advertised precision of $\pm$ 1 percent at the $3\sigma$, the user can be assured that 99.73 percent of the time the equipment will be reading better than $\pm$ 1 percent of the true measurement.

The precision of the measurement systems as determined for this report is summarized as follows:

1) The general equation for determining the precision of a measurement system will be based upon manufacturer's specifications.

2) The data specified by the manufacturer is normally specified with a confidence interval of 99.73 percent of a $3\sigma$ precision. In essence, the manufacturer's number is a conservative one as he is confident that his instrument will read within the tolerance that he specifies 99.73 percent of the time or can be in error greater than the tolerance specified by one time in 370.

3) The sigma ($\sigma$) or one standard deviation precision is determined by using manufacturers data and the following equation:

$$\sigma = \frac{1}{6} \sqrt{A^2 + B^2 \ldots \text{etc.}}$$

Specific deviation precision data for thrust, flow, stand pipe flow, pressures (wiancko and taber), cell pressure, and temperature are given on pages 33 to 40 of the Marquardt Monthly Progress Report MR-1-5, dated 15 July 1963, Summary data are presented in Figure 4-32.

## Product Support

The Phase I engineering model propellant transfer equipment has been fabricated, cleaned, pressure checked, and sealed for shelf storage until Hughes requests its use.

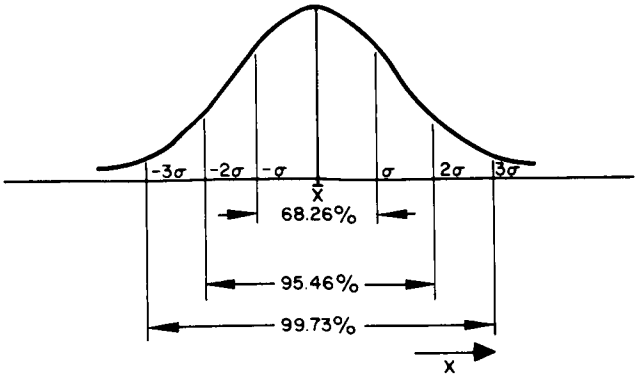


Figure 4-31. Gaussian Distribution Curve

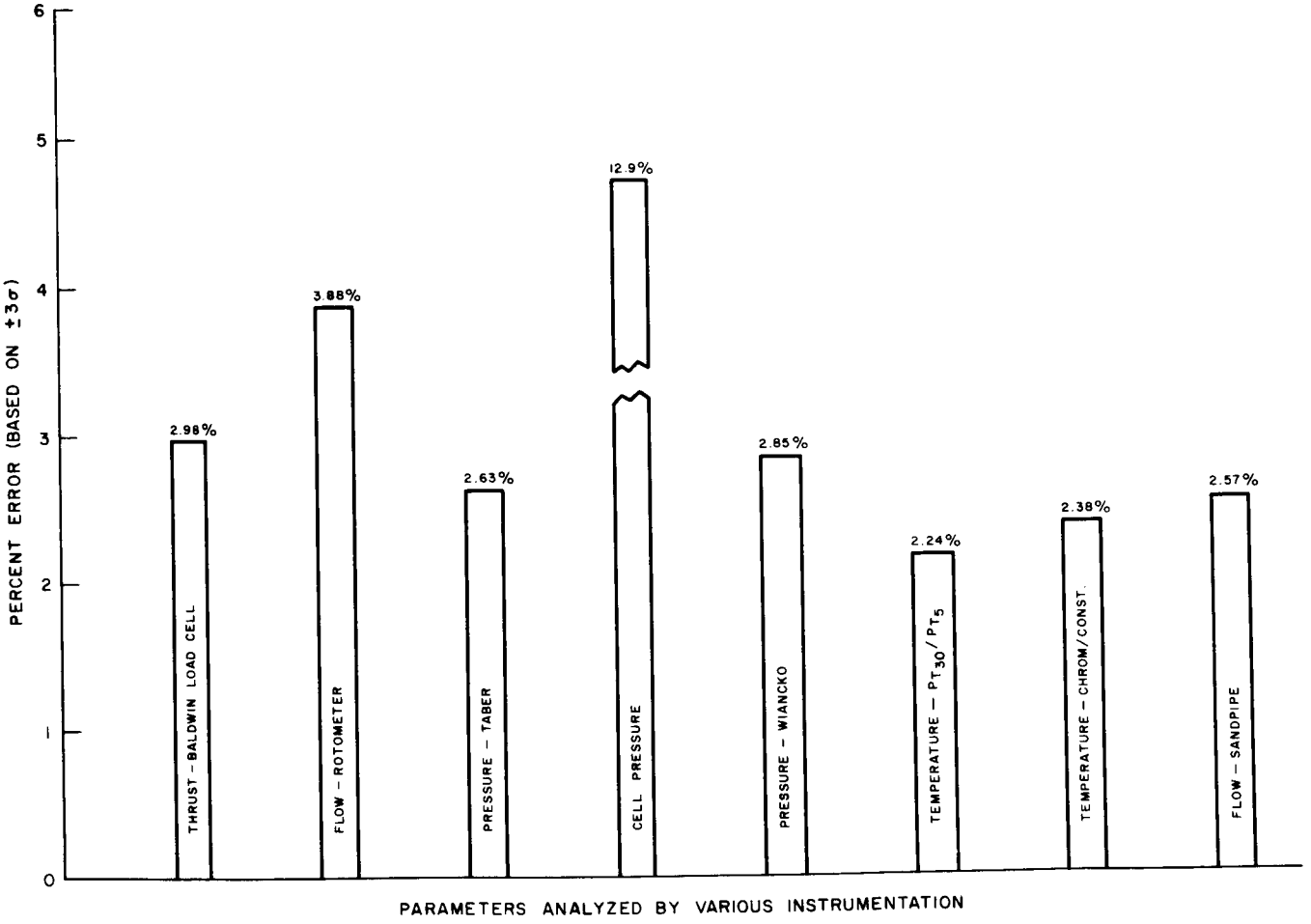


Figure 4-32. Summary of Steady-State Syncom Rocket Parameters

## TELEMETRY AND COMMAND

### Telemetry Encoder Circuit Design

The Advanced Syncom telemetry will be the NASA Goddard Space Flight Center standard pulse frequency modulation (PFM) system with the following exceptions:

1) Information rate — 48.5 ± 5 percent data channels per second.

2) Reference frequency — above 15.5 kcps, noncoherent, ± 1 percent long-term stability.

3) Reference bursts are omitted for the second half of each frame, during which time data signals are continuously telemetered.

4) The command execute tone, at 3.62 kcps, replaces the PFM signal when it is detected by the command execute tone filter.

5) If the command being executed is operation of one of the four bipropellant motors, the amplitude of the telemetered command execute tone is attenuated. The attenuation control signal is taken from the motor solenoids. The degree of attenuation indicates which of the motors is operated.

6) Solar sensor pulses psi and psi-2 directly modulate the telemetry carrier.

Figure 4-33 is a block diagram of the Advanced Syncom telemetry encoder. The selection counter time base is provided by the central timer. The commutator, in conjunction with the selection counter, time-division-multiplexes the data to produce the PFM format. The reference and frame synchronization frequencies are obtained by applying the appropriate voltages to the subcarrier oscillator at the appropriate times. The dc to dc converter provides positive voltages which permit considerable simplification of the commutator and use of the subcarrier oscillator to generate the 4500 cps frame sync frequency.

The transducer excitation circuit provides an accurate -10 volt reference voltage for the temperature and pressure transducers. The solar sensor amplifier amplifies the psi and psi-2 pulses and directly modulates the telemetry carrier.

The telemetry format is shown in Table 4-5.

### Command Decoder Circuit Design

The preliminiary designs of the read tone circuits, the reset circuits, the clock circuits, the command register flip-flops with associated gating, the count inhibit power circuit, and the enable and matrix power circuits are complete. A re-evaluation of the interface between the command decoder and the rest of the spacecraft showed that a change in the configuration of the output of the decoder would simplify the interface problem and

# TABLE 4-5. ADVANCED SYNCOM TELEMETRY FORMAT

| Frame | Channel 0 | 1* | 2 | 3 | 4 | 5 | 6 | 7 | 8** | 9 | 10 | 11 | 12 | 13 | 14 | 15 |
|---|---|---|---|---|---|---|---|---|---|---|---|---|---|---|---|---|
| 0 | 000 | Space-craft ident | TM ident | TM calibration | | | | TM power out | Transponder No. 1 Received signal strength | | | | | | | |
| 1 | S | Bus No. 1 | | | Bus No. 2 | | | Spare | Transponder No. 2 Received signal strength | | | | | | | |
| | | Current | Battery No. 1 voltage | Battery No. 2 voltage | Current | Battery No. 1 voltage | Battery No. 2 voltage | | | | | | | | | |
| 2 | 100 | Decoder No. 1 | | Decoder No. 2 | | Decoder No. 3 | | Spare | Transponder No. 3 Received signal strength | | | | | | | |
| | | Enable, command register, mode | | Enable, command register, mode | | Enable, command register, mode | | | | | | | | | | |
| 3 | S | Decoder No. 4 | | $\psi_2$ angle | | | Bipropellant system No.1 | | Transponder No. 4 Received signal strength | | | | | | | |
| | | Enable, command register, mode | | | | | Fuel pres-sure | Fuel temper-ature | | | | | | | | |
| 4 | 010 | Bipropellant system No.1 | | Bipropellant system No. 2 | | | | Spare | Bus voltage Unregulated bus No. 1 | | | | | | | |
| | | Oxidizer | | Fuel | | Oxidizer | | | | | | | | | | |
| | | Pres-sure | Temp-erature | Pres-sure | Temp-erature | Pres-sure | Temp-erature | | | | | | | | | |
| 5 | S | PACE Lock, timer selection transmitter beam position | | | Trans-ponder 1 trans-mitter power | Trans-ponder 2 trans-mitter power | Trans-ponder 3 trans-mitter power | Trans-ponder 4 trans-mitter power | Bus voltage Unregulated bus No. 1 | | | | | | | |
| 6 | 011 | TWT Area Temperature | | | | Spares | | | Bus voltage Unregulated bus No. 2 | | | | | | | |
| | | No. 1 | No. 2 | No. 3 | No. 4 | | | | | | | | | | | |
| 7 | S | Solar panel temp-erature** | Structure temp-eratures*** | | | Spares | | | Bus voltage Unregulated bus No. 2 | | | | | | | |

*A typical channel for channels 1 through 7 is composed of a reference burst followed by a data burst.
**Channels 8 through 15 contain no reference bursts and, therefore, are composed entirely of continuous data bursts.
***Different sensor for each encoder.

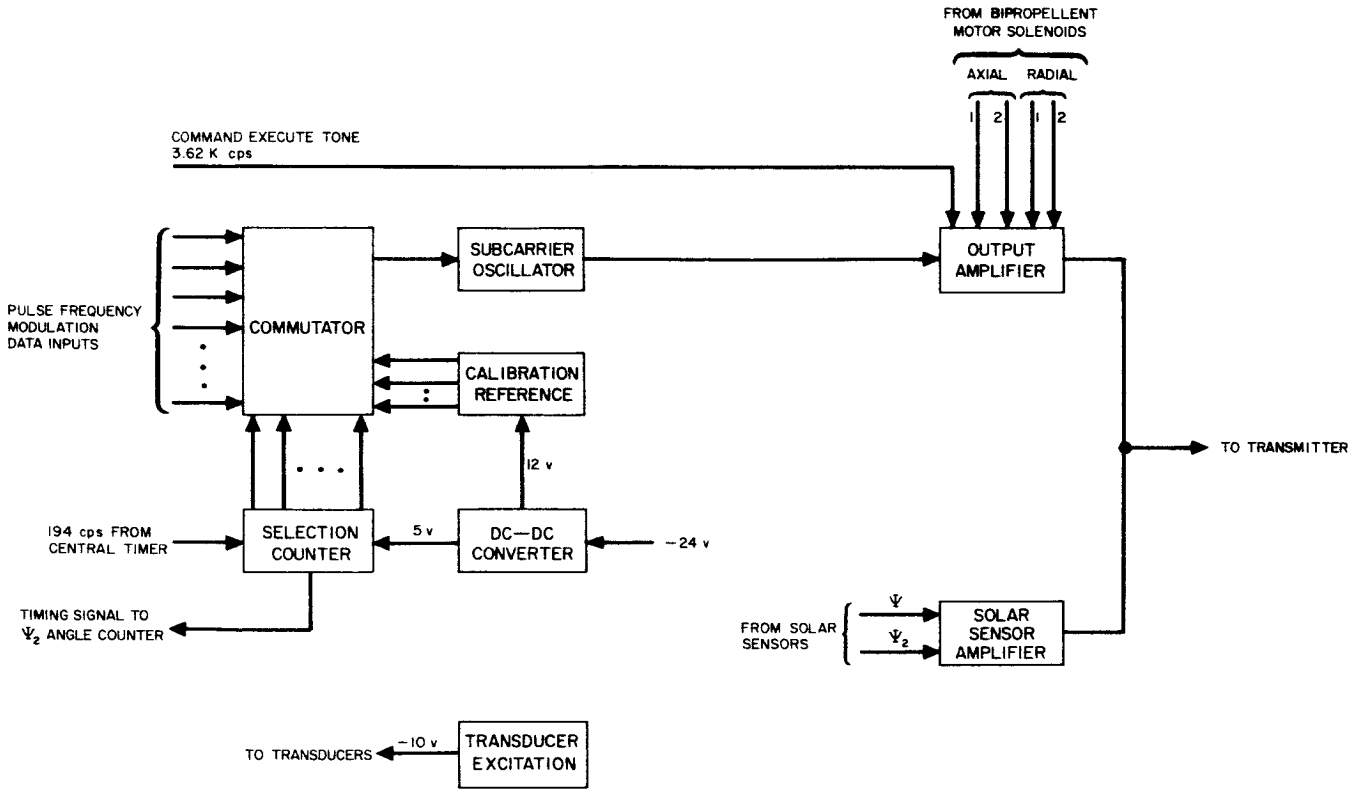


Figure 4-33. Advanced Syncom Telemetry Encoder Block Diagram

reduce the complexity of the interface circuitry. The configuration change in the output of the decoder made necessary several minor revisions in the output amplifier circuits. These changes are being made, and the output amplifiers are nearly complete.

The layouts of all circuits for which the preliminary design is complete are nearly finished. Fabrication of these circuits for the decoder breadboard will begin when the layout and wire list are complete.

### Telemetry Transmitter and Command Receiver

Fabrication of these units is proceeding on schedule. At the present time both units are in the sheet-metal (chassis and box) fabrication stage.

## ELECTRICAL POWER

### Simplified Electrical Power System

Further analysis has been conducted on the simplified system design as presented during the May Design Review. Figures 4-34, 4-35, and 4-36 are main array capabilities calculated for several temperatures. The main array bus voltages necessary to charge a 22-cell battery are superimposed on the array chacteristics. The array voltage plus the battery discharge diode logic drop is equal to the battery on-charge voltage.)

### Battery Cycling Tests

During the 24-hour cycling sequence, one of the Syncom I 0.81 amp-hr cells failed in a shorted condition and was removed from the test. The cycling sequence is not considered to have precipitated the failure. (One of the predominate failure modes of this cell is to fail shorted.)

The end-of-charge and end-of-discharge voltages are plotted in Figure 4-37. At the end of the 28 cycles shown, a rated discharge test was conducted (see Figure 4-38). Under the low rates of the test cycle, the battery effective capacity decreased from normal (see curve) because of the memory effects exhibited by nickel-cadmium cells. The battery capacity returned to normal when operated through a full charge-discharge cycle (see dates on curve).

The General Electric 12 amp-hr cells were started on the 24-hour synchronous orbit cycle (see Figure 4-39). At this point insufficient data is available to support conclusions. Tests will be started in August to determine the amp-hr efficiency of the General Electric cells as a function of charge rate, and also the effect of reduction of on-charge voltage on the battery capacity operating point.

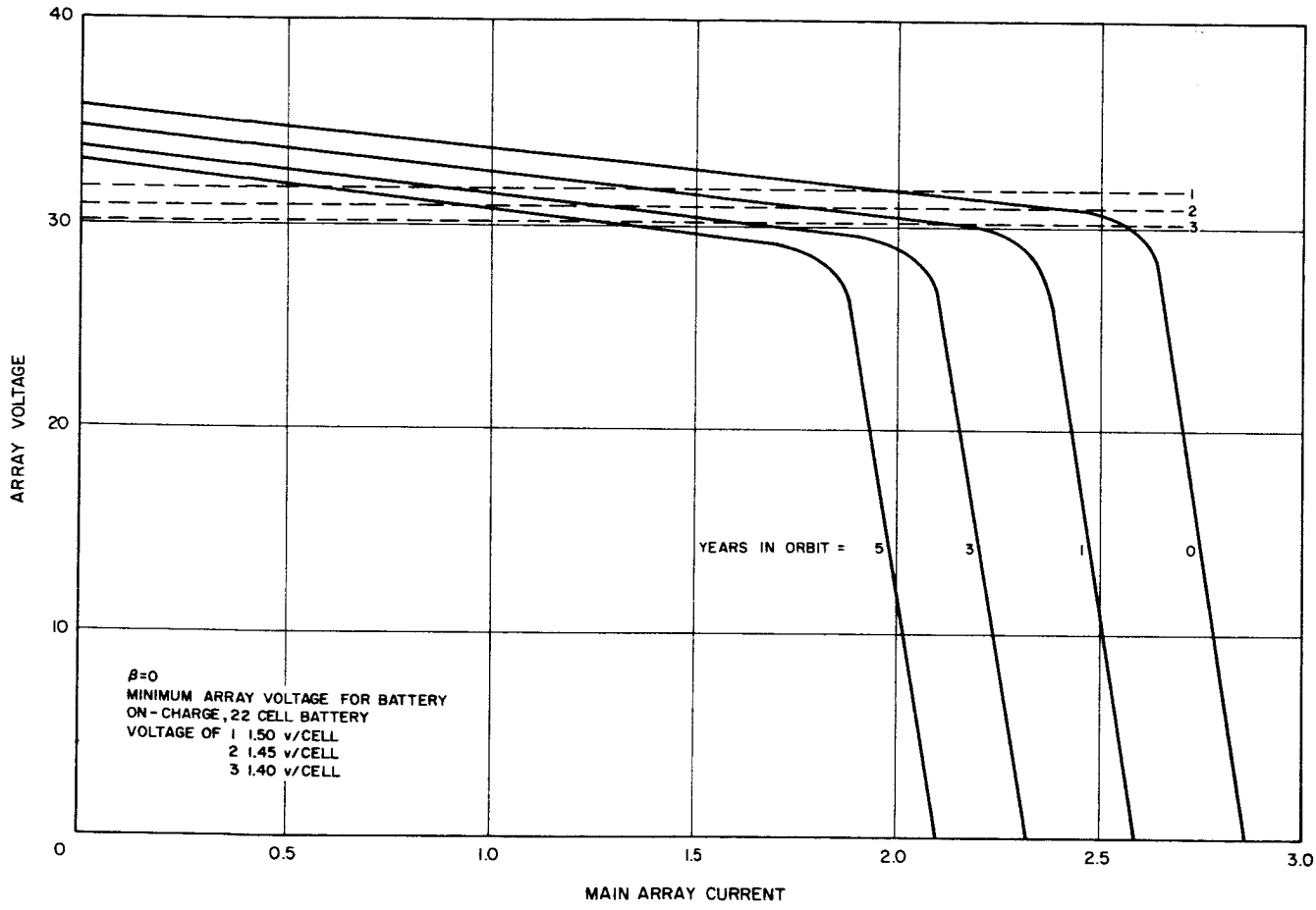


Figure 4-34. Solar Array Characteristics, 60° F

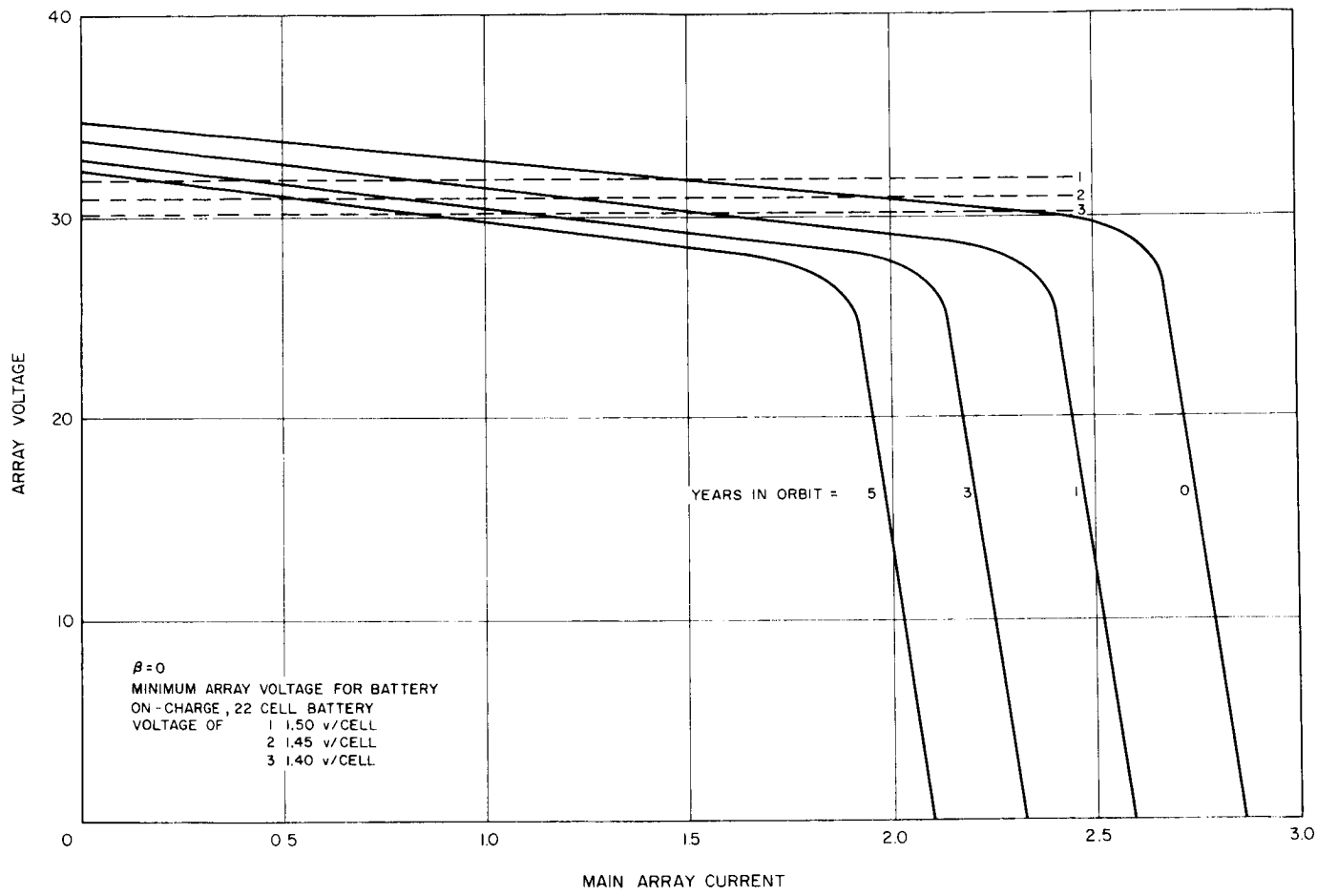


Figure 4-35. Solar Array Characteristics, 70° F

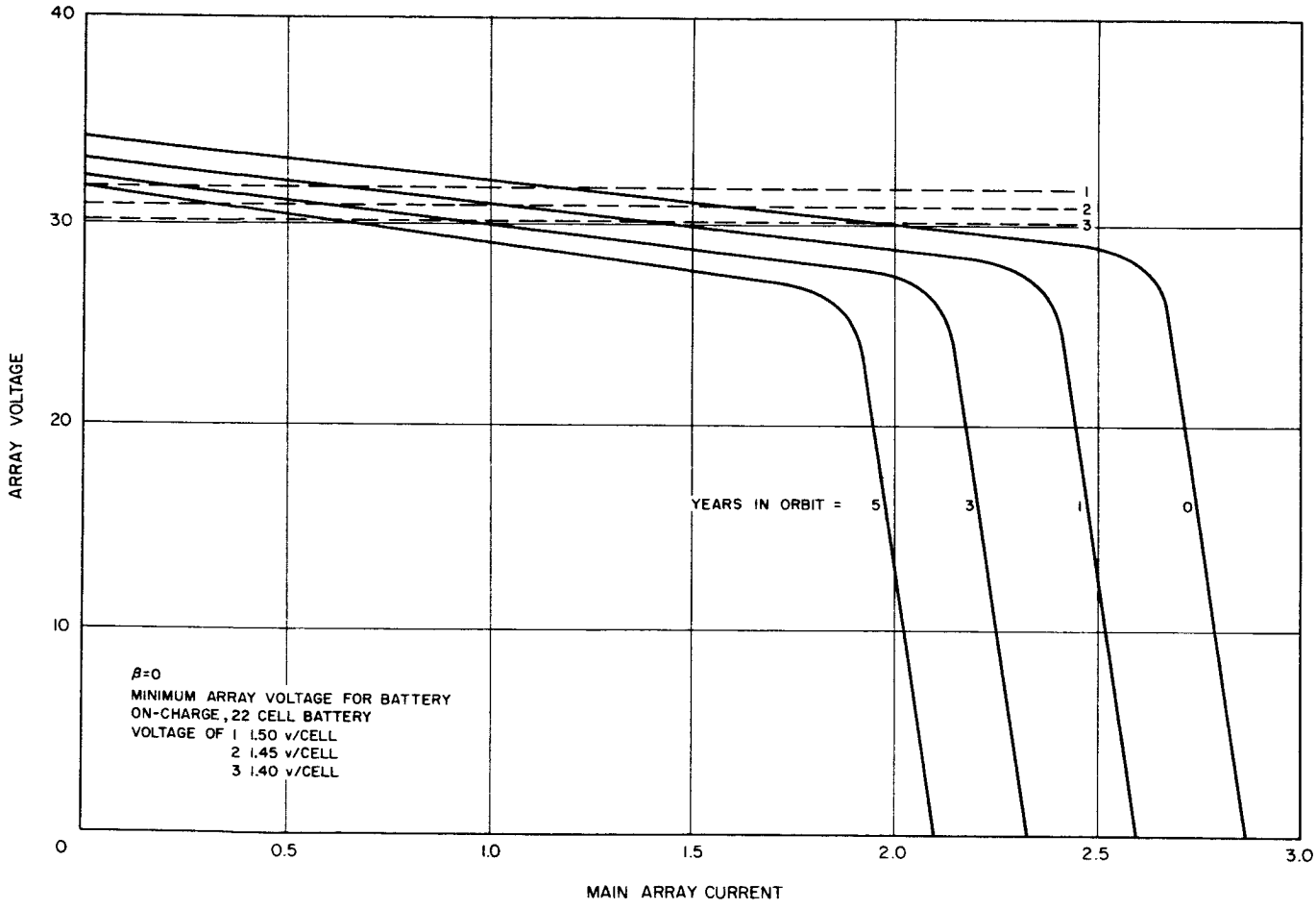


Figure 4-36. Solar Array Characteristics, 77° F

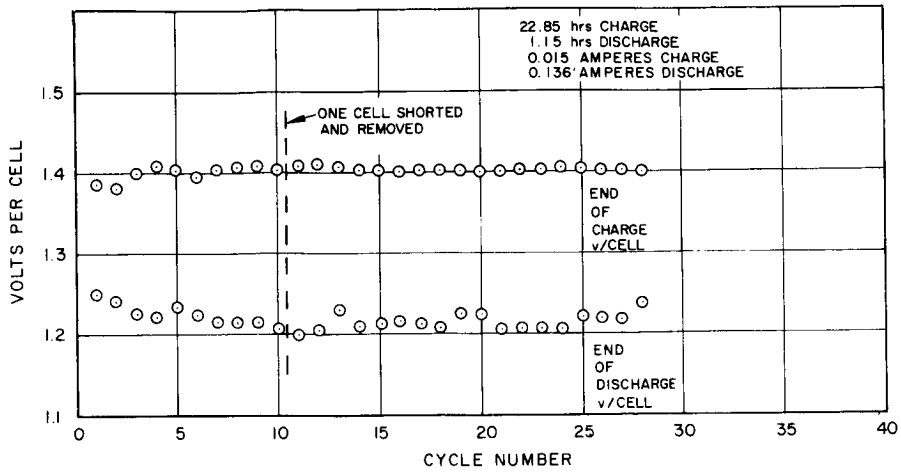


Figure 4-37. Syncom I Battery Test

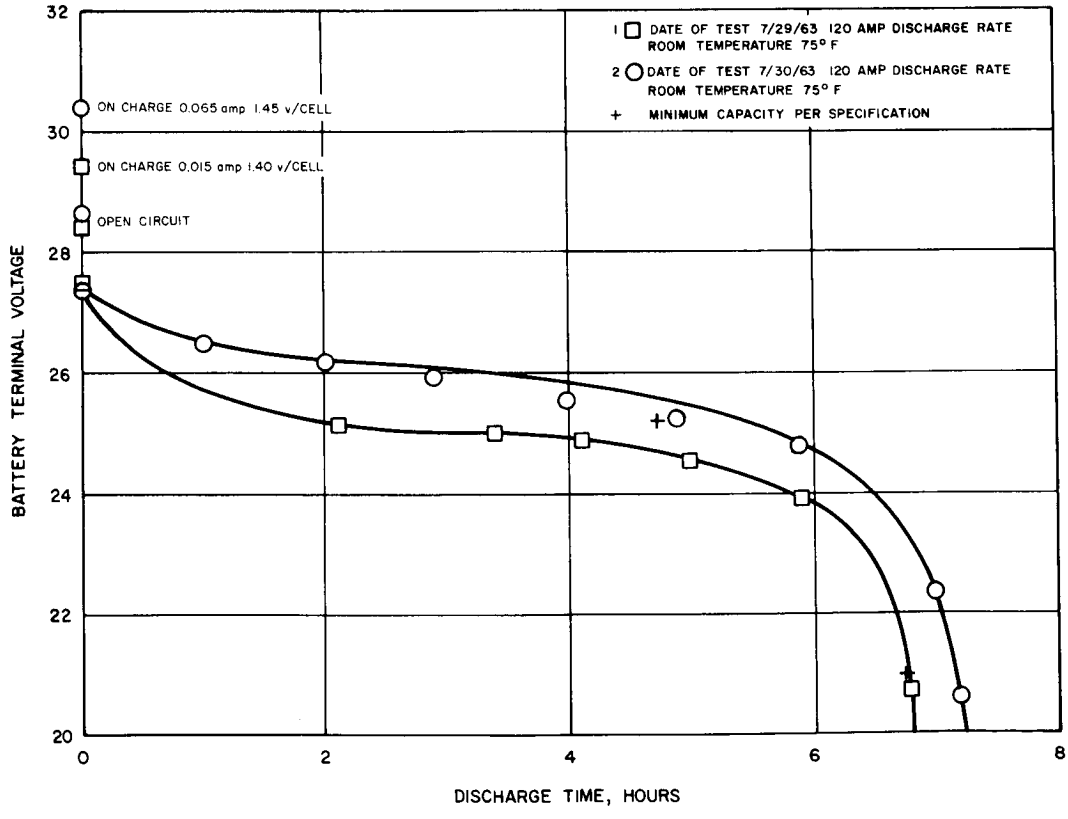


Figure 4-38. Nicad Battery Discharge Curve

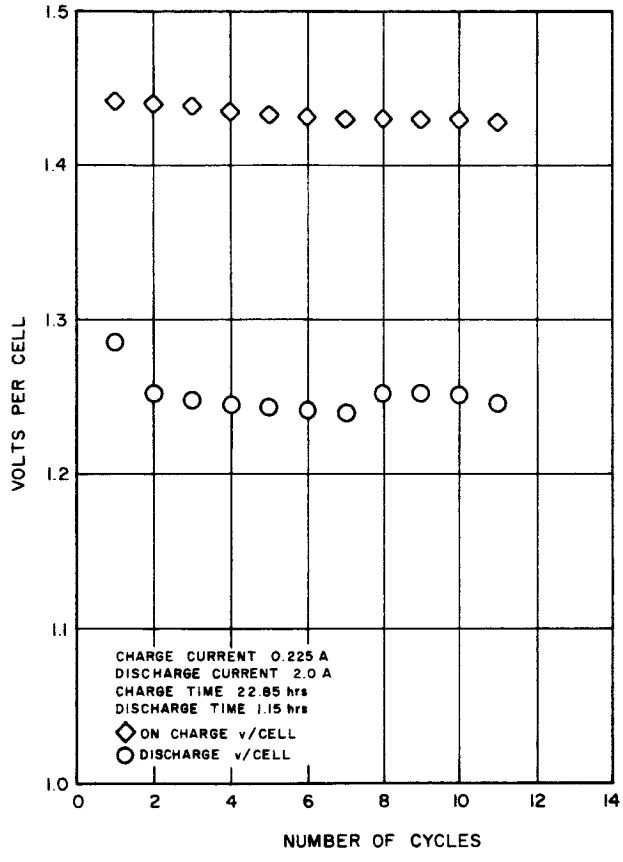


Figure 4-39. General Electric
12 Amp-Hr, 22-Cell Battery

Figures 4-40 and 4-41 depict the test setup and show the power supplies, automatic cycle timers, and current limiters used in the test. Figure 4-42 is a photograph of the General Electric 12 amp-hr cells (in restraining cases) in the temperature-controlled test facility.

### Fabrication Status of Two Battery Strings

Source selection should be completed during the month of August and cells ordered at that time.

## STRUCTURE

### Structural Design

#### Redesign

The general structure arrangement is essentially unchanged from the previous report. The design effort has been directed toward the refinement of the structure to provide a greater degree of homogeneity to the primary structure and to reduce its weight. Minor revisions have been made in the arrangement of structure to provide continuity and eliminate or reduce load eccentricity. Excess material is being trimmed from presently designed parts and, where a reduction of weight may be accomplished and heat conductivity is not a criterion, aluminum alloy parts have been changed to magnesium alloy.

The interface between the spacecraft and the Agena interconnect structure has been revised to reduce weight of the spacecraft at the interface and to provide higher reliability against tip-off during separation. The aft thrust tube and radial bulkhead structure have been revised to provide greater clearance for the trajectory of the V clamp assembly at separation. This revision is shown in Figure 4-43.

The structure arrangement was presented to a comprehensive Design Review Board for a review prior to detail design and engineering drawings. As a result of Board comments, flexibility will be maintained during the engineering drawing period that will permit design for greater transmissibility of heat through the structural joints and allow for an increased amount of heat insulation between the structure and the apogee motor case.

#### Engineering Drawings

Approximately 80 percent of the investigations, layout, and coordination of the design has been accomplished, and about 10 percent of the manufacturing drawings have been completed.

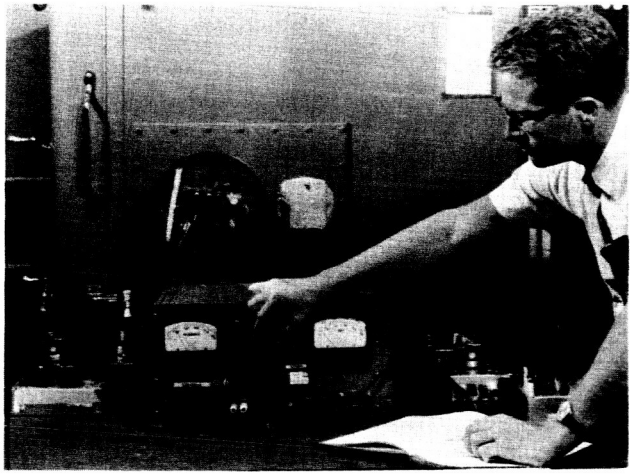

Figure 4-40. Battery Cycling Test Power Supplier

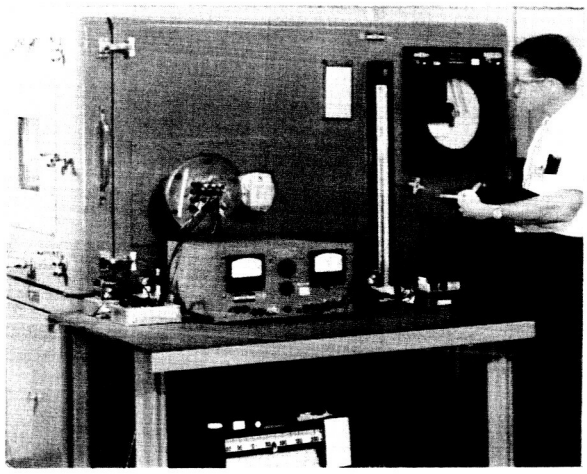

Figure 4-41. Battery Cycling Test Equipment

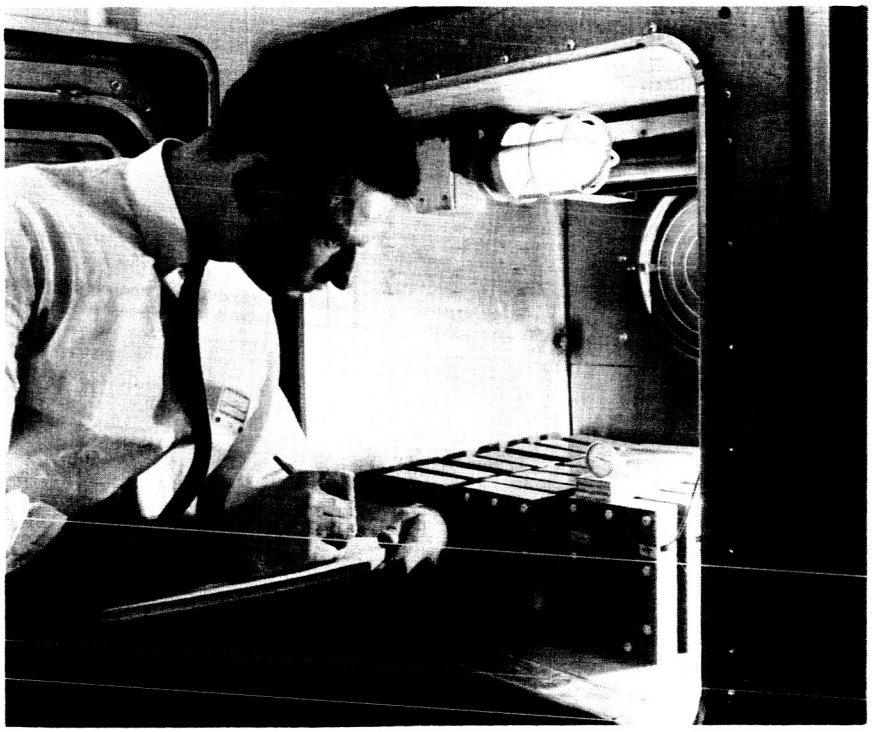

Figure 4-42. General Electric Batteries on Cycling Test

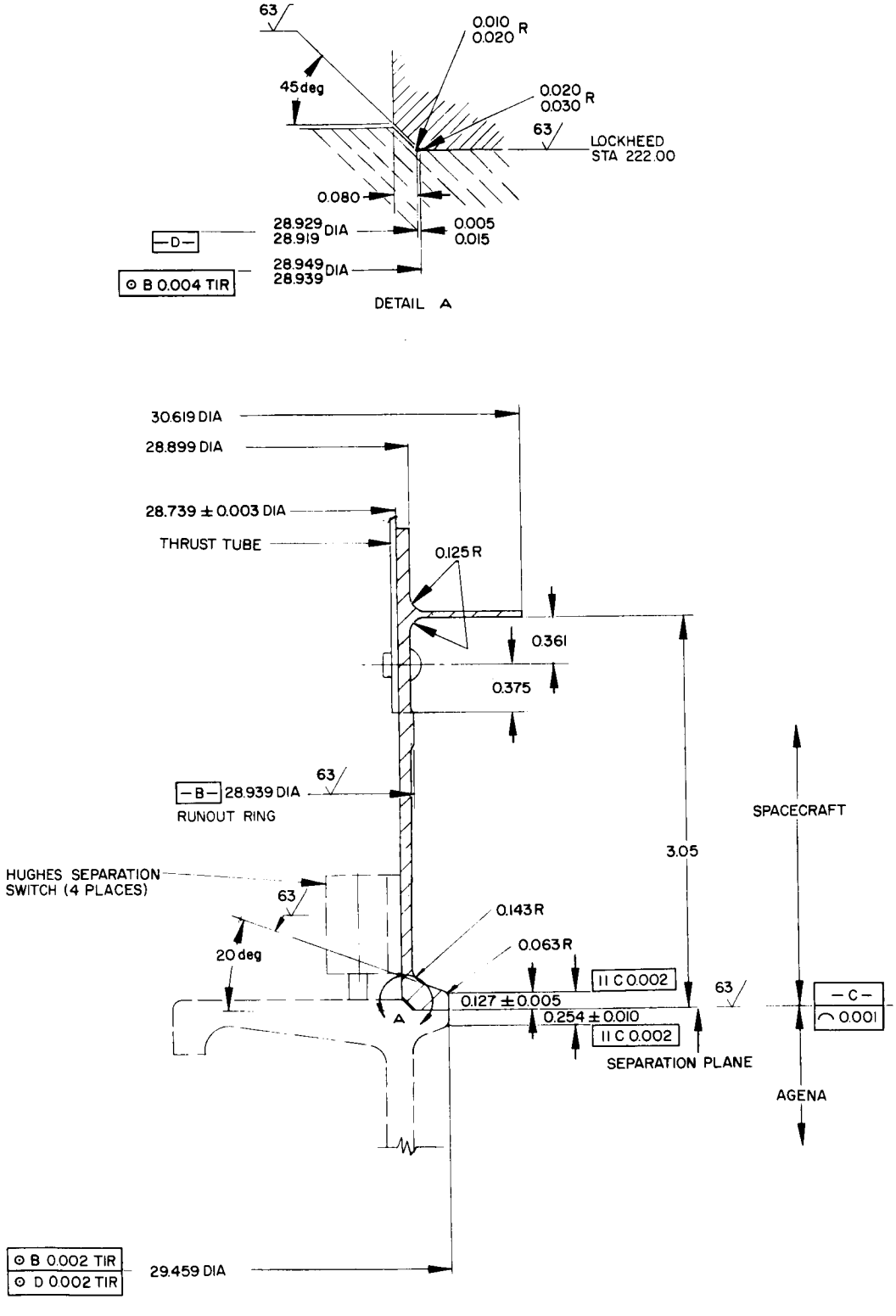


Figure 4-43. Spacecraft – Booster Interface

## Structural Analysis

Stress effort during this report period has been concentrated in four areas.

1) Analysis of the three-point support solar panel has been completed, and drawings have received stress approval. Analysis is proceeding on the brackets attaching the panels to the basic structure.

2) Analysis of the forward equipment support structure is continuing on the basis that the tubular truss structure will be used.

3) The thrust tube ring is being analyzed for loads transferred through the interconnect structure.

4) Preliminary gauges have been chosen for the thrust tube and bulkhead stiffener ribs. These are subject to change, pending further parametric studies to be performed with the dynamic model.

## Structural Dynamic Tests and Analyses

A preliminary structural dynamic analysis has been completed on the T-2 vehicle. All studies were performed on models cantilevered from the interface. During this period the 6 degree-of-freedom lateral model was expanded to 10 degrees of freedom, and a 5 degree-of-freedom longitudinal system was established.

In order to easily calculate the fundamental modes and quickly conduct parametric studies, simple 3 degree-of-freedom systems in both the longitudinal and lateral directions were established. These systems gave results almost identical to their larger counterparts. The response of the system to various force inputs and the effect of material gauge changes on the fundamental frequency will be studied.

Preliminary Comparison of T-1 and T-2. The thrust tube is the predominant structural element in the cantilevered system. It was thought that the bulkhead stiffener ribs added stiffness to the thrust tube, but T-1 studies indicate otherwise. Table 4-6 compares the fundamental frequencies obtained during T-1 and shows calculated T-1 frequencies, and fundamental frequencies calculated for T-2.

TABLE 4-6 FUNDAMENTAL FREQUENCY COMPARISON

| | Test | T-1 (analytical) | | T-2 (analytical) | |
|---|---|---|---|---|---|
| | | No Rib Action | Estimated Rib Action | No Rib Action | Estimated Rib Action |
| Longitudinal | 125 | 135 | 182 | 139 | 170 |
| Lateral | 47 | 48 | 67 | 50 | 64 |

The frequency studies show that the T-2 model has approximately the same fundamental frequency as the T-1 model. Examination of the mode shapes indicates flexibility in the forward structure of T-2.

In addition to the studies indicated above, a study of the fundamental torsional frequencies will be conducted.

## Design Loads and Recommendations

Acceleration levels are presented here for the Syncom II HSX-302-F2 configuration, based on qualification level vibration tests of the T-1 vehicle. The levels represent a partial reduction of test data (responses to excitation at the apogee motor interface are not included) and will be revised and supplemented as additional information becomes available. Some differences are to be expected between the data presented and the levels measured on the T-2 vehicle because of differences in configuration. The following acceleration data are included:

1) Sinusoidal and random qualification test input spectra for the complete spacecraft (Figure 4-44).

2) Design vibratory accelerations for component supports and basic structure (Tables 4-7, 4-8 and 4-9).

3) Sinusoidal and random qualification test spectra for components (Figures 4-45 through 4-53). The sinusoidal tests are to be performed at a logarithmic sweep rate of 2 octaves per minute, 4.35 minutes duration per axis. Random tests are to be of 6 minutes duration. Lateral tests are to be performed on two lateral axes having an included angle of 45 degrees.

The following are criteria for application of these accelerations to the components and structure:

1) All loads given are ultimate loads (i.e., 1.5 times maximum anticipated flight loads).

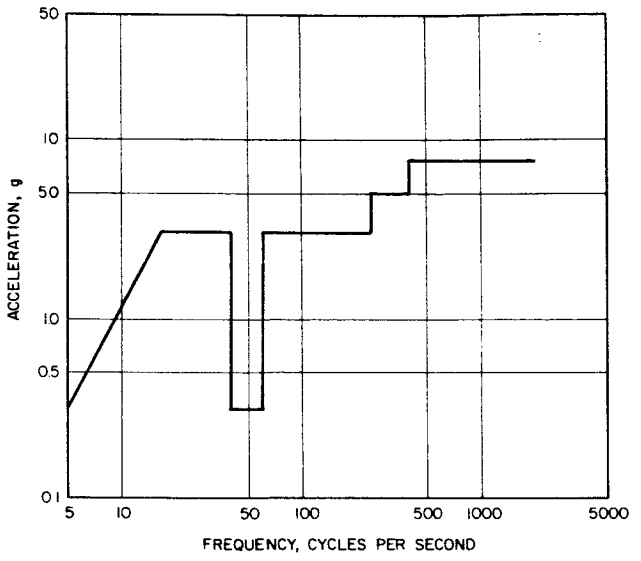


a) Lateral Axes Input at the Agena Interface

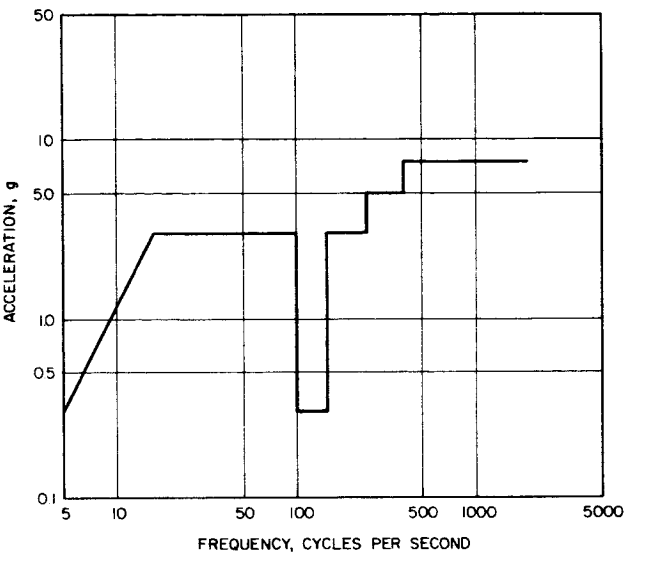


b) Longitudinal Axes Input at the Agena Interface

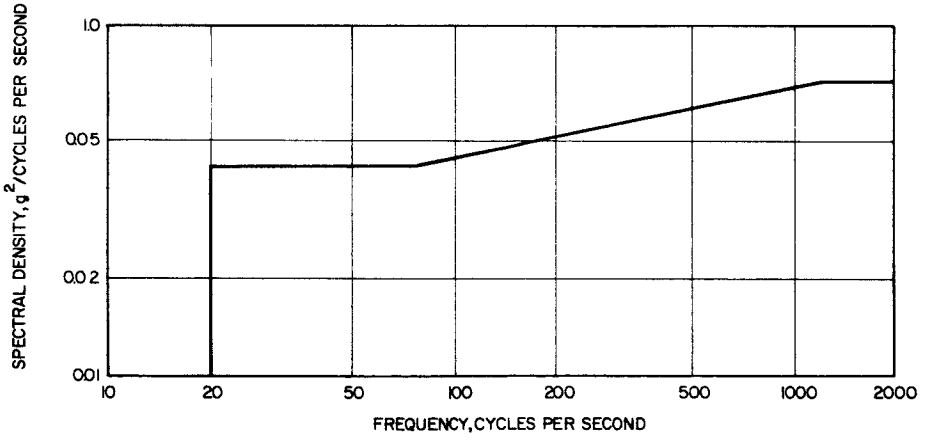


c) Longitudinal and Lateral Axes Input at the Agena Interface or Apogee Motor Attachments

Figure 4-44. Spacecraft Sinusoidal Qualification Test Spectrum

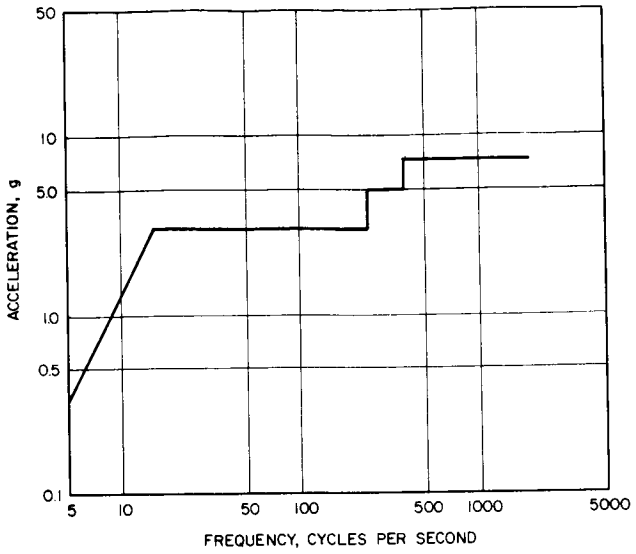


a) Longitudinal and Lateral Sinusoidal Qualification Test Spectra

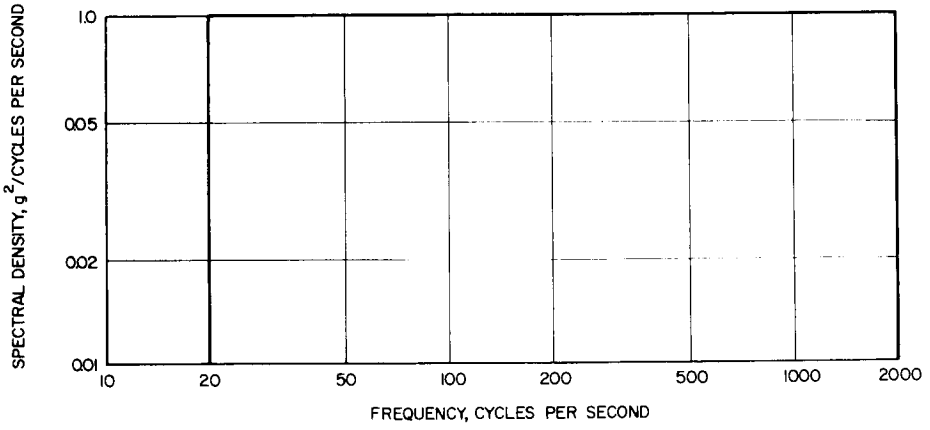


b) Longitudinal Random Qualification Test Spectrum

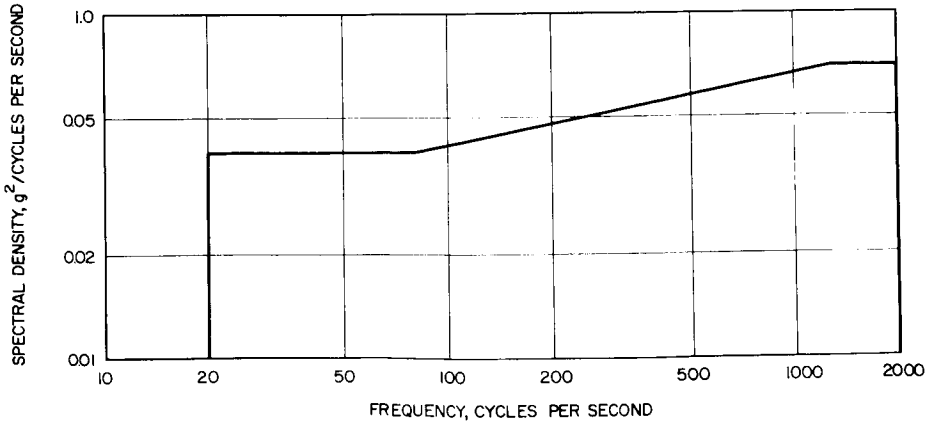


c) Lateral Random Qualification Test Spectrum

Figure 4-45. Apogee Motor Attachment

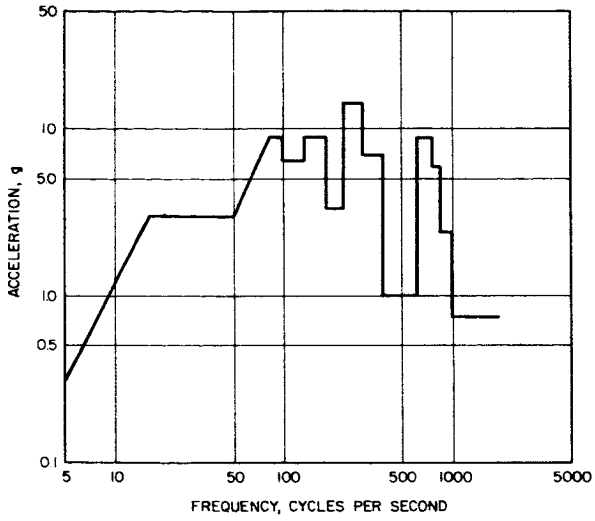


a) Longitudinal Sinusoidal Qualification Test Spectrum

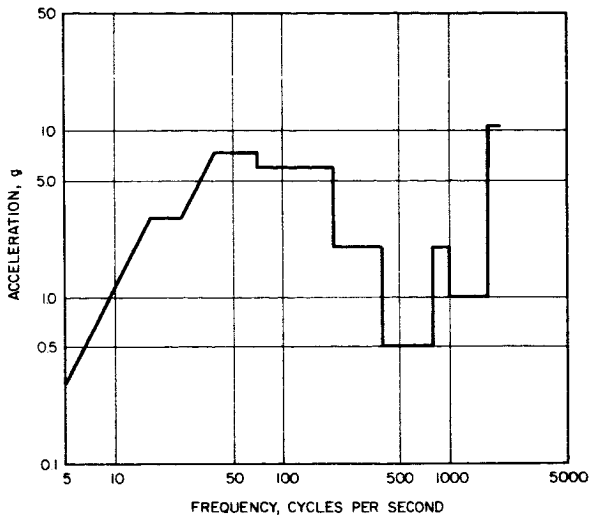


b) Lateral Sinusoidal Qualification Test Spectrum

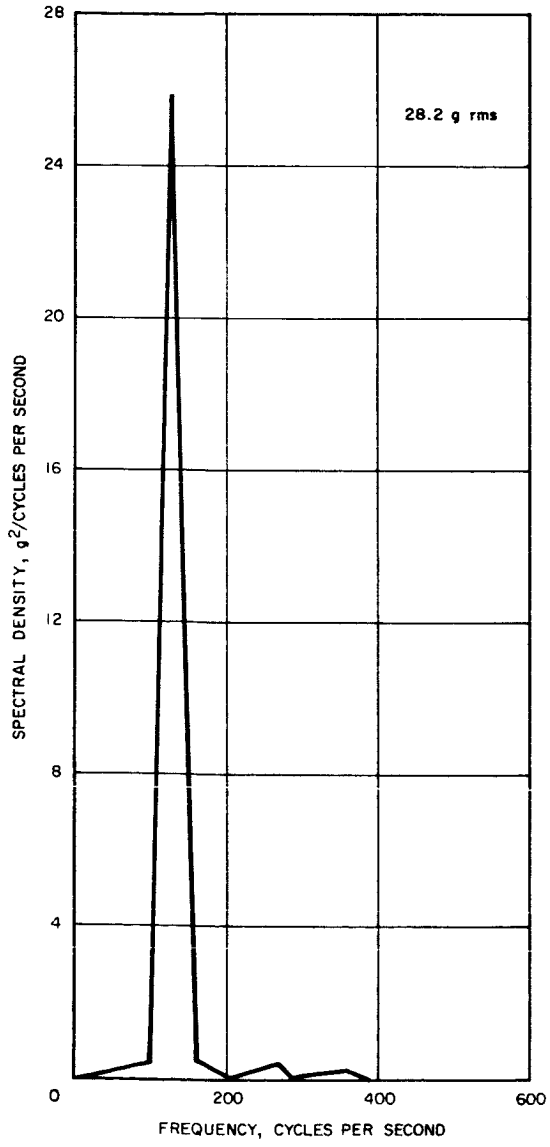


c) Longitudinal Random Qualification Test Spectrum

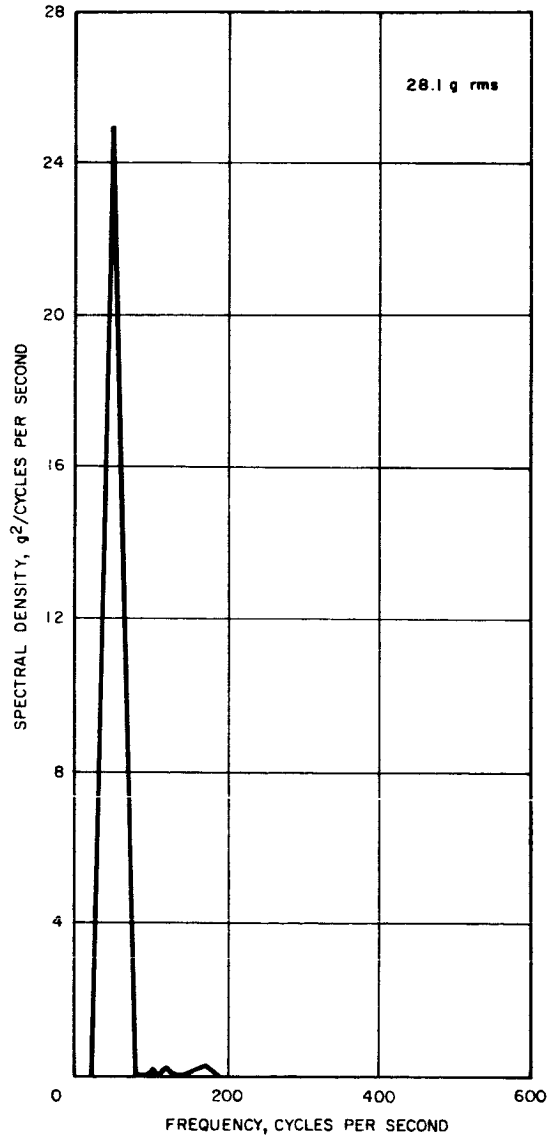


d) Lateral Random Qualification Test Spectrum

Figure 4-46. Apogee Motor Nozzle Attachment

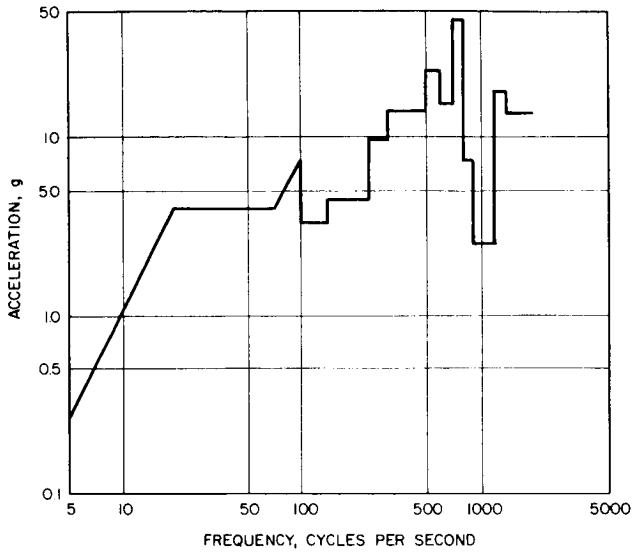


a) Longitudinal Sinusoidal Qualification Test Spectrum

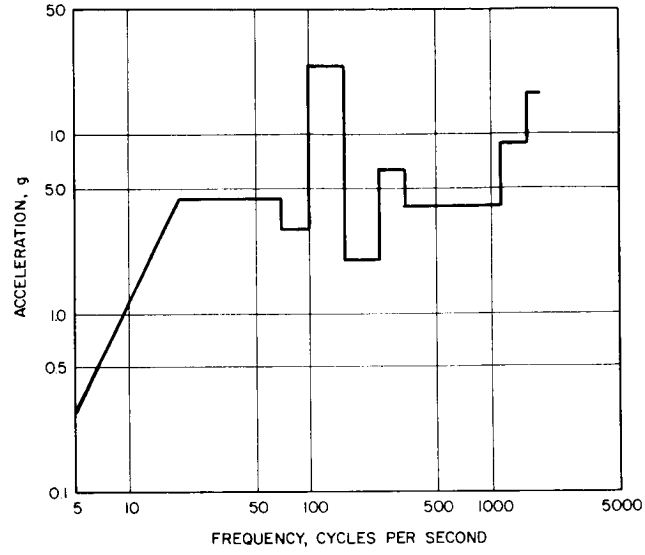


b) Lateral Sinusoidal Qualification Test Spectrum

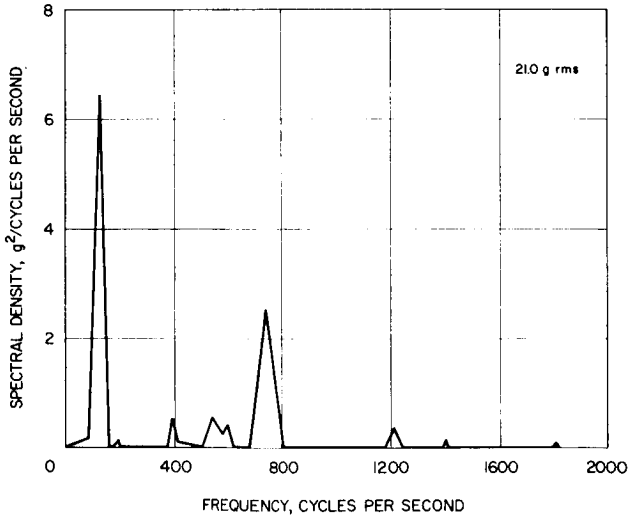


c) Longitudinal Random Qualification Test Spectrum

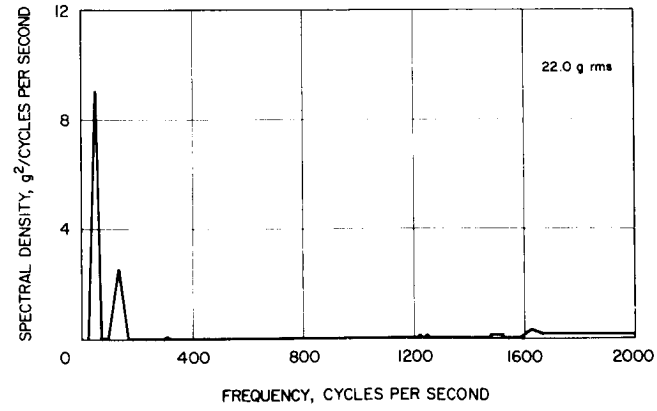


d) Lateral Random Qualification Test Spectrum

Figure 4-47. Quadrant Electronics Package and Fuelled Bipropellant Tank

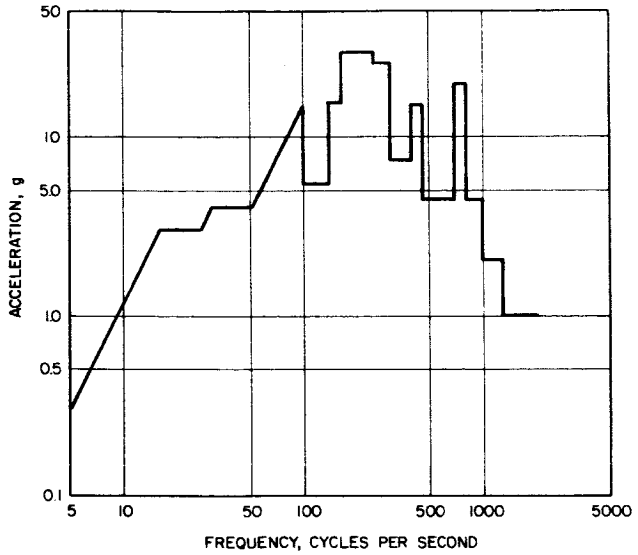


a) Longitudinal Sinusoidal Qualification Test Spectrum

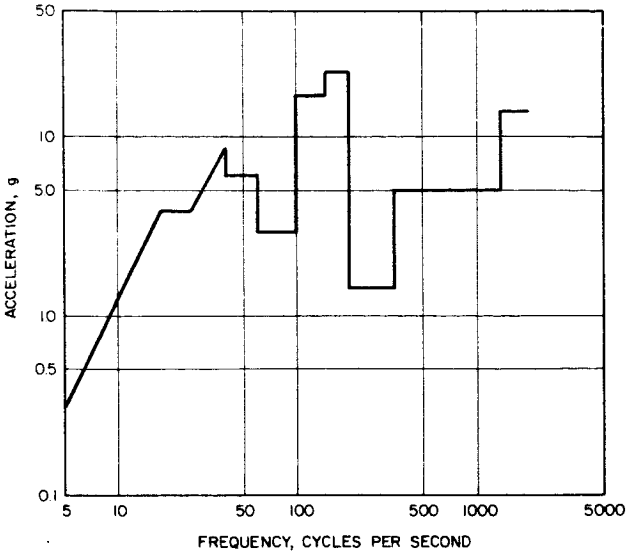


b) Lateral Sinusoidal Qualification Test Spectrum

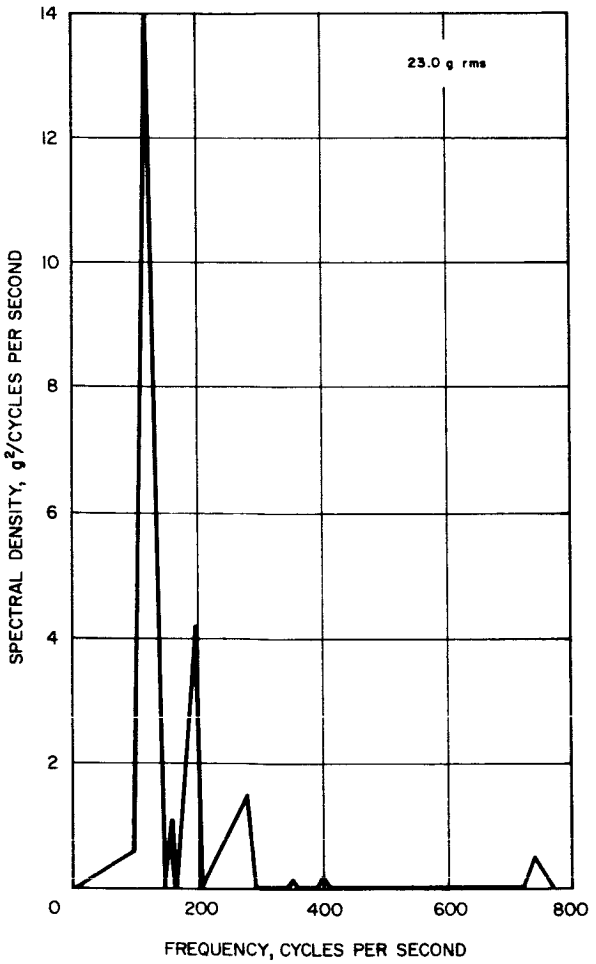


c) Longitudinal Random Qualification Test Spectrum

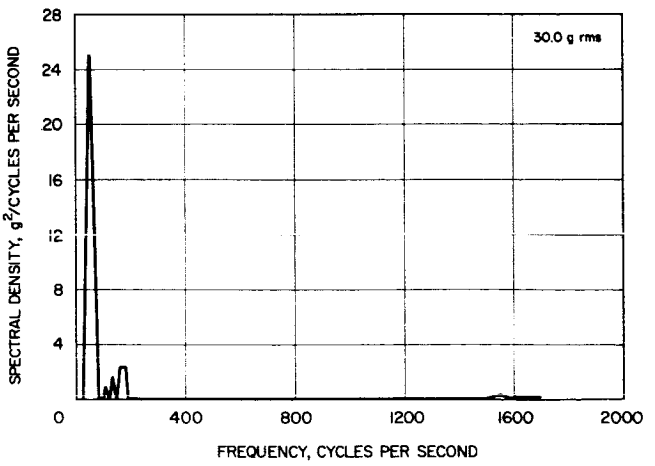


d) Lateral Random Qualification Test Spectrum

Figure 4-48. Forward Battery Pack Center of Gravity

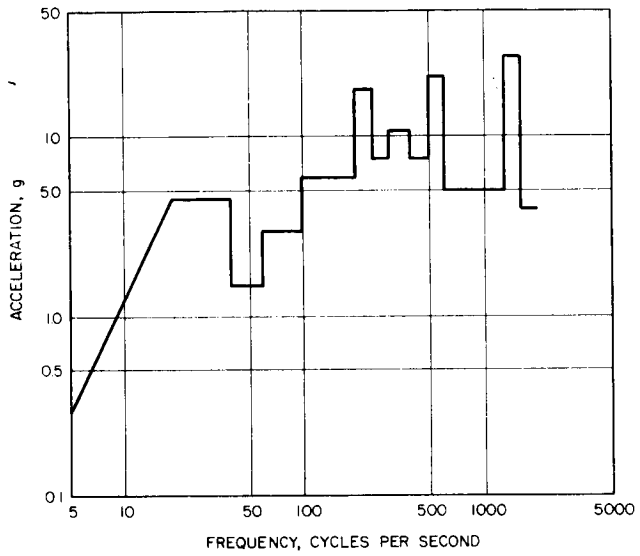


a) Lateral Sinusoidal
Qualification Test Spectrum

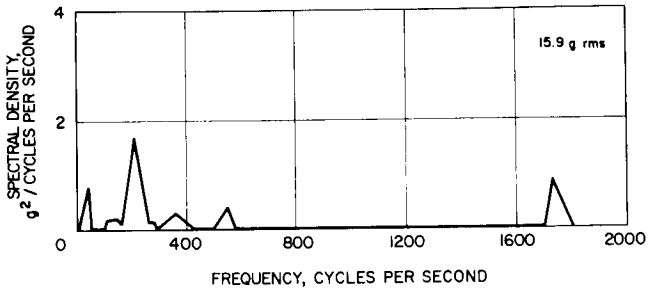


b) Lateral Random
Qualification Test Spectrum

Figure 4-49. Aft Battery Pack Center of Gravity

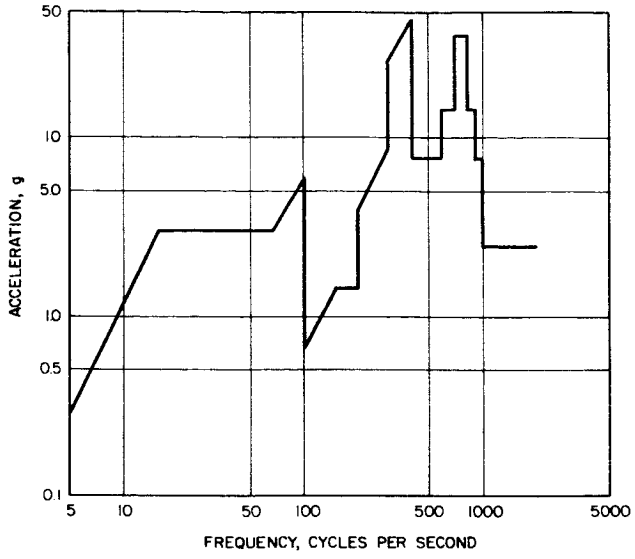


a) Longitudinal Sinusoidal Qualification Test Spectrum

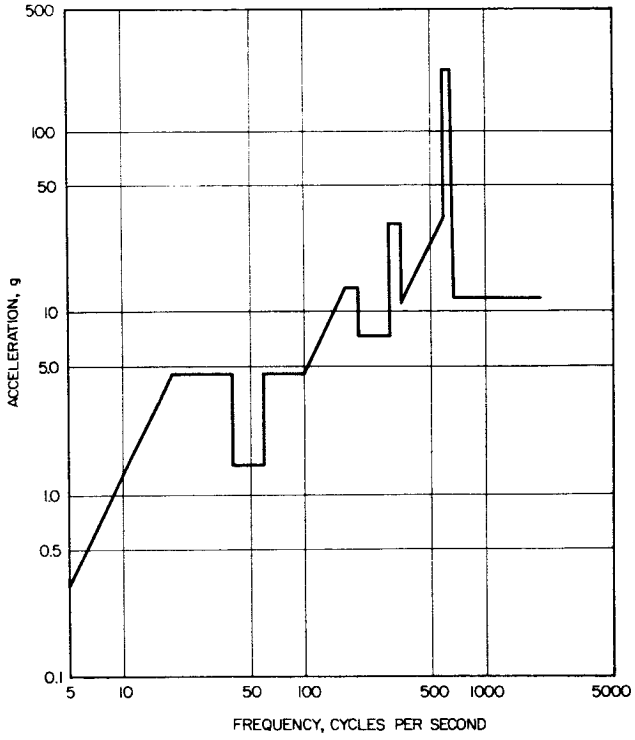


b) Lateral Sinusoidal Qualification Test Spectrum

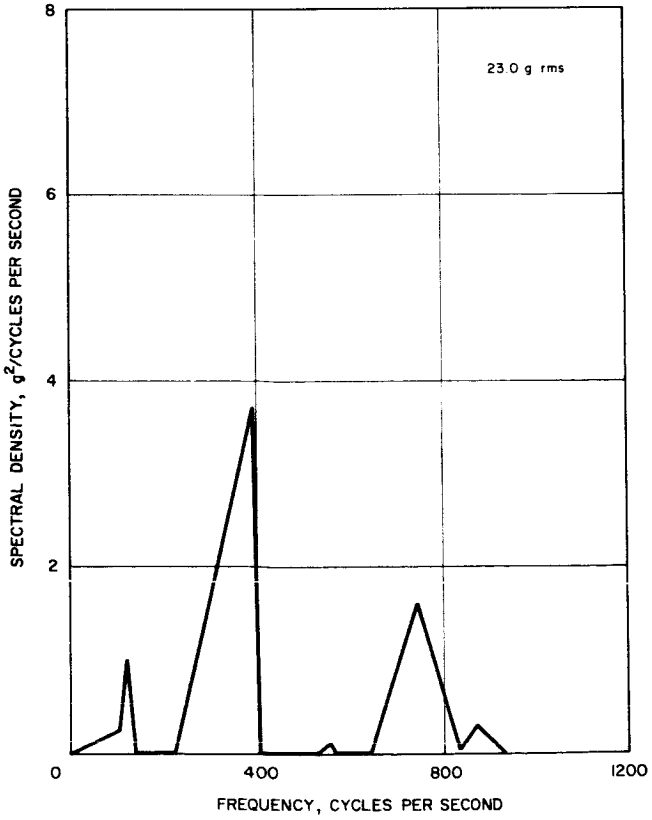


c) Longitudinal Random Qualification Test Spectrum

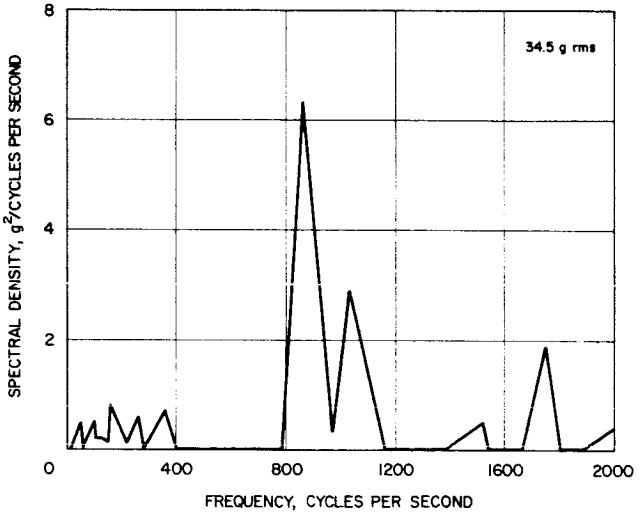


d) Lateral Random Qualification Test Spectrum

Figure 4-50. Traveling-Wave Tube Power Supply

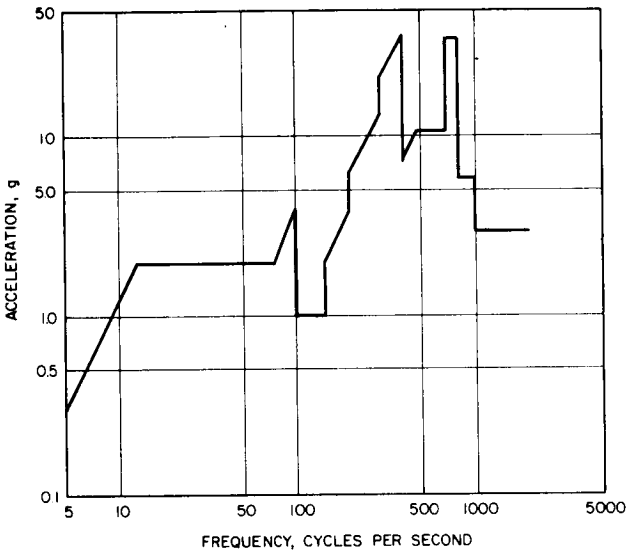


a) Longitudinal Sinusoidal Qualification Test Spectrum

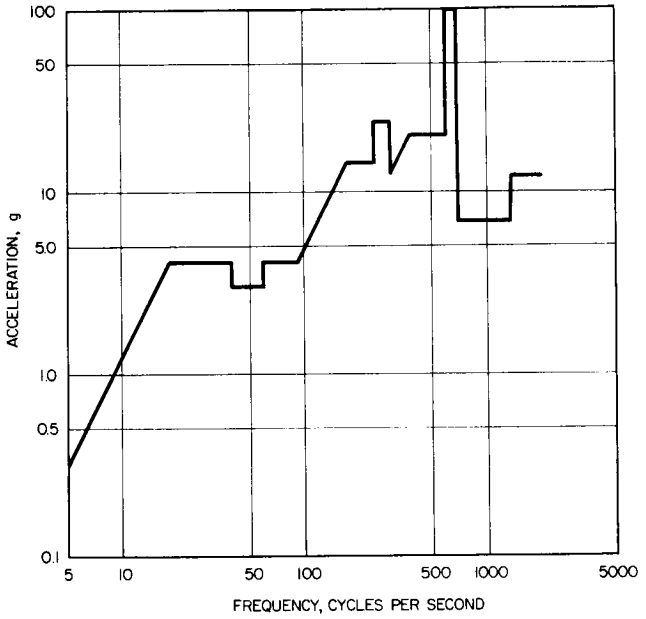


b) Lateral Sinusoidal Qualification Test Spectrum

Figure 4-51. Traveling-Wave Tube and Rib-Mounted Antenna Electronic

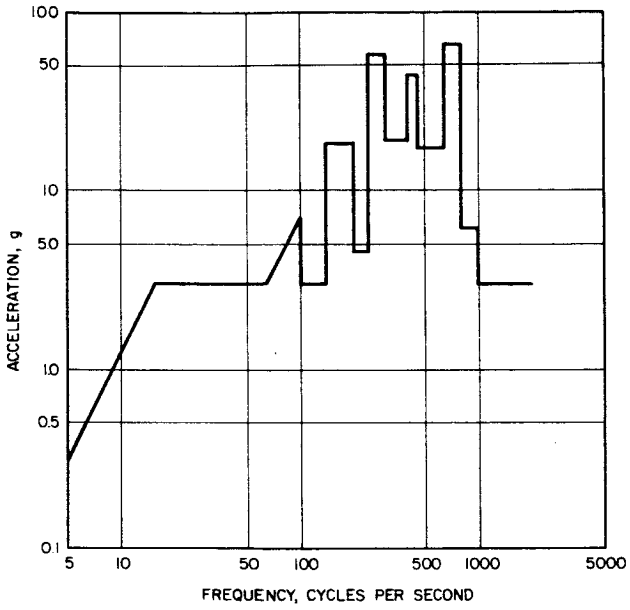


a) Longitudinal Sinusoidal Qualification Test Spectrum

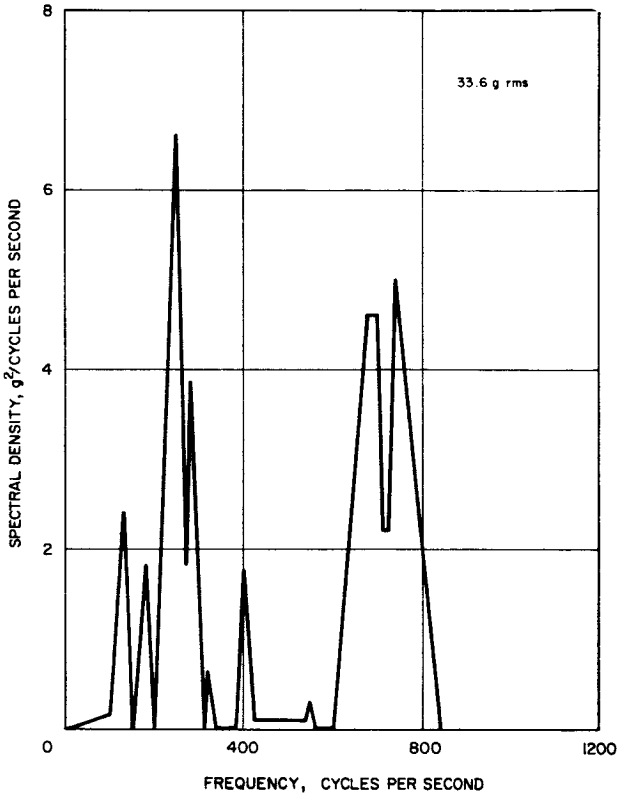


b) Longitudinal Random Qualification Test Spectrum

Figure 4-52. Communication Antenna Attachment

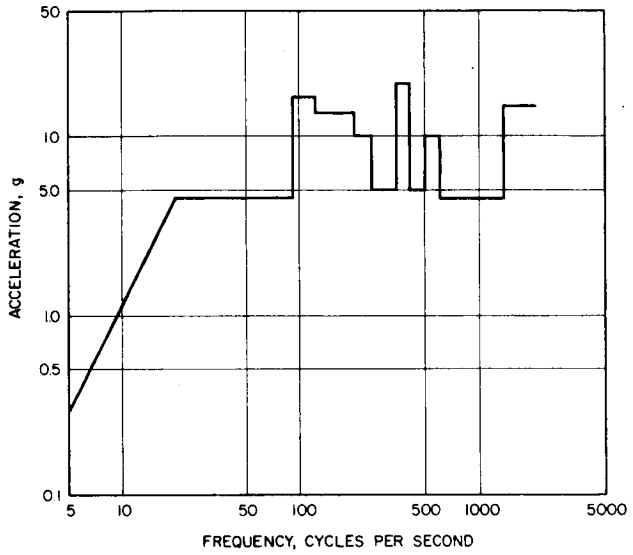


a) Lateral Sinusoidal
Qualification Test Spectrum

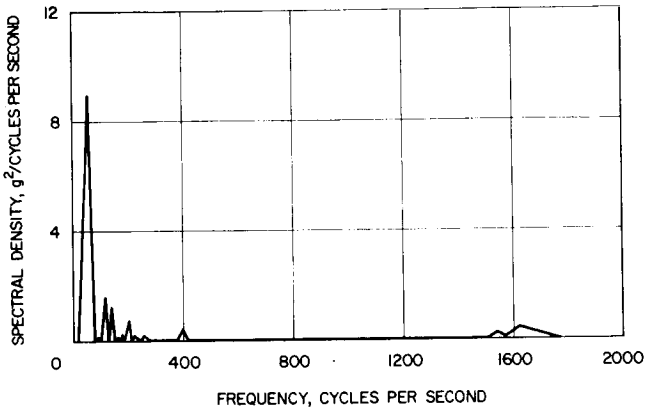


b) Lateral Random
Qualification Test Spectrum

Figure 4-53. Forward Solar Panel – Forward Attachment

2) Vibratory levels given in Tables 4-7, 4-8, or 4-9 are to be superimposed on the simultaneously applied longitudinal and lateral quasi-static accelerations for design purposes. Possible combinations of qualification level quasi-static accelerations are given below.

3) Component vibratory accelerations act through the component center of gravity (or through the attachments to basic structure), as specified in the figures. Basic structure includes trusswork, quadrant electronics support brackets, aft bulkhead, ribs, and thrust tube.

4) Lateral accelerations act in any radial direction unless otherwise indicated. Longitudinal accelerations act along the thrust axis. Longitudinal and lateral vibratory accelerations are separately applied.

5) Random and sinusoidal accelerations are separately applied.

6) The vibratory accelerations given in Tables 4-8 and 4-9 are applied as follows:

   a) The accelerations under each frequency heading are separately applied.

   b) The directions of the applied accelerations are indicated by the upper or lower set of algebraic signs. For example, all of the accelerations at 125 cps are in phase.

The random acceleration levels given in Table 4-9 assume that the rms ($1\sigma$) response in a frequency band of $2\Delta f$ at a frequency f is

$$\left[\int_{f-\Delta f}^{f+\Delta f} \Phi_o \, df\right]^{1/2}$$

where $\Phi_o$ is the response acceleration spectral density and $2(\Delta f)$ is a narrow frequency band around f. The accelerations shown in Table 4-9 are 3 levels.

The following are design recommendations based on observation of the spacecraft during vibration testing at qualification levels:

1) The sun sensor bracket thickness should be increased. The bracket failed during sinusoidal vibration tests.

TABLE 4-7. DESIGN VIBRATORY ACCELERATIONS FOR COMPONENT ATTACHMENTS

MAXIMUM SINUSOIDAL OR $3\sigma$ RANDOM

| Component | Longitudinal g | Lateral g |
|---|---|---|
| Antenna compartment attachment | 120 | 33 |
| Communication antenna attachment | 101 | - |
| Traveling-wave tube attachment | 120 | 85 |
| Rib-mounted antenna electronics attachment | 40 | 85 |
| Traveling-wave tube power supply attachment | 120 | 104 |
| Forward battery pack center of gravity | 69 | 90 |
| Aft battery pack center of gravity | 69 | 48 |
| Loaded propellant tank attachment | 63 | 66 |
| Quadrant electronics attachment | 63 | 66 |
| Apogee motor attachment | 88 | 47 |
| Apogee motor nozzle attachment | 85 | 84 |
| Solar panel attachment | - | 64 |
| Orientation rocket platform | 98 | - |

TABLE 4-8. DESIGN VIBRATORY ACCELERATIONS FOR BASIC STRUCTURE

SINUSOIDAL INPUT AT THE AGENA INTERFACE

| Component | Longitudinal 0 to peak g | | | Lateral 0 to peak g | | |
|---|---|---|---|---|---|---|
| | 125 cps | 190 cps | 270 cps | 50 cps | 100 cps | 140 cps |
| Antenna compartment attachment | ±1.5 | ± 1.5 | ∓ 7 | ±1.5 | ± 4.5 | ± 8 |
| Communication antenna attachment | ±3.0 | ∓19.0 | ∓57 | ±1.5 | ± 4.5 | ± 8 |
| Traveling-wave tube attachment | ±1.0 | ± 4.0 | ∓12 | ±3.0 | ∓ 5.0 | ± 9 |
| Rib-mounted antenna electronics attachment | ±1.0 | ± 4.0 | ∓12 | ±3.0 | ∓ 5.0 | ± 9 |
| Traveling-wave tube power supply attachment | ±2.0 | ± 4.0 | ∓ 7 | ±1.5 | ± 4.5 | ± 8 |
| Forward battery pack center of gravity | ±5.5 | ∓30.0 | ±27 | ±6.5 | ∓ 3.0 | ±18 |
| Aft battery pack center of gravity | | | | ±1.5 | ± 6.0 | ± 6 |
| Loaded propellant tank center of gravity | ±3.5 | ± 4.5 | ±10 | ±4.5 | ∓23.0 | ∓23 |
| Quadrant electronics attachment | ±3.5 | ± 4.5 | ±10 | ±4.5 | ∓23.0 | ∓23 |
| Apogee motor attachment | ±2.0 | ± 2.0 | ± 9 | ±3.5 | ∓ 3.5 | ± 2 |
| Apogee motor nozzle attachment | ±6.5 | ∓ 9.0 | ±15 | ±7.5 | ± 6.0 | ∓ 6 |
| Solar panel attachment | | | | ±4.5 | ∓18.0 | ±15 |

TABLE 4-9. DESIGN VIBRATORY ACCELERATIONS FOR BASIC STRUCTURE

RANDOM INPUT AT THE AGENA INTERFACE

| Component | Longitudinal 3$\sigma$ g | | | Lateral 3$\sigma$ g | | |
|---|---|---|---|---|---|---|
| | 125 cps | 190 cps | 270 cps | 50 cps | 100 cps | 140 cps |
| Antenna compartment attachment | ±10.5 | ± 6.5 | ∓11.5 | ±12.0 | ±12.0 | ±11.5 |
| Communication antenna attachment | ±23.5 | +20.0 | ∓29.5 | ±12.0 | ±12.0 | ±11.5 |
| Traveling-wave tube attachment | ±10.5 | ± 6.5 | ∓11.5 | ±25.0 | ∓ 0 | ±17.2 |
| Rib-mounted antenna electronics attachment | ±10.5 | ± 6.5 | ∓11.5 | ±25.0 | ∓ 0 | ±17.2 |
| Traveling-wave tube power supply attachment | ±13.4 | ± 0 | ∓15.0 | ±12.0 | ±12.0 | ±11.5 |
| Forward battery pack center of gravity | ±56.0 | ∓27.4 | ±23.2 | ±83.0 | ∓10.0 | ±14.0 |
| Aft battery pack center of gravity | ±56.0 | ∓27.4 | ±23.2 | ±12.0 | ∓ 0 | ± 3.0 |
| Loaded propellant tank center of gravity | ±42.5 | ± 3.0 | ± 8.5 | ±54.0 | ∓ 0 | ∓28.0 |
| Quadrant electronics attachment | ±42.5 | ± 3.0 | ± 8.5 | ±54.0 | ∓ 0 | ∓28.0 |
| Apogee motor attachment | ±19.0 | ± 0 | ± 9.5 | ±33.0 | ∓ 0 | ∓ 0 |
| Apogee motor nozzle attachment | ±82.0 | ∓ 8.5 | ±12.0 | ±82.0 | ∓ 2.5 | ± 3.0 |
| Orientation rocket platform | ±41.0 | 69.0 | 15.9 | | | |

2) The batteries should be restrained against slippage by a flanged cover.

3) Trusswork joints should not be welded. The three trusswork failures during the T-1 vibration test occurred near welded joints. A probable cause of the failures was a flow of the tubing material away from the weld which was significant in the thin walled (0.028 inch) tubing.

4) Attachment of the spin control rocket motors to the trusswork should be made as short as possible to minimize the bending moments in the truss and torus. The attachment bolts should fit snugly to eliminate "chattering." This type of motion is evident in the T-1 test data, prior to a spin motor truss failure.

5) The spin motor locking pin, which restrains the flexure pivots during launch, should be modified to eliminate "brinelling" of the hole under vibratory loads. Increasing amounts of motor free play were observed during testing.

6) The solar panels should be inspected during manufacture to eliminate areas of inadequate bonding between the honeycomb core and the face sheets.

7) Rib mounted components should be backed by stiffeners to prevent large deflections of the web.

8) Bolts should be restrained against vibration by safety wire or by a liquid bonding agent such as "Loctite."

Design Quasi-Static Accelerations. Vibratory accelerations given in Tables 4-7, 4-8, or 4-9 are to be superimposed on the simultaneously applied longitudinal and lateral quasi-static accelerations for design purposes. Possible combinations of qualification level quasi-static accelerations include:

1) Liftoff

+2.6g longitudinal, 3.8g lateral

2) Maximum dynamic pressure

+3.0g longitudinal, 0.8g lateral

3) Atlas booster engine burnout

+11.4g longitudinal, 1.5g lateral

4) Agena booster burnout

+7.5g longitudinal, 0g lateral, radial acceleration due to spin of 6.7 x (radius-feet) g

5) Apogee motor burnout

-13.5g longitudinal, 0g lateral, radial acceleration due to spin of 6.7 x (radius-feet) g

The positive longitudinal direction is forward on the spacecraft (in the direction from the separation plane to the apogee motor nozzle). Quasi-static accelerations act through components centers of gravity.

Mass Properties Analysis

Basic changes in the weight distribution for the Advanced Syncom since the last reporting period have occurred as follows:

| Subsystem | Weight Change, Bounds |
|---|---|
| Electronics | (+2.7) |
| Addition of isolators and regulators | +2.1 |
| Revised weight estimates | +0.6 |
| Power Supply | (-8.4) |
| Deletion of voltage regulators | -4.5 |
| Solar cell substrata redesign | -3.7 |
| Miscellaneous | -0.2 |
| Controls | (+3.7) |
| Amended Marquardt estimate to reflect flight spacecraft weights | +3.7 |
| Structure | (-0.8) |
| Miscellaneous | -0.8 |
| Ballast | (+2.8) |
| To provide for maximum spacecraft weight at booster separation | +2.8 |

Table 4-10 excludes a redistribution of equipment to achieve better roll-to-pitch moment-of-inertia ratios. Changes in mass property data for the apogee motor are also excluded. Present weight (122.2 pounds) for the propulsion subsystem represents the weight of an inert case. A considerable

TABLE 4-10. ESTIMATED WEIGHT STATUS, HSX 302-T2

| Subsystem | Δw, Pounds* | Weight, Pounds | $\phi$** | $\phi$*** | Target Weight, Pounds |
|---|---|---|---|---|---|
| Electronics | ∓2.7 | 185.1 | 0.296 | 0.122 | 140.45 |
| Wire harness | | 19.9 | 0.032 | 0.013 | 16.40 |
| Power supply | -8.4 | 119.1 | 0.190 | 0.078 | 122.68 |
| Control | ∓3.7 | 51.0 | 0.081 | 0.034 | 48.86 |
| Propulsion | | 122.2 | 0.195 | 0.081 | 122.20 |
| Structure | -0.8 | 97.5 | 0.156 | 0.064 | 96.25 |
| Miscellaneous | | 19.9 | 0.032 | 0.013 | 16.40 |
| Ballast | ∓2.8 | 11.0 | 0.018 | 0.007 | 62.50 |

| | Weight, Pounds | Z – Z, Inches | $I_{z-z}$, Slug-ft$^2$ | $I_{x-x}$, Slug-ft$^2$ | R/P |
|---|---|---|---|---|---|
| Final orbit condition | ( 625.7) | 21.5 | 56.8 | 53.9 | 1.05 |
| $N_2$ | 2.9 | | | | |
| $N_2H_3$-$CH_3$ fuel | 53.0 | | | | |
| $N_2O_4$ oxidizer | 84.1 | | | | |
| Total at apogee burnout | ( 765.7) | 21.5 | 71.0 | 61.1 | 1.16 |
| Apogee motor propellant | 752.3 | | | | |
| Total payload at separation | (1518.0) | 22.6 | 87.9 | 78.5 | 1.12 |

* Change in subsystem weight since last report.
** Ratio of subsystem weight to final orbit condition weight.
*** Ratio of subsystem weight to total payload at separation.

reduction in weight (on the order of 20 pounds) is anticipated to reflect the fired case weight data. Written confirmation of the Jet Propulsion Laboratory's latest estimates is required before this change can be included. The optimum placement of equipment is dependent upon this data.

## Thermal Control

Thermal analysis of the Advanced Syncom spacecraft has continued in the form of bulk temperature estimates and specialized thermal calculations for various spacecraft subsystems. The detailed nodal temperature analysis, which has been under preparation for several months, has been summarized and will be temporarily discontinued.

## Nodal Analysis

The nodal analysis of the spacecraft consists of a lumped parameter model of one-fourth of the vehicle represented by 52 nodes in an effort to simulate as much of the spacecraft internal detail as is presently feasible. The analytical model is shown in Figure 4-54; nodal locations are indicated and the nodal numbers listed and identified. Much of the input data required to run the computer program has been calculated and tabulated for future computation on the IBM 7090 computer. This data includes thermal capacity, internal heat generation, thermal conductance, thermal radiation coefficient, and spacecraft geometry. The thermal capacity of each node in the analysis has been calculated on the basis of current structure geometry and dimensions.

The internal heat generation at each node of the network requires a knowledge of the electrical energy dissipation or a function of time at each of the spacecraft control items as well as solar heat inputs occurring at the outside surfaces of the vehicle. The calculation of these values is only about 5 percent complete because of a lack of heat dissipation information available from the spacecraft electrical systems suppliers.

Thermal conductance calculations are essentially completed based on existing spacecraft geometry, mounting methods, and material thicknesses. These values are subject to change as design progresses and materials and gauges are finalized.

Thermal radiation coefficients are incomplete primarily because of inability to compile all of the necessary radiation view factors. The only feasible means of obtaining many of the complex view factors between spacecraft internal items is to measure them with the "form factometer" apparatus which requires the use of a vehicle structure mock up.

Spacecraft geometry has been completely defined for computer use. Each node of the network has been specified as to thermal coupling to adjoining nodes with respect to all of the means of heat transfer that can occur. Figure 4-55 is an example of such a nodal geometrical representation

NODAL LUMPED MASS SYSTEM

| | | | |
|---|---|---|---|
| 1, 53 | UPPER SOLAR PANELS | 34 | SUPPORTS (QUADRANT ELECTRONICS) |
| 2, 54 | LOWER SOLAR PANELS | 35 | ANTENNA ELECTRONICS |
| 3 | THERMAL BARRIER | 36, 37, 38 | TRAVELLING WAVE TUBE NO. 1 |
| 4, 5, 6 | INNER CYLINDER RING | 39 | TRANSMITTER |
| 7, 8, 9 | AFT BULKHEAD | 40, 41 | DC CONVERTER NO.1 AND 2 |
| 10, 11, 12 | FWD BULKHEAD | 42 | ANTENNA BASE RING |
| 13, 14, 15 | THRUST TUBE | 43 | ANTENNA |
| 16, 17, 18 | GROUND PLANE | 44 | ANTENNA PROBE |
| 19, 20, 21 | AFT BULKHEAD STIFFENERS | 45, 46, 47 | TRAVELLING WAVE TUBE NO. 2 |
| 22, 23, 24 | TOP CIRCULAR FRAME | 48 | SUN SENSOR |
| 25, 26, 27 | LOWER CIRCULAR FRAME | 49 | THRUST RING |
| 28, 29, 30 | STRUTS | 50 | RADIAL JET UNIT |
| 31 | QUADRANT ELECTRONICS | 51 | AXIAL JET UNIT |
| 32 | OXIDIZER TANK | 52 | RADIAL JET UNIT SUPPORT |
| 33 | FUEL TANK | | |

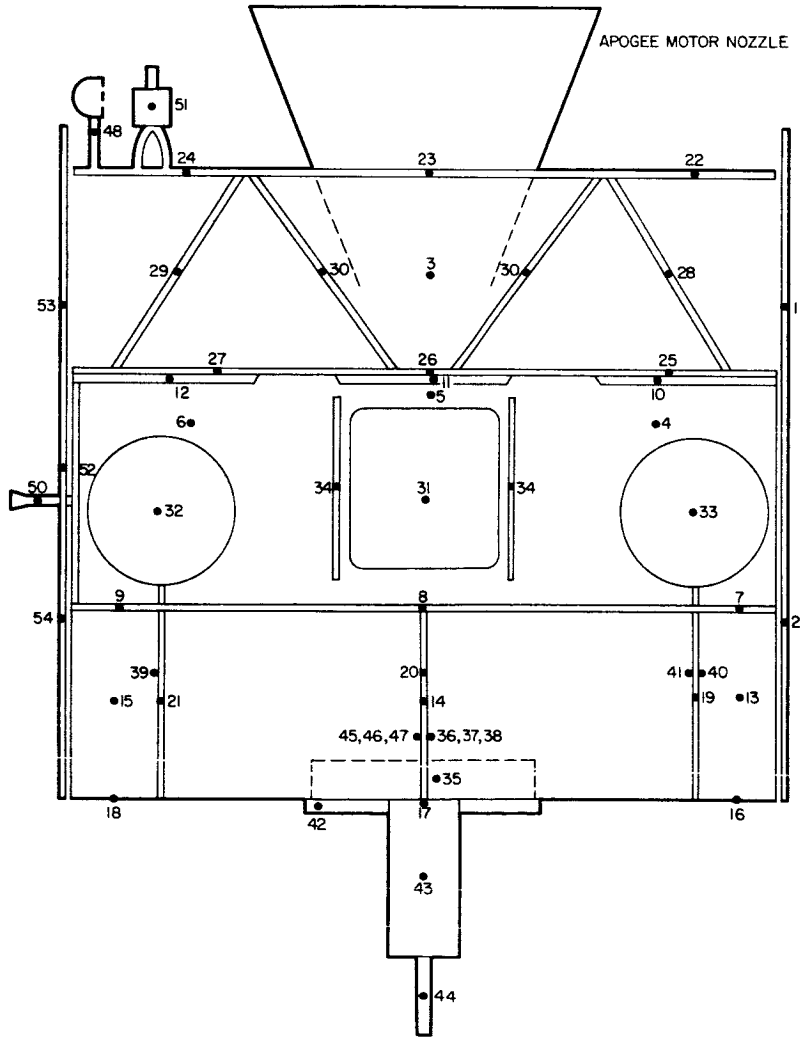


Figure 4-54. Advanced Syncom Nodal Representation

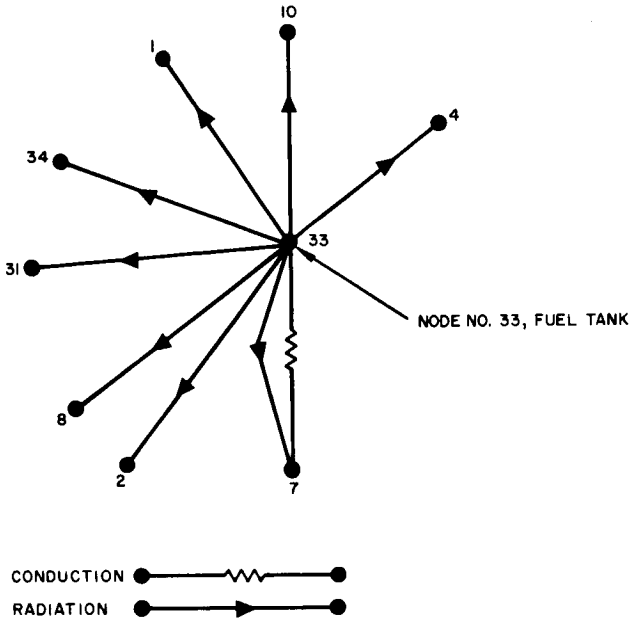


Figure 4-55. Typical Nodal Network Schematic

for a typical spacecraft node (node No. 33, the fuel tank). It can be seen that node 33 is radiantly coupled to nodes 2, 8, 31, 34, 1, 10, 4, and 7, and conductively coupled to node 7.

Reaction Engine Analysis. Preliminary studies have been made to determine radial engine temperatures and insulation requirements. In accordance with specifications, the radial engine package external surface temperature is not to exceed 200° F in order to limit radiative heat transfer to the vehicle. The analysis did not attempt to include vehicle heating effects caused by the engine exhaust products during combustion. The only heat contribution was assumed to be from the hot engine exhaust nozzle. Preliminary tests of the radial reaction jet performed at Marquardt indicated that steady-state temperatures for the radiation shield facing the engine ranged from 1200° F at a point opposite the nozzle exit to 1400° F at a point opposite the throat. An analytical model, shown in Figure 4-56, was assembled and steady-state heat balances made to determine engine assembly external temperatures for various insulation configurations. With the original opening of approximately 3 inches in the solar panel, Marquardt tests have indicated temperatures of approximately 900° F at the external shroud of the engine assembly. The high external temperature has probably resulted from radiation or conduction from the nozzle tip to the external shroud, across the uninsulated gap. Since the opening in the solar panel has been increased to over 5 inches, the insulation can be extended to the nozzle tip, and maximum temperatures in the region of 200° F at the external shroud are expected. This assumes that thermal conduction from the inner radiation shield to the external shroud can be eliminated or reduced to a negligible quantity (compared to heat transfer through the insulation).

Since this type of thermal radiation analysis is dependent on emittance of outer shroud and the spacecraft enclosure and also the relative area of the shroud and enclosure, these variables were changed to several different values. Results shown in Table 4-11 indicate that shroud external temperatures of approximately 200° F are reasonable to expect for the 5-inch diameter engine package.

Thermal Properties. To incorporate a satisfactory thermal control system into the spacecraft design, certain basic information pertaining to thermal radiation properties of several surface types must be obtained. Requests have been made for the required information divided into two distinct groups:

1) Radiation properties before prolonged space exposure. This information is required in order to select the proper spacecraft external energy balance to obtain a predetermined nominal spacecraft temperature level. It is necessary that this information be accurate to within ± 5 percent.

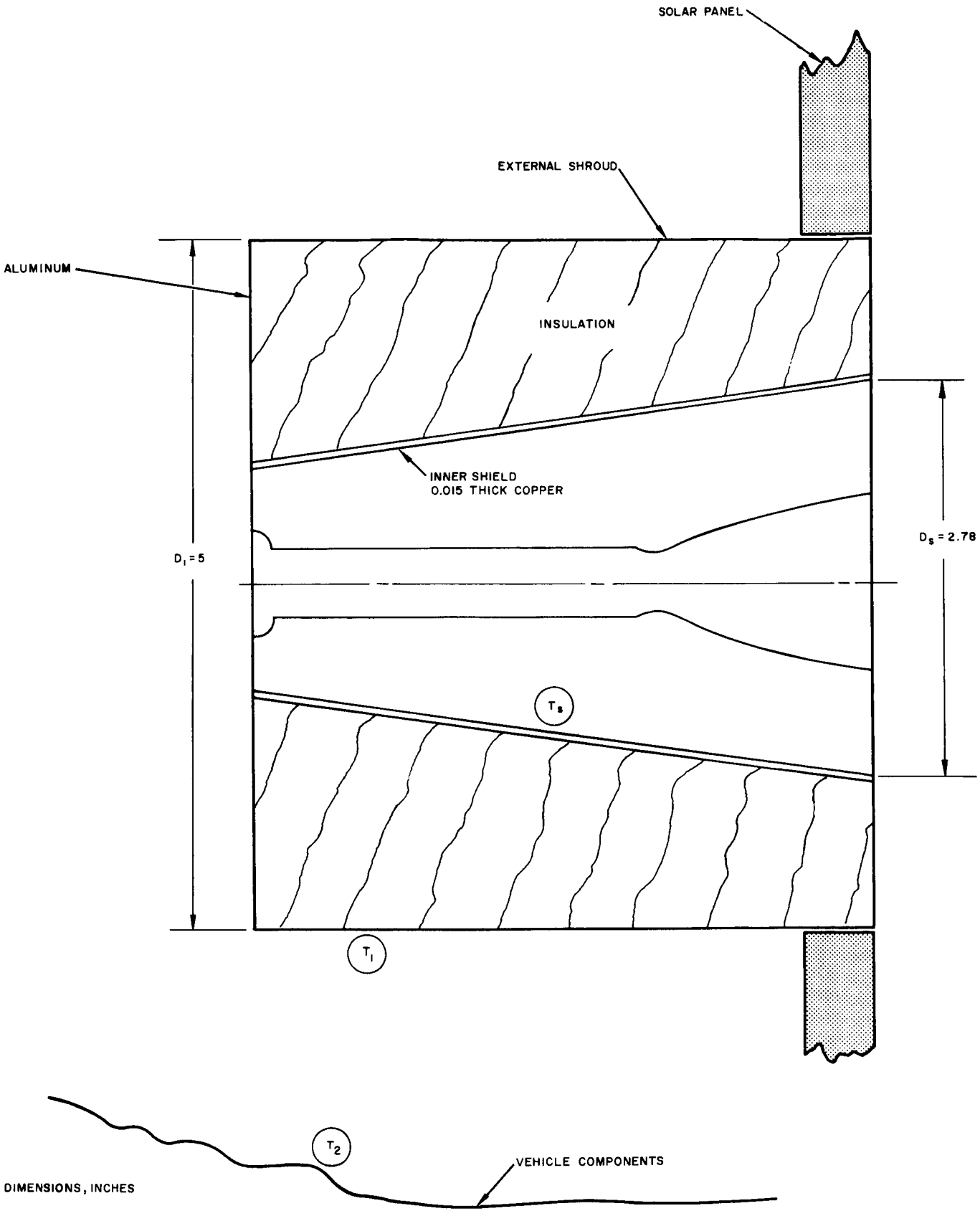


Figure 4-56. Radial Engine Normal Analytical Model

2) Radiation properties after prolonged space exposure. The long-time space effects on the external surfaces of the vehicle must be predictable in order that temperature variations from nominal values can be predicted. In addition, provisions can be made to minimize variations and make adjustments to compensate for the surface property variations during the lifetime of the spacecraft.

The required information is listed in Table 4-12. Since all of the various means of surface degradation attributable to the long-time effects of outer space are not known, it has been requested that ultra violet exposure data be provided as soon as possible. Ultra violet exposure is presently felt to be a major contributor to surface property changes with respect to time.

In addition to the normal spectral properties of materials, it has been requested that the specular absorptance of solar cells, white paint, and vapor deposited aluminum be investigated. Although it has been reported that solar cells in general exhibit a fairly constant value of solar absorptance with angle of incidence, it is essential that this property be known for the actual solar cells since the cylindrical geometry of the solar panels allows for all-angle absorptance. Specular absorptance of other materials such as white paint and vapor deposited aluminum shows a high variation especially at low angles.

TABLE 4-11. RADIAL ENGINE EXTERNAL SHROUD TEMPERATURE

| $D_1^*$ = 5.0<br>$D_S$ = 2.22<br>$T_2$ = 140° F<br>$T_S$ = 1200° F | $\frac{A_1}{A_2}$ = 0 | $\frac{A_1}{A_2}$ = 0.5 | $\frac{A_1}{A_2}$ = 1.0 |
|---|---|---|---|
| $\epsilon_1 = \epsilon_2$ = 0.2 | $T_1$ = 196° F | = 210 | = 224 |
| $\epsilon_1 = \epsilon_2$ = 0.5 | = 162 | = 168 | = 175 |
| $\epsilon_1$ = 0.2<br>$\epsilon_2$ = 0.5 | = 196 | = 197 | = 200 |

*Subscripts refer to figure.

TABLE 4-12. THERMAL PROPERTY MEASUREMENTS

| Variable Property | Before Space Exposure | After Space Exposure |
|---|---|---|
| 1) Advanced Syncom solar cells | | |
| a) Solar absorptance | 0 | 0 |
| b) IR emittance | 0 | 0 |
| 2) Hughes inorganic white paint (HP4-135) | | |
| a) Solar absorptance | X | 0 |
| b) IR emittance | X | 0 |
| 3) Hughes organic white paint (HP4-144) | | |
| a) Solar absorptance | 0 | 0 |
| b) IR emittance | 0 | 0 |
| 4) Hughes black paint (HP4-143) | | |
| a) Solar absorptance | X | 0 |
| b) IR emittance | X | 0 |
| 5) Vapor deposited aluminum (HP4-142) | | |
| a) Solar absorptance | X | 0 |
| b) IR emittance | X | 0 |
| 6) Advanced Syncom solar cells | | |
| a) Solar absorptance (specular) ($\alpha$ versus solar angle) | 0 | |
| 7) Hughes inorganic white paint (HP4-135) | | |
| a) Solar absorptance (specular) | 0 | |
| 8) Vapor deposited aluminum (HP4-142) | | |
| a) Solar absorptance (specular) | 0 | |

Note: 0 = required, X = completed

## Apogee Injection Rocket Engine

The apogee injection rocket engine is under development at the Jet Propulsion Laboratory. Because of the necessity of diverting engineering effort to provide Syncom I launch support, development progress has largely been limited to loading the first heavywall engine and completing the flight-weight nozzle design.

The initial heavywall engine loading was accomplished by mixing three equal propellant batches in the 25-gallon mixer at Edwards Air Force Base. Following inspection, the engine will be tested early in August 1963, indicating a slip of approximately 2 weeks. The new 150-gallon mixer will be installed and checked out at Edwards Air Force Base during August, September, and October 1963, and will be integrated into the development schedule during November 1963, coincident with the loading of development engine C-3. This revised schedule represents a slip of approximately 6 weeks.

The contour nozzle design has been completed and will be submitted for fabrication vendor quotation during August 1963. The initial test of the full contour design is planned for October 1963. Flight engine delivery will be initiated in September 1964.

# 5. SPACECRAFT RELIABILITY AND QUALITY ASSURANCE

## QUALITY ASSURANCE

A Quality Control Instruction is being developed to audit the Advanced Syncom quality program. The instruction will be based on the existing Quality Control Instruction for Internal Quality Audits and will be used to measure the effectiveness of the quality program during the flight hardware fabrication and test phase of the Advanced Syncom program. A Quality Control representative has been monitoring the development and fabrication of the bipropellant control system at Marquardt and the filters being supplied by Rantec. The status of these suppliers is as follows:

Marquardt Corporation

1) Component and systems testing on the engineering model to Marquardt specifications Nos. 0601-0622 was conducted during this period. The complete bipropellant control system was tested to specifications No. 0622 and from all indications was successful.

2) Additional testing on the system has been suspended awaiting further instructions regarding the interim phase of the program.

3) Discrepancies as recorded on the facility survey of 12 June 1963 were discussed in detail with E. Bodie of Marquardt Quality Control Engineering. A report listing the discrepancies will be presented to Marquardt for corrective action.

Rantec Corporation

1) A visit to Rantec Corporation was made on 15 July 1963. The purpose of the visit was to determine compliance with Quality Control requirements of purchase order 4-753011-FF31-A. Some minor discrepancies existed.

2) Rantec drawings are being used for manufacturing and testing to requirements specified on the purchase order.

3) A product production schedule was obtained from Rantec. The requirements of Hughes Aircraft Company Quality Assurance Attachment Q-4 was discussed in detail with Rantec Quality Control. The Quality Control Manager stated that Hughes would be notified when parts were to be tested. These tests will be under the surveillance of Hughes Quality Control.

4) The clean room does have Class II capabilities although it is not presently being operated as such. Procedures to control this area are in process.

## QUALITY CONTROL

Quality Program Plans for all suppliers will be similar to those already written for semiconductor suppliers.

### Operations

In-process inspection is being performed on a limited basis on items being fabricated during this phase.

### Instructions

Instructions will be prepared for all special processes and packaging techniques.

# 6. MATERIAL PROCESSES AND COMPONENTS

A structure for solar panel substrates was proposed and accepted by designers. Materials for fabrication of panels for test are being procured.

A program for optimizing the behavior of the adhesive used for bonding solar cells to the substrate has begun.

The development of a technique and material for potting connectors is nearly complete. This technique employs a flexible material that cures at room temperature and does not outgas in vacuum. It will be useful for repair work when a material that cures at a higher temperature, already available for original fabrication, may not be easily used.

Discussions of materials and processes to be used in antenna structures are in process with designers.

For several months, the material used for encapsulating the collector end of the Syncom I traveling-wave tubes has been exposed in dummy assemblies to the expected maximum temperature of Advanced Syncom tube operation and in vacuum to determine its potential stability. Tests show no indication of any degradation under these conditions; therefore, tests of another possible material have been deferred for the present.

## PARTS

The basic philosophy in selection of parts is to use as far as possible parts that have been qualified for other space programs and have a history of dependable behavior. New parts are considered critically to determine the actual need for them and to evaluate their potential reliability.

Discussion of proposed part applications continued with designers resulting in the possibility of reducing the total number of different semiconductor devices from 67 to 44. Reduction in device types should provide better reliability control over larger quantities of fewer device types.

A simplified circuit was suggested for a specific application which saved eight active and eight passive parts per spacecraft. A number of parts, either new or requiring modifications of presently qualified parts, are being evaluated. Procurement specifications will be prepared as required.

A unique method, based on defect density, has been developed for predicting the lifetime of silicon solar cells (or semiconductor devices) in a combined field of electrons and protons having a given energy spectral distribution. Silicon solar cell lifetime in Van Allen radiation, in solar flare radiation, and in galactic cosmic-ray radiation has been roughly estimated using this method. These estimates are based on the best estimates available of the various energy spectra and of the energy-dependent damage constant for diffusion lengths obtained experimentally. A great degree of uncertainty in these life estimates exists because of uncertainties in the environmental conditions, including flux, energy spectrum, and temporal fluctuations at Advanced Syncom altitudes.

A detailed description and discussion of this lifetime prediction technique will be presented in a report now being prepared, "A Survey of the Effects of Electron and Proton Radiation on Silicon Solar Cells."

A number of transformers and chokes have been designed and samples made for breadboard circuit tests, principally for transponder power supplies. Circuit requirements are not yet established, however, for either these or the other magnetic parts which will ultimately be required.

A small adjustable air capacitor of 0.1 to 1.0 pf range was designed here and samples are being constructed. A commercial vendor has since proposed a design which will be evaluated in comparison to the one developed here.

# 7. SPACECRAFT SUPPORT EQUIPMENT, RELATED SYSTEM TESTS, AND INTERFACES

## INTERFACE DOCUMENTS

The following Interface Requirements are under preparation:

Launch Vehicle/Spacecraft
Apogee Engine/Spacecraft
Bipropellant Control System/Spacecraft
Telemetry and Command Station/Spacecraft
Communication Terminal/Spacecraft

These documents contain a general description of the interface and detailed requirements for electrical, mechanical, test, and ground support interface parameters. Early release of these documents is planned although some requirements may not be defined. The requirements will be periodically updated.

## GROUND CONTROL EQUIPMENT

### Specifications

Ground support equipment (GSE) is to be provided for maintaining and verifying the proper operation of all spacecraft subsystems, calibrating all sensors and the telemetry system, and monitoring and control of spacecraft functions during system tests and launch operations.

The specifications tree outlined in the June monthly report has been modified by the addition of a spacecraft access panel specification under Integration Subsystem. This specification will document the interface between the ground support equipment and the spacecraft during system test and while the spacecraft is on the spin machine.

Preparation of the outlined specifications is continuing, and it is anticipated that first drafts will appear in the August report. This will constitute a major accomplishment in the design of GSE.

## Equipment Design and Fabrication

### Communications Transponder RF Test Equipment

Figure 7-1 is a revised block diagram of the transponder RF test equipment. It is identical to the block diagram included in the June 1963 progress report except for the following change in the receiver IF circuitry: the power splitter and two limiter amplifiers have been replaced by one limiter and three two-stage amplifiers.

The various blocks in Figure 7-1 may be classified into three categories: (1) spacecraft hardware, (2) modified spacecraft hardware, and (3) special-purpose test hardware. The development status of special-purpose test hardware is given below.

### Special - Purpose Test Hardware

Amplifiers, Limiter, and Discriminator. The output signal from the frequency dividers is amplified by a two-stage amplifier with a bandwidth of about 20 mc. It then passes through a passive limiter employing biased diodes. Any amplitude modulation present on the signal due to noise or other causes is eliminated almost entirely by the limiter, provided that initially amplitude modulation is not greater than 50 percent and frequency of the modulation is not greater than 5 mc.

The output signal of the limiter is amplified by a two-stage amplifier and delivered to the frequency discriminator, which detects the frequency modulation present on the signal for all modulating frequencies up to 5 mc.

On the input side of the discriminator, part of the signal energy is diverted into a two-stage amplifier that drives the phase detectors. Since these are two phase detectors, the latter two-stage amplifier has two outputs which are isolated from each other.

The two-stage amplifiers, limiter, and discriminator have been set up and operated in breadboard form (Figure 7-2). Laboratory work is in progress to improve the linearity of the frequency discriminator and to make the gain of the amplifiers more uniform over the 20 mc frequency band.

To check the operation of the limiter for amplitude modulation of frequencies above the audio range, two immodulated carrier waves from two signal generators were used simultaneously. One carrier wave was adjusted to one-half the amplitude of the other so the resultant amplitude modulation would be 50 percent. Satisfactory functioning of the limiter was obtained with the two carrier waves separated in frequency by various amounts up to 5 mc.

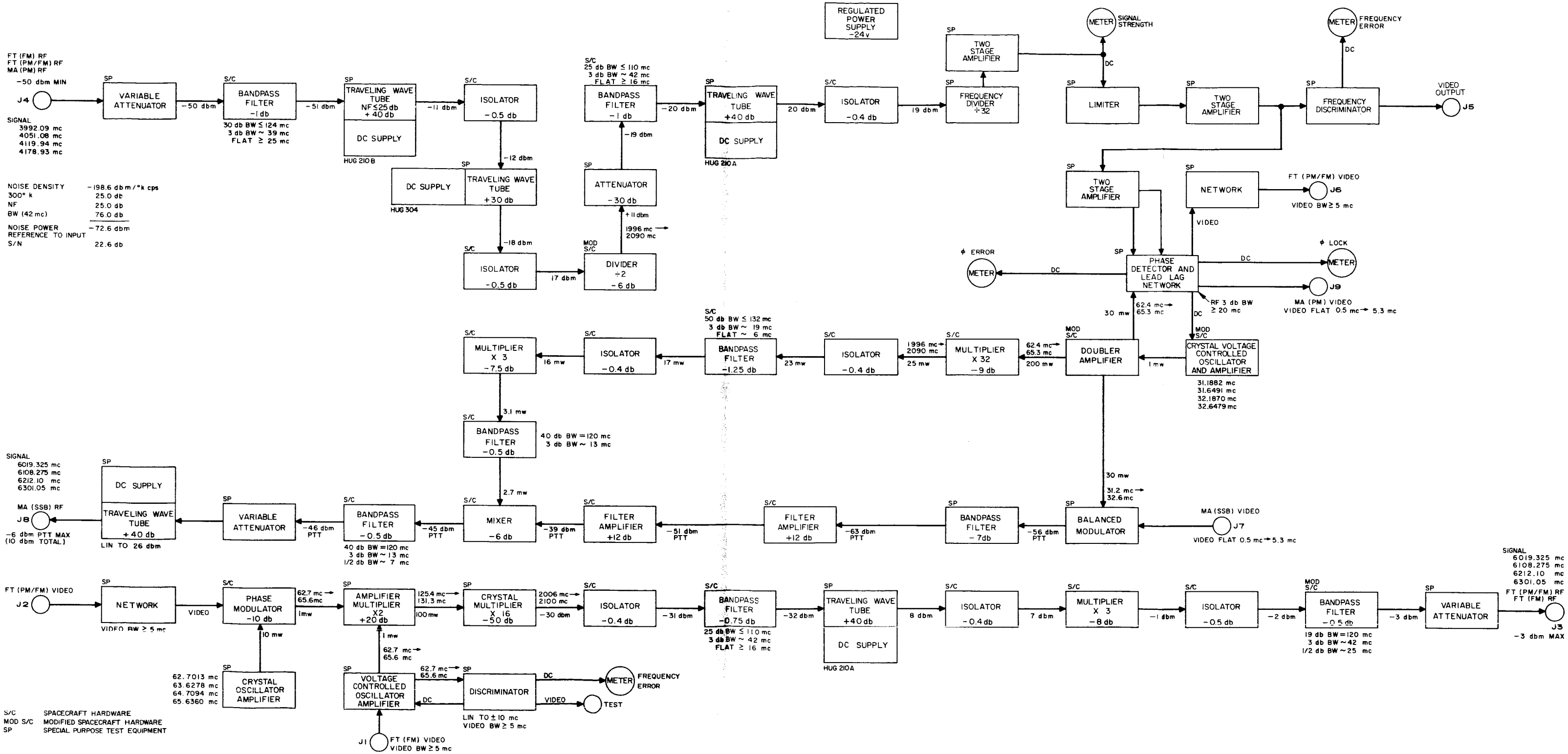


| | |
|---|---|
| NOISE DENSITY | −198.6 dbm/°k cps |
| 300° k | 25.0 db |
| NF | 25.0 db |
| BW (42 mc) | 76.0 db |
| NOISE POWER REFERENCE TO INPUT | −72.6 dbm |
| S/N | 22.6 db |

Figure 7-1. Revised Block Diagram of Advanced Syncom Transponder RF Test

GSE Phase-Lock Loop (Inner Loop). The phase detector, low-pass loop filter, and voltage-controlled oscillator were completed and joined to form a phase-lock loop as shown in Figure 7-3. The laboratory test setup is shown in Figure 7-4. Experimental data for the loop pull-in or capture range is plotted in Figure 7-5. Voltage-controlled oscillator frequency at pull-in was determined by opening the loop at the phase detector signal input and loading that input with 50 ohms.

The voltage-controlled oscillator package is a modified spacecraft master oscillator containing a doubler and amplifiers. It has 100- and 290-milliwatt outputs at 64 mc and a 30-milliwatt output at 32 mc.

Divide-By-Two. This divider is basically the spacecraft X2 multiplier connected in reverse. Investigation of tuning and bias requirements is continuing.

X16 Multiplier. An experimental X16 multiplier has been fabricated using a crystal mount with a twin-stub tuner. This unit is undergoing tests to ascertain its suitability for the application.

Divide-By-32. The divide-by-32 network is essentially the spacecraft X32 multiplier connected in reverse. Preliminary measurements on a breadboard circuit indicate a 13-db insertion loss. Good stability was obtained when the input power level was adjusted properly.

Traveling-Wave Tubes. Purchase orders have been placed for all TWTs. Huggins Laboratories Inc., will be the supplier. The vendors part numbers are indicated in the block diagram.

Variable Attennators. Purchase orders have been placed for the variable attennators. All attennators are 50 db and will be supplied by ARRA Inc.

## Equipment Design and Fabrication

### Synchronous Controller

During the report period the logic design effort on the command generator and telemetry processor was discontinued. Prior to discontinuation of the effort, logic design for the command generator and synchronous controller was 90 percent complete. This includes logic for 1) command generator, 2) command and status displays, 3) execute-mode selector, and 4) synchronous controller.

Command generator logic included mechanization of the primary (shift), secondary (count), and fault isolation modes of operation. The fault isolation mode was available when operating in either the shift or count mode, and permitted the address portion of the message to be transmitted and

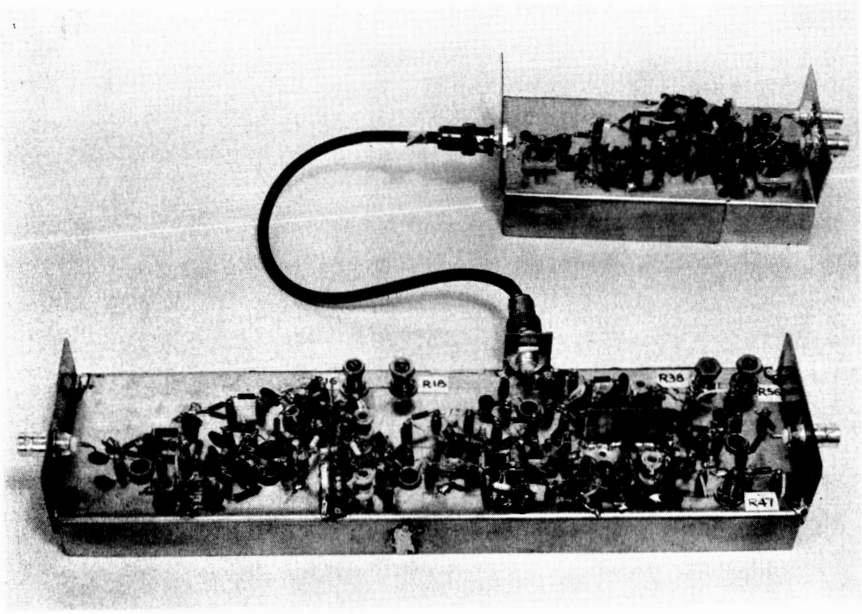


Figure 7-2. Breadboard of Amplifier Limiter and discriminator

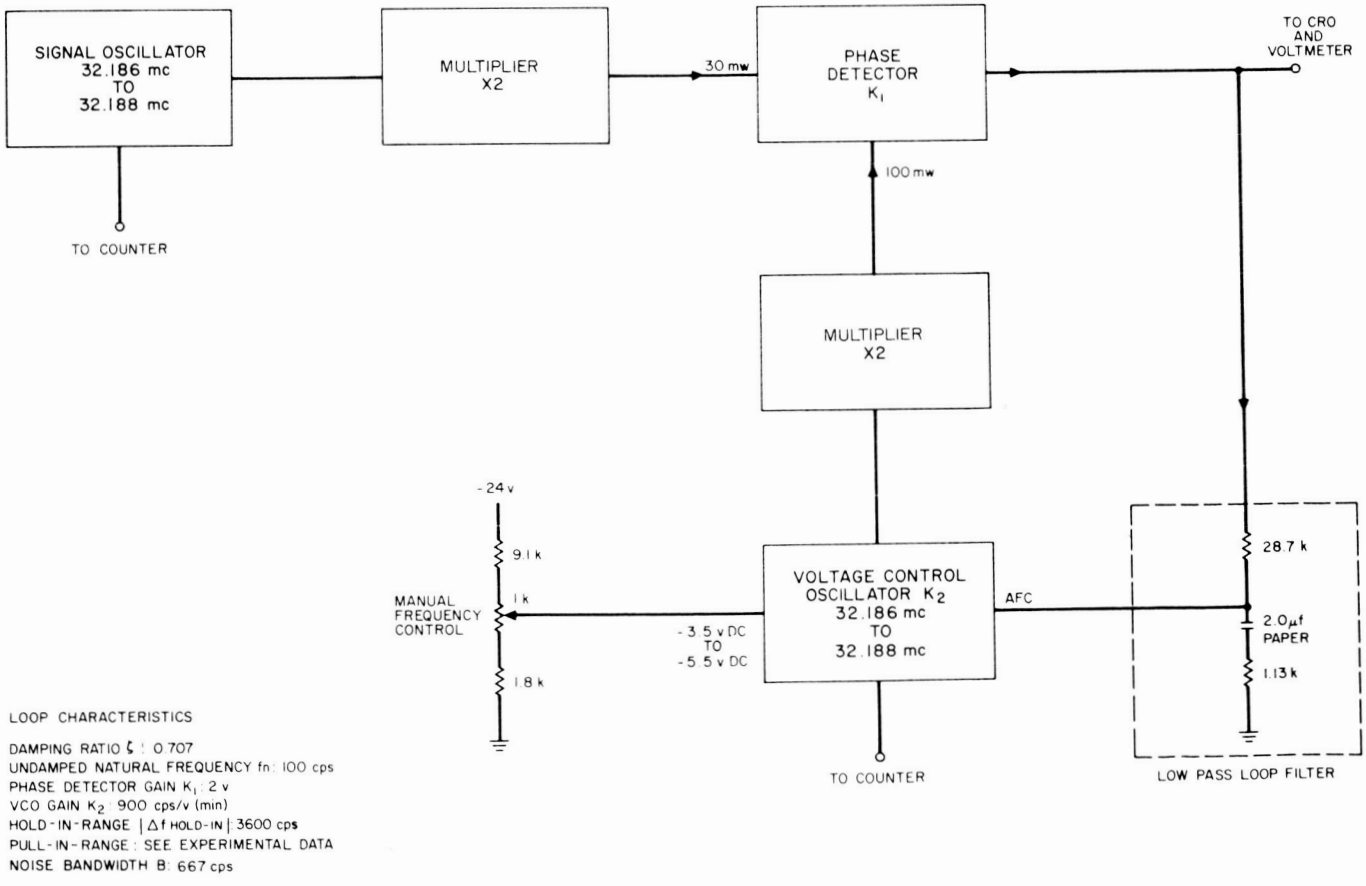


LOOP CHARACTERISTICS

DAMPING RATIO $\zeta$ : 0.707
UNDAMPED NATURAL FREQUENCY fn: 100 cps
PHASE DETECTOR GAIN $K_1$: 2 v
VCO GAIN $K_2$: 900 cps/v (min)
HOLD-IN-RANGE $|\Delta f_{HOLD-IN}|$: 3600 cps
PULL-IN-RANGE : SEE EXPERIMENTAL DATA
NOISE BANDWIDTH B: 667 cps

Figure 7-3. Phase Lock-Loop Test Setup

Figure 7-4. Laboratory Test Setup for Measuring Performance of Phase-Lock Loop

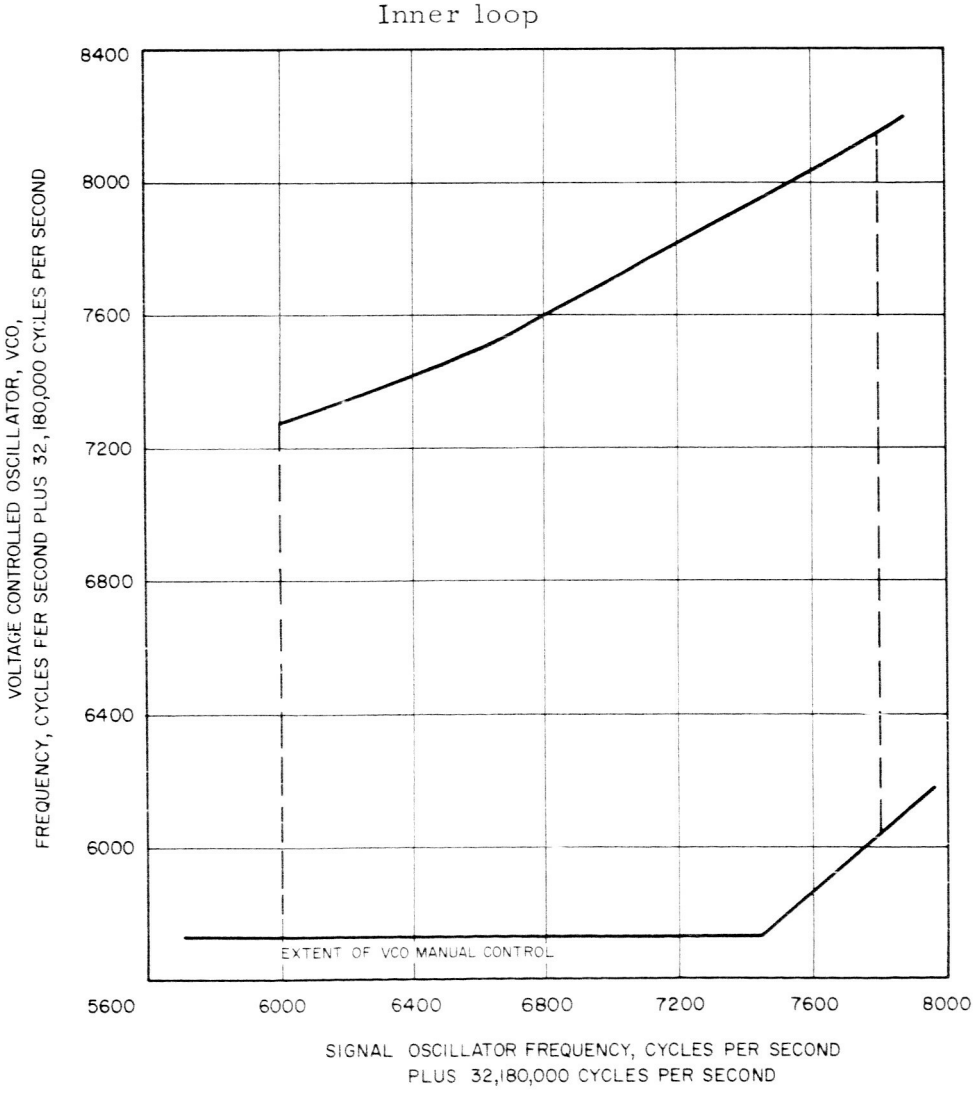


Figure 7-5. Pull-in Range of Phase-Lock Loop

verified before transmitting the command portion of the message. Error detection, verification logic, and internal self test features were also provided.

Present design effort is being directed toward integrating the Hughes-designed synchronous controller into the OGO command generator to be furnished by NASA. The majority of the existing logic for the synchronous controller and execute mode selector can be used in the new design task with slight modifications.

An execute mode selector provides the interface buffering between the OGO console and synchronous controller. The following execute modes would be provided:

1) Normal execute consisting of a one-shot pulse of variable width (10- to 150- millisecond duration)

   a) Execute and clear spacecraft decoder

   b) Execute and hold; no decoder clear

2) A continuous execute signal that is terminated upon releasing the push button switch

3) Real-time execute pulse controlled by the synchronous controller

4) Programmed count for positioning antenna beam

5) Eclipse mode for generating pseudo psi pulses.

PACE Module Tester

All fabrication, including painting, has been completed for the front panel. The components have been mounted and wiring is 90 percent complete. Module test procedures are now being written.

PACE Function Board and Unit Tester

The logic and circuit design is approximately 50 percent complete. About 10 percent of the circuitry has been fabricated on flat cards. Panel layout was initiated.

Eclipse Mode Oscillator

An oscillator will be required at the ground station to generate pseudo psi pulses during eclipse periods. These pulses will be sent to the spacecraft where, when so commanded, the PACE circuitry will use these to maintain the antenna beam in the correct position throughout the eclipse.

A description of the proposed method of generating the pseudo psi pulses and correctly phasing them to lock the antenna beam in the desired direction follows.

Measurement of the Satellite Spin Rate (psi frequency) Prior to the Eclipse. It is assumed that no spin rate or attitude correction will be made preceding the eclipse, during an interval of sufficient length for the satellite's spin rate to stabilize and for all hunting transients of the voltage-controlled oscillator in the psi tracker to die out.

The measurement can be made with a commercial counter or by using the precision oscillator. In the latter case, the 5 mc oscillator drives the 24-stage counter through a gate that is opened for 12 psi interval by the most significant bit of the 36:1 divider chain in the psi tracker. The count obtained in this way is the number of cycles of the 5 mc oscillator in psi interval. This should be noted and the measurement repeated a sufficient number of times to resolve the uncertainty in the least significant bit of the count. The psi interval is then determined within ±0.5 period of the oscillator.

Generation of the Artificial Psi Pulses. Again, the 5 mc oscillator drives the 24-stage counter. A gate driven by the appropriate counter outputs, as determined in the preceding measurement, resets the counter when the psi count is reached. This counter reset gate is periodic in the psi interval and can be used to trigger a one-shot that produces a suitably wide replica of the psi pulse for transmission to the satellite.

Phasing. It is imperative that when the switchover from sun-sensor generated to transmitted psi pulses occurs, the two pulse trains are in phase at the satellite. If correct phasing is to be established before switchover, the round trip transmission delay between ground station and satellite must be known. It is then a fairly simple procedure, knowing the psi frequency, to determine the phase difference at the ground station that will result in in-phase pulse trains at the satellite. Phasing is then established by an initial setting of the 24-stage counter at:

$$\text{total psi count} \left( 1 - \frac{\text{required phase difference}}{360 \text{ degrees}} \right)$$

and starting the counter (by gating in the 5 mc frequency source) with the leading edge of a received psi pulse.

Accuracy. Assuming perfect stability of the measured pre-eclipse spin rate during the eclipse, there are two sources of cumulative error in the proposed system, crystal instability and quantization of the psi interval into 0.2 microsecond increments (the period of the 5 mc oscillator). The effect of cumulative error is a gradual shift off-center of the phased-array beam, and would be most pronounced during a long (66-minute) eclipse and with the satellite spinning at its maximum rate (150 rpm).

A crystal is obtainable with a short-term (24-hour) stability of one part in $10^9$ in a $\pm 0.01^{\circ}$ C proportional control oven. This would yield a worst-case cumulative error attributable to instability of

$$66 \text{ minutes} \times \frac{150 \text{ revolutions}}{\text{minutes}} \times \frac{360 \text{ degrees}}{\text{revolutions}} \times 10^{-9} = 0.00356 \text{ degree}$$

which is negligible. An order-of-magnitude decrease in short-term stability would still yield a negligible error of 0.0356 degree, and this could possibly be achieved with a less expensive crystal in a thermostatically controlled oven.

The maximum quantization error during one revolution of the satellite is $\pm 0.5$ period of the 5 mc oscillator,

$$\pm \frac{0.5 \text{ period at 5 mc}}{\text{minutes, period of revolution}} \times 360 \text{ degrees} =$$

$$\frac{1 \times 10^{-7} \text{ second}}{0.4 \text{ second}} \times 360 \text{ degrees} = \pm 0.00009 \text{ deg/revolution}$$

The worst-case cumulative quantization error is then

$$\pm \frac{0.00009 \text{ degree}}{\text{revolution}} \times \frac{150 \text{ revolution}}{\text{minutes}} \times 66 \text{ minutes} = \pm 0.89 \text{ degrees}$$

which is acceptable. It would be possible to reduce this quantization error by using a higher-frequency oscillator driving a longer count-down chain, but the disadvantages of incorporating the additional high-speed circuitry this would require and the extreme difficulty of obtaining ultra-stable crystals in the frequency range beyond 5 mc outweigh the small improvement in beam position accuracy that would result.

## Power Supply Functional Operation

The dc power panel has been modified so that there are now 2-connector power switches, one on each side of the panel power switch. The dc power supply functional (Figure 7-6) contains identical halves. Each contains a power supply with its associated circuitry (test position) and load and battery (spacecraft). The power supply functional is symmetrical and only one circuit, No. 2, shall be discussed.

Power supply No. 2 is applied to the spacecraft bus loads by the following method: panel power switch (S10) is depressed, p. s. No. 2 (position 4) selected by power supply select switch (S12). The voltage is adjusted before application to the spacecraft by depressing external power switch (S5) and monitoring the voltage on voltmeter (M3). After the voltage has been adjusted to the appropriate value, power may be applied to the spacecraft load No. 2 by depressing connecting power system No. 2

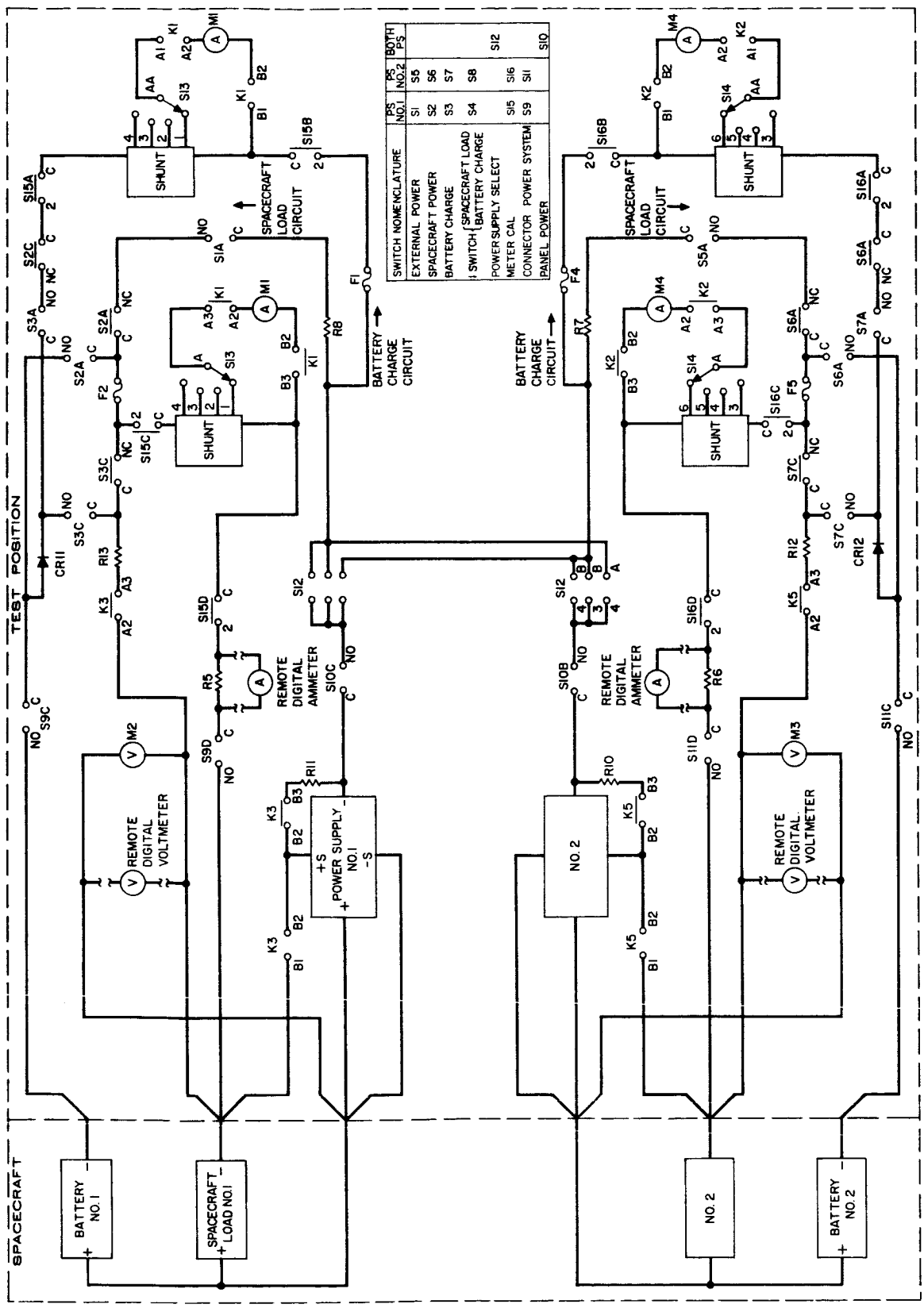


Figure 7-6. Dc Power Supply Functional Diagram

switch (S11). Power supply No. 2 may be applied to spacecraft load No. 1 by following the above discussion except now the voltage is adjusted by depressing external power switch (S1) and monitor the voltage on voltmeter (M2), after the voltage has been adjusted, power is applied to spacecraft load #N by depressing connecting power system No. 1 switch (S9). Both loads may be supplied by the same power supply simultaneously. Switches S11 and S9 actuate relays K5 and K3 which switch the power supply negative sensing lead and the voltmeters from the power supply to the spacecraft load.

The load current or the battery charging current can be monitored by pressing either spacecraft load or battery charge switch (S4) which energizes or de-energizes relay K2 respectively. Ammeter M4 has a safety feature which prevents an operator from switching the ammeter from battery charge (milliamps) to spacecraft load (amperes).

Test Data Recording.

Figure 7-7 shows the proposed data flow for the recording facilities. The major difference over the method previously shown is that the analog data is recorded in parallel rather than serial format. Most major test and all recording equipments are shown in separate blocks. Additional test data signals are received from miscellaneous equipments and the spacecraft.

Data are recorded on a strip chart recorder, x-y plotter, high-speed oscillograph, and a printer for quick-look purposes and on a magnetic tape recorder to obtain a permanent record of the test. Patching for individual tests is accomplished by exchanging prepatched boards, one audio, and one video for each test. The method of operation is described in the following paragraphs.

Digital voltmeters and milliammeters with binary coded decimal (BCD) outputs were chosen for compatibility with outputs of frequency counters and digital recording equipment. The output of the digital test equipment is recorded on four tracks of a seven-track magnetic tape recorder. Analog signals developed in the spacecraft or by test equipment will usually be converted to digital form before recording. The parallel recording of BCD characters described below was chosen because 1) standard digital printers can readily be used for readout of recorded data, 2) number of recorded data channels can be increased with little additional equipment, 3) recorded data can be converted easily into IBM format, and 4) it offers substantial saving in amount of equipment needed compared to serial recording of the digital data.

The digital data are time multiplexed and recorded on four tracks of a magnetic tape recorder, one binary coded decimal character per line. Tape speed is 3-3/4 ips which provides more than six hours of recording time using 14-inch reel and 1-mil tape. The data sampling rate is two

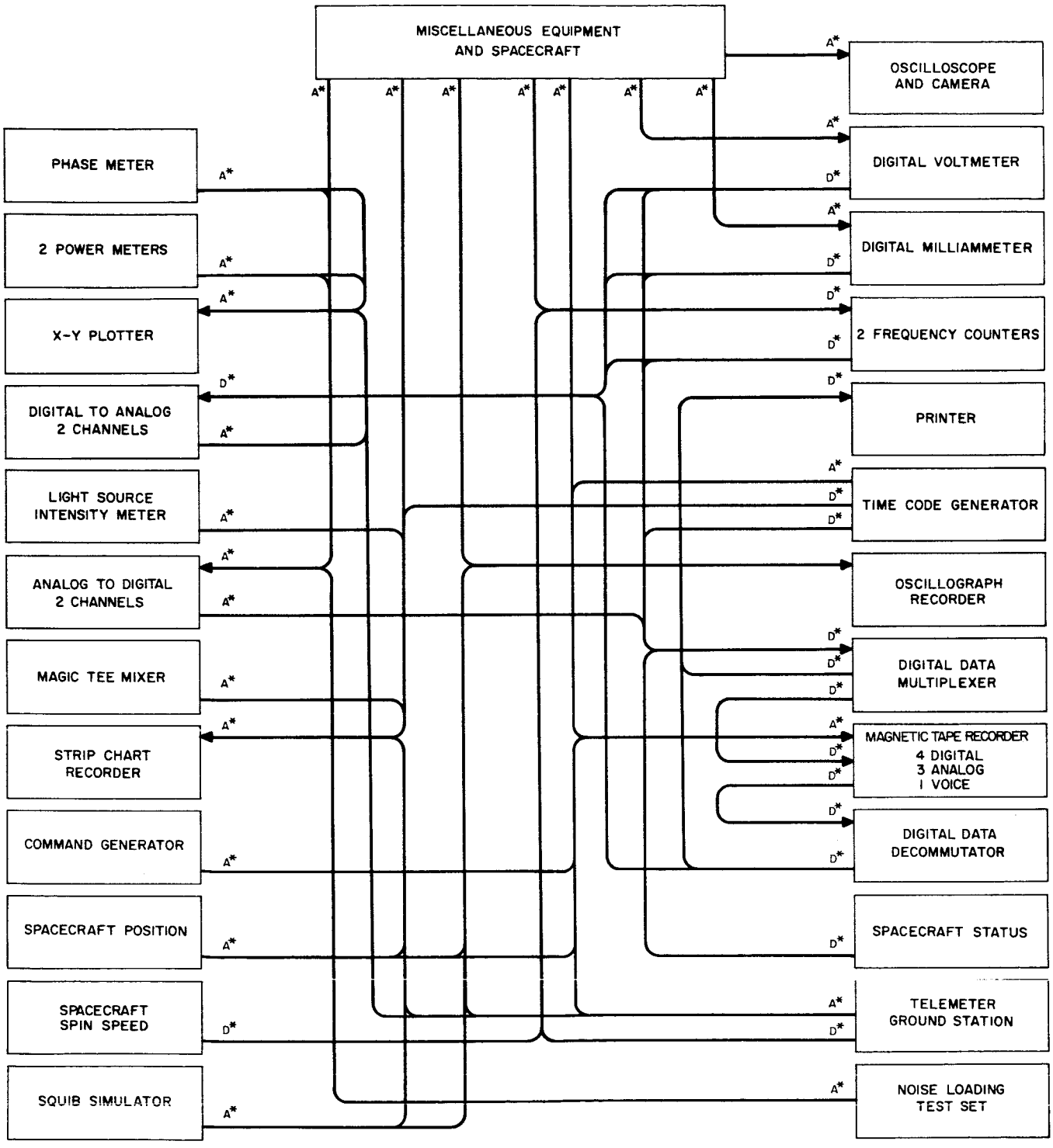


* A-CONNECTED VIA ANALOG PATCH PANEL
D-CONNECTED VIA DIGITAL PATCH PANEL
PATCHING PERFORMED BY EXCHANGING PRE-PATCHED BOARDS

Figure 7-7. Data Flow Chart

Data recording facilities

samples per second per channel. Five channels would be recorded as follows: time, spacecraft status 1, spacecraft status 2 (27 on-off indications each), data 1, and data 2 (nine digit words). At a data rate of one sample per second per channel and with additional input gates, this system will accommodate five more data channels. Data can be recovered from the tape by the use of a simple decommutator and be printed on a nine-column digital printer. Tape can also easily be transformed into IBM format and printed out by an IBM data processor.

The multiplexer (Figure 7-8) consists of 36 input gates per channel, one 36-bit shift register, a four-line output gating circuitry and IBM zero generator, and a sequencer. Sample pulses are generated in the sequencer in synchronization with the time code generator at a pulse rate of two pulses per second (five channel system) and are fed to the input equipment to initiate measurement. The parallel digital outputs of the input equipments are applied sequentially to the shift register via the input gates which are controlled by timing pulses originating at the sequencer. During the time between arrivals of data at the shift register, the stored data are read into the tape recorder through the output gates in groups of four. Following recording of each BCD character the data in the shift register are shifted four times until the total of 36 bits originally stored in the shift register have been recorded on magnetic tape. IBM zeros are generated in place of zeros to maintain synchronization pulses in the playback equipment; and spacing pulses are provided to reset counters in decommutator during playback and to group readings of each sampling period when data are reproduced.

The decommutator (Figure 7-9) consists of four input driver amplifiers, a 36-bit register, two counters, and associated circuitry. Clock pulses are derived from an OR gate which samples the 4-bit BCD characters at the input. Spacing or reset words are detected using a 4-bit input AND gate. Through the four power drivers, nine groups of four flip-flops are supplied all input BCD characters at the steering inputs; however, only the group receiving a timing pulse accepts the BCD character. Nine time pulses are generated by the counter during the time the nine BCD characters are received and these pulses are fed sequentially, one each, into the nine flip-flop groups that make up the 36-bit register. With the ninth pulse, the register contains a 9-decimal word in BCD form which can then be accepted by the printer or similar equipment upon receiving the data available signal. A counter which is triggered by every ninth pulse supplies word identification facilitating display or printout of one or more data channels.

Command signals, undemodulated (or demodulated) telemetry signals, time code signal, and a 14.5-kc subcarrier are recorded on the three analog tracks with voice recorded on the auxiliary track. Digital-to-analog converters are available to convert digital data into analog data for display on analog equipment.

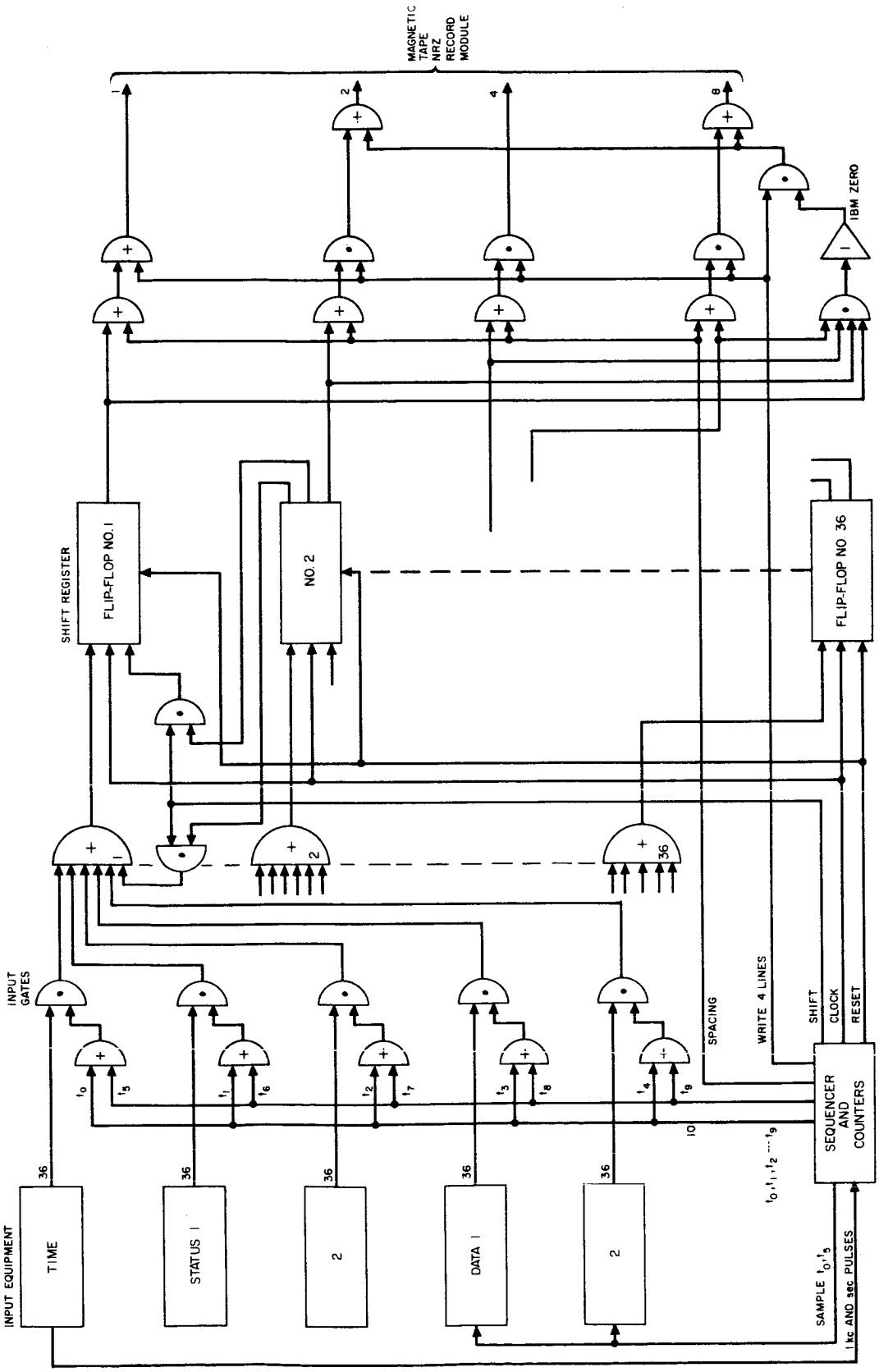


Figure 7-8. Digital Data Multiplexer

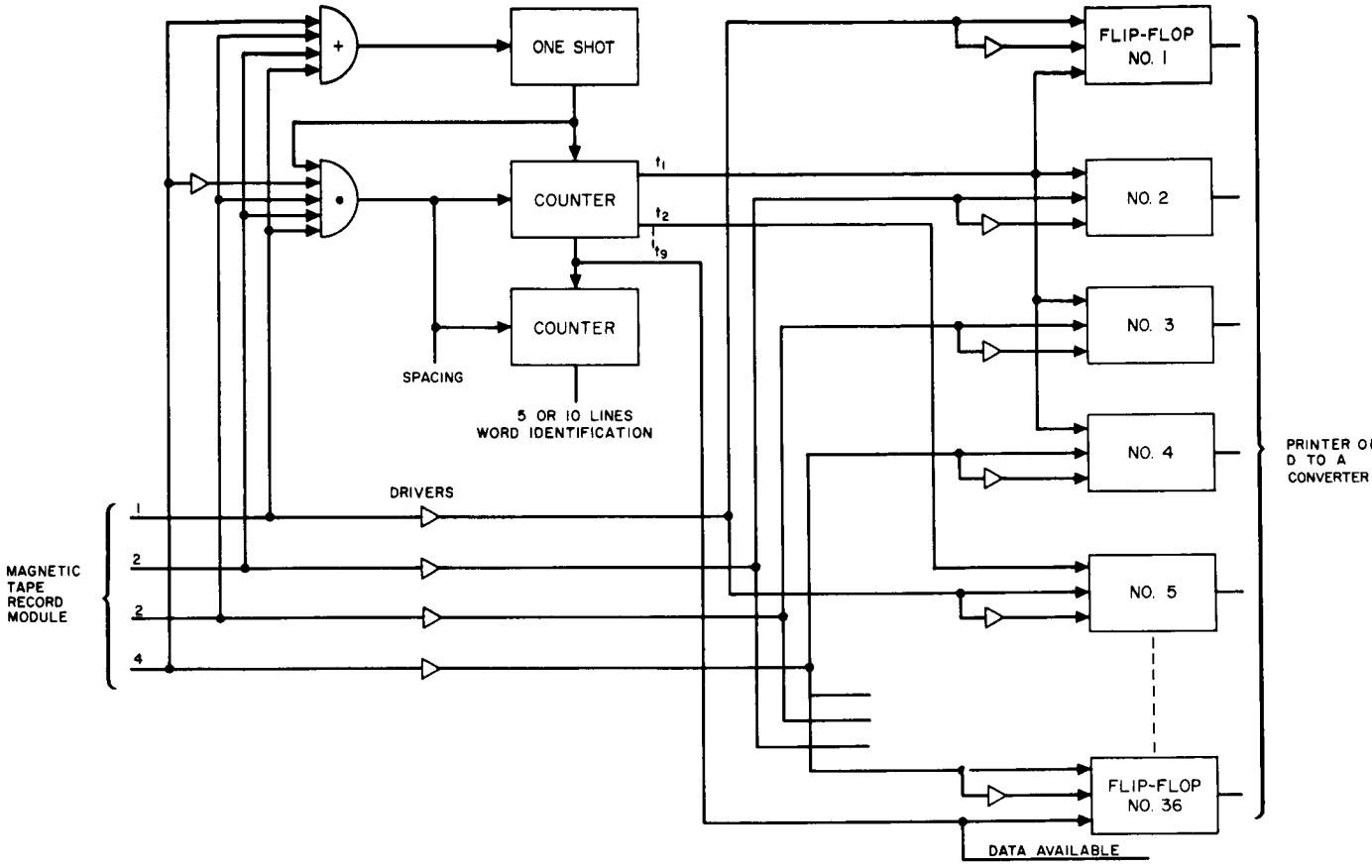


Figure 7-9. Digital Data Decommutator

Spacecraft position and spacecraft spin-speed signals are pulses generated at the spin machine. Pulses are generated as a function of spacecraft position at a rate proportional to the spacecraft spin speed.

Test Equipment Requirements Evaluation.

The system tests as outlined in the supplementary summary report are being reviewed in detail to define the equipment requirements. Each test is blocked out to indicate the specific commercial and special test equipment needed in addition to the connections through the various patch panels. Figure 7-10 shows the block diagram for one of the frequency translation transponder tests. All equipment and connections are shown, and based on this block diagram. A test equipment list is produced. The connection requirements for the video and audio patch panels will be determined on the basis of similar test analysis. Approximately 90 percent of the tests have been analyzed.

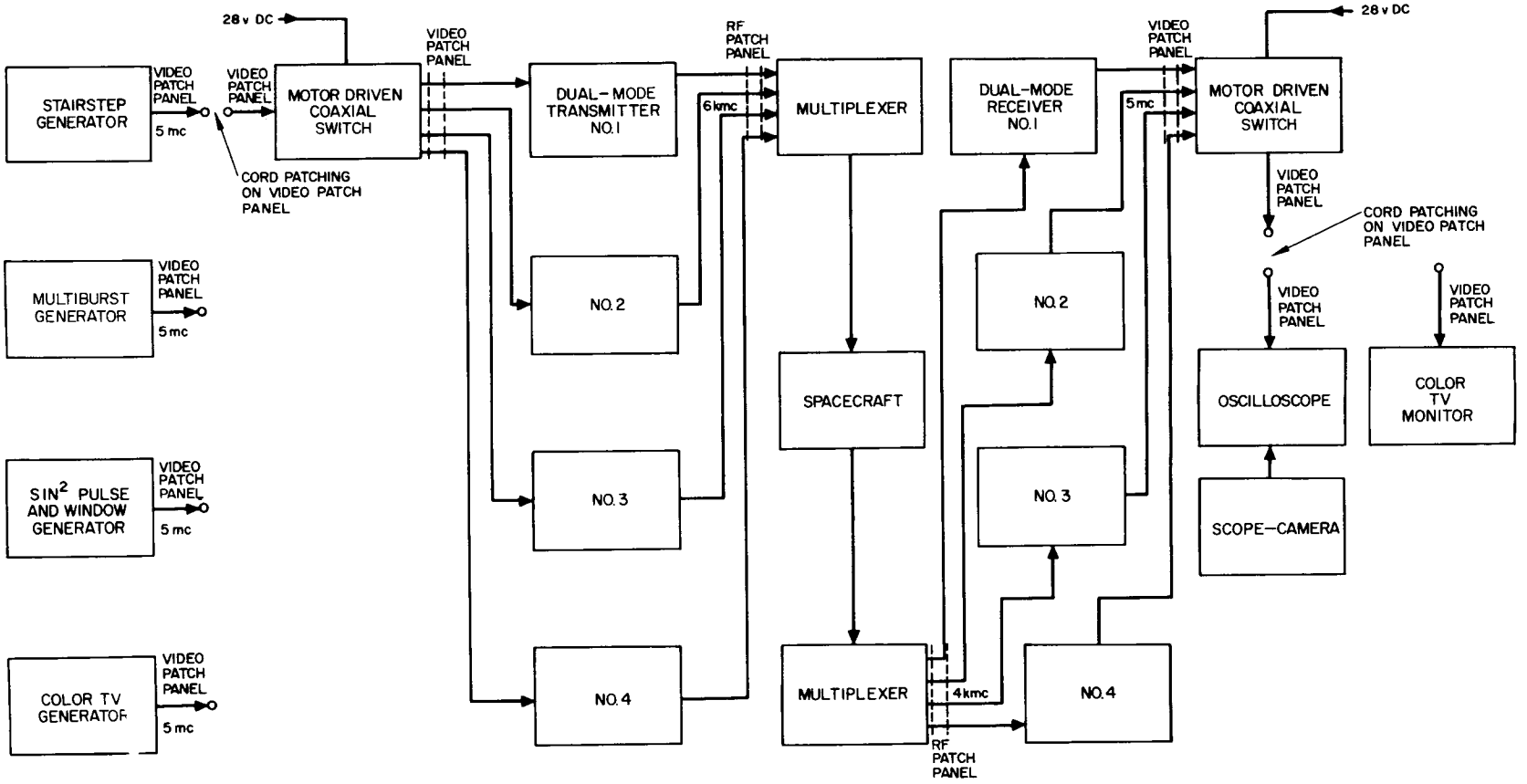


Figure 7-10. Demonstrated Response of Frequency Translation Transponders to Various TV Test Signals

# 8. SPACECRAFT HANDLING EQUIPMENT

## MOBILE ASSEMBLY FIXTURE

The drawings of this fixture are almost ready for checking and stress analysis (Drawing No. X209823).

## WEIGHT, CENTER-OF-GRAVITY, AND MOMENT-OF-INERTIA EQUIPMENT

Design work on this equipment (Drawing No. X209819) will commence during the first portion of the next report period.

## SYSTEM TEST AND SPIN FIXTURE

The power requirements for this fixture are still being evaluated. The present layout (Drawing No. X209817) contains a 1.5 hp variable drive dc motor operating at a 3:1 ratio through sheaves and belts. Another layout with a 2.0 hp ac motor will be completed pending further dimensional data on motor and accessories from the vendor.

A specification for the slip rings was prepared and issued to a vendor.

Design work is continuing on alignment adjustment of mounting surface, size and location of control panel, and the position of a strobe light. Additional parameters on noise level and alignment are being prepared.

## BALANCING MACHINE

The parameters issued by the Mass Properties Engineering Section have been modified during July as the design has developed. On the present layout (Drawing No. X209818, Figure 8-1) viscous-type dashpot pickups are used instead of knife edges or flexures. The pendulum has been eliminated, and a rectangular machine has been substituted for the tripod base.

A 2 hp vertical, low-noise level dc motor with speed control to within 0.1 rpm has been selected.

Additional information on the force required to overcome the resistance of the dashpots is being obtained to evaluate with a knife-edge mounting.

Figure 8-2 shows the complete schematic of this balancing machine.

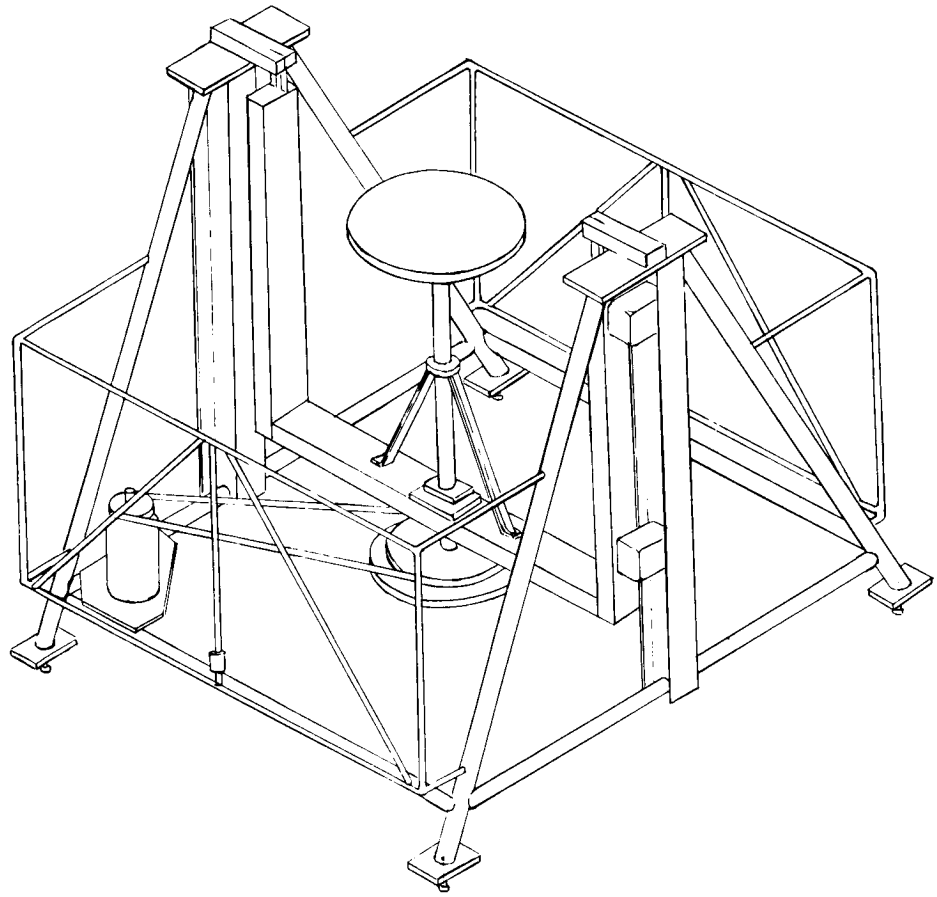

Figure 8-1. Balancing Machine

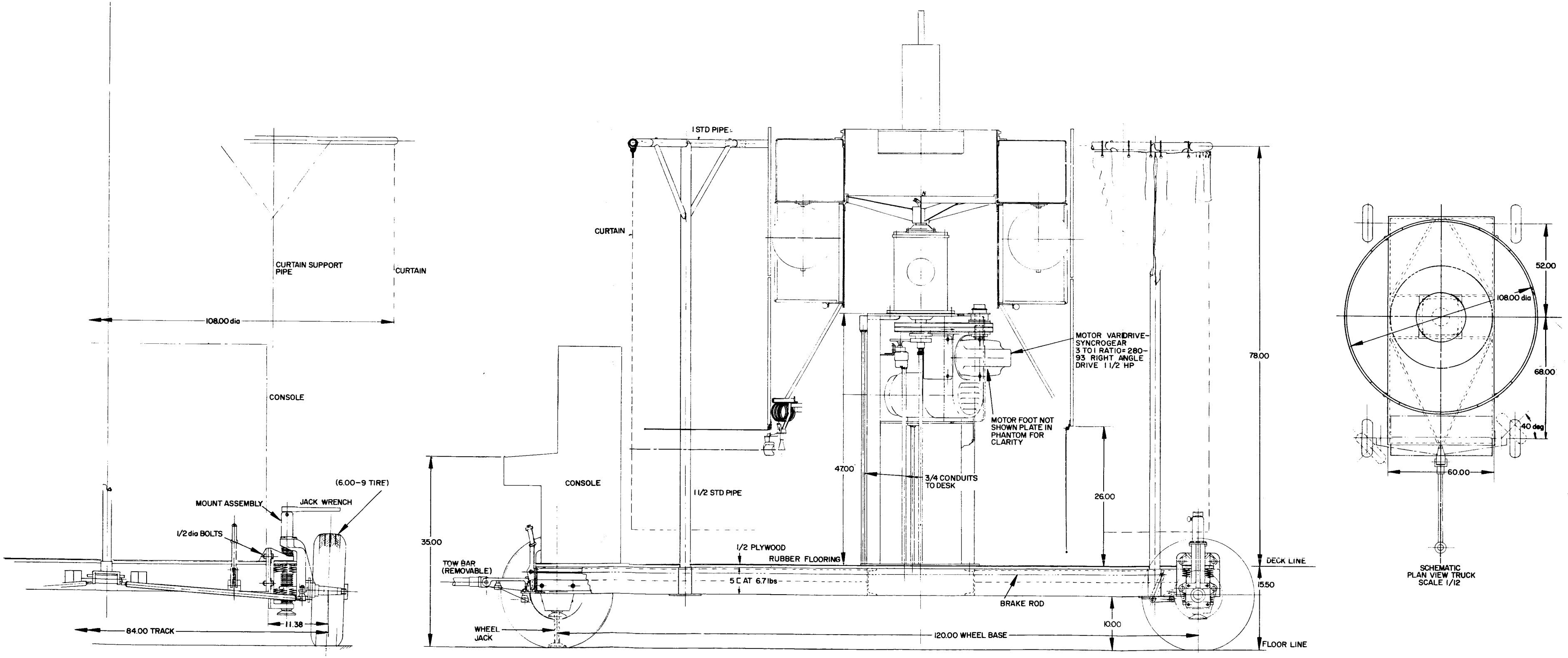


Figure 8-2. System Test and Spin Fixture

# 9. NEW TECHNOLOGY

## SOLAR CELL SUPPORT PANELS ATTACHMENT

The unique mounting arrangement used to attach the solar cell support panels to the spacecraft is believed to be a new application of basic mechanical principles. This arrangement, illustrated in Figure 9-1, was first reported in the Syncom Monthly Progress Report for May 1963.

> "The three attachment points for each solar cell support panel are on 120-degree spaced radial lines from the center of the panel and are located near the edge of the panel. These attach points provide constraint normal to the plane of the panel, and within the plane of the panel they provide constraint only in the direction perpendicular to the radial lines from the center. The attachments are hinged or slotted so that no reaction loads will be applied in a direction of the radial lines. This arrangement ensures that deformation of the spacecraft structure will not introduce loads into the solar cell support panels."

The arrows shown in Figure 9-1 indicate the directions of freedom of movement, and not the directions of constraint, which are perpendicular to the indicated directions.

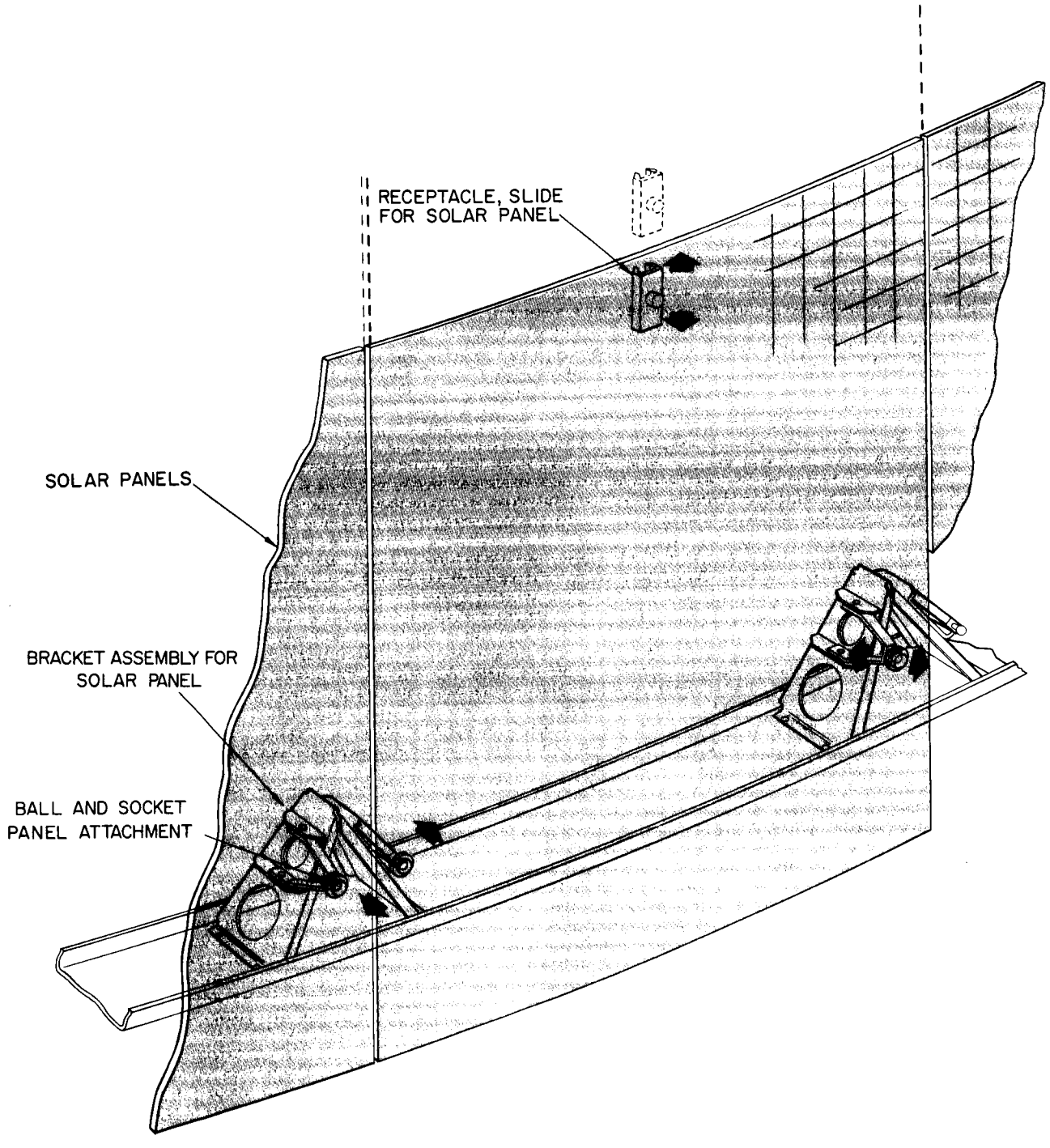


Figure 9-1. Solar Cells Support Panels Attachment

# 10. PROJECT REFERENCE REPORTS

J. M. Ferry, "RCS Installation Procedures," IDC, 15 July 1963.

K. Z. Bradford, "Syncom New Development Coordination," IDC, 15 July 1963

R. A. Browne, "Report on Peak g Response vs Frequency at Various Locations on the Advanced Syncom T-1 Spacecraft for Sinusoidal Qualification Level Input at the Base of the Thrust Tube," 17 July 1963.

J. P. Wrzesinski, "Advanced Syncom Coordination Control Summary Report," IDC, 19 July 1963.

P. J. Fisher, "Advanced Syncom System Test Equipment Wiring Specification," 22 July 1963.

P. J. Fisher, "Advanced Syncom System Test Equipment Packaging Specification," 22 July 1963.

J. S. Culver, Trip Report – LMSC, Sunnyvale, Booster-Spacecraft Interface Coordination, 23 July 1963.

L. Korba, "Weight Reduction Proposal," 15 July 1963.

R. J. Smith, "Advanced Syncom Power Amplifier Regulators," IDC, 18 July 1963.

P. A. Rubin, "Rosman II – NASA Experimental Communication Station," IDC, 17 July 1963.

Paul E. Norsell, "384H-33 Compression Curves," IDC, 17 July 1963.

J. B. Beaumont, "Minutes of Advanced Syncom 3 July 1963 Meeting to Define RCS Alignment Procedures," IDC, 10 July 1963.

J. B. Beaumont, "Minutes of Advanced Syncom 10 July Meeting for Requirements for Velocity Jet Clearance Hole in Solar Panel," IDC, 10 July 1963.

L. I. Ivey, "Advanced Syncom PACE Regulators," IDC, 10 July 1963.

F. B. Bjorklund, "Advanced Syncom Passive Thermal Control System Sensitivity to Surface Property," IDC, 8 July 1963.

F. B. Bjorklund, "Advanced Syncom Preliminary Thermal Analysis," IDC, 8 July 1963.

L. W. Geary, "Advanced Syncom Parts Program," IDC, 9 July 1963.

J. M. Ferry, "Syncom II, Bi-Propellant Engine Durability," IDC, 9 July 1963.

B. Finver, "Minutes of Syncom II RCS Interface Meeting," IDC, 8 July 1963.

R. N. Ely, "Advanced Syncom Organic Thermal Control of Solar Panels," IDC, 3 July 1963.

J. G. Lotta, "Advanced Syncom Mass Property Data," IDC, 3 July 1963.

B. Finver, "Minutes of Advanced Syncom RCS Interface Meeting," IDC, 28 June 1963.

J. B. Beaumont, "Coordination Item Meeting Report for Advanced Syncom Clearance Hole for Velocity Jet," IDC, 3 July 1963.

B. N. Smith, "Advanced Syncom Damper Vibration Fixture," IDC, 28 June 1963.

L. A. Gustafson, "Summary of LMSC-Hughes Interface Meeting," IDC, 1 July 1963.

T. Hudspeth, "Advanced Syncom Telemetry and Command Antenna," IDC, 1 July 1963.

I. Baker, "Structural Evaluation of Advanced Syncom Solar Panel Designs," IDC, 28 June 1963.

R. A. Houghten, "Advanced Syncom Coordination Control Summary Report," IDC, 28 June 1963.

R. A. Houghten, "Advanced Syncom Umbilical Disconnect Time," IDC, 27 June 1963.

D. T. Dupree, "Master Index-Advanced Syncom Electronic Ground Support Equipment," 1 July 1963.

P. E. Norsell, "Apogee Motor Squib Access Requirements," IDC, 28 June 1963.

F. B. Bjorklund, "Advanced Syncom Solar Panel Temperature Control," IDC, 27 June 1963.

A. M. Liebschutz, "Semiconductors Used on Advanced Syncom Spacecraft," IDC, 26 June 1963.

"Reporting of New Technology" Syncom and Advanced Syncom Project Notice No. 66 (Rev. A), 7 July 1963.

"Use of Torq-Set Screws for Advanced Syncom," Advanced Syncom Project Notice No. 16, 15 July 1963.

"Telemetry System and Format" Advanced Syncom Project Notice No. 17, 16 July 1963.

"Telemetry System and Format" Advanced Syncom Project Notice No. 17 (Rev. A), 29 July 1963.

"Definition of Command System" Advanced Syncom Project Notice No. 18, 17 July 1963.